DUBLIN CITY UNIVERSITY

Standardized Development of Microarray Technology via Substrate-Independent Surface Coatings

by

Scott D. Spillman

A thesis submitted in partial fulfillment for the
degree of Doctor of Philosophy

in the
School of Physical Sciences

under the supervision of
Brian D. MacCraith

September 2009

Declaration of Authorship

I hereby certify that this material, which I now submit for assessment on the programme of study leading to the award of Doctor of Philosophy is entirely my own work, that I have exercised reasonable care to ensure that the work is original, and does not to the best of my knowledge breach any law of copyright, and has not been taken from the work of others save and to the extent that such work has been cited and acknowledged within the text of my work.

Signed (Candidate):

ID No.:

Date:

Abstract

by Scott D. Spillman

While microarray technology has provided a versatile and high-throughput analytical tool for many research purposes, poor cross-platform assay dataset correlation has prevented the technology from finding common usage for real-world applications due to difficulties regarding the ability to validate results obtained on different platforms. Although large-scale investigations in the literature have demonstrated that cross-platform dataset correlation can be increased through the implementation of standardized interlaboratory probes, assay methodology, and analysis techniques, the degree of cross-platform concordance achievable remains significantly limited due to inherent differences in the platforms themselves. Much of the inherent cross-platform differences limiting the extent of cross-platform dataset comparability lies with dissimilar surface properties between platforms, resulting in differential probe and target behaviors. To overcome these limitations regarding cross-platform dataset comparability, the development and use of multifunctional substrate-independent surface coatings was explored as a method to eliminate the initial differences in cross-platform surface properties and their effects on microarray performance. Specifically, two types of substrate-independent surface coatings were examined: an electrostatically self-assembled polyelectrolyte multilayer and a self-polymerized polydopamine film.

The results of this investigation determined that both multifunctional substrate-independent surface coatings were capable of depositing onto a broad range of materials and converting their surface properties into the properties of the coating itself. Additionally, when using these surface coatings as a common cross-platform interface, it was possible to obtain highly concordant microarray datasets between platforms constructed from glass, mica, silicon, and polymer. In particular, multianalyte DNA and protein dose-response assays performed on platforms with substrate-independent surface coatings yielded significantly higher correlation coefficients in comparison to platforms without substrate-independent surface coatings. Furthermore, it was shown how the surface properties of the multifunctional substrate-independent surface coatings can be manipulated through chemical modification in order to tailor and optimize microarray performance to suit specific applications. Utilization of substrate-independent surface coatings in such a manner can provide researchers and manufacturers with a simple, yet effective, method to standardize microarray fabrication across different platforms while still enabling sustainable development of the technology in terms of platform material, design, and application.

Acknowledgements

First and foremost, I would like to thank my parents, Joni and Steve, whose support, guidance, and bailouts have enabled me to pursue my goals and get to where I am today. Also, I would like to thank all of the foreigners I have met over the years who encouraged me to broaden my horizons and inspired me to become a foreigner myself: Ronen, Alfredo, Michael, Alex, Sompong, Madhu, and especially Avril, whose friendship I dearly miss. A special thanks is also deserved to Joseph Wang, who gave me my first opportunity and taught me the meaning of hard work and perseverance. Additionally, many thanks go to those at DCU, especially Helen and Rob, whose valuable discussions helped me to formulate the concepts presented within this thesis. And finally, thanks go to Prof. Brian MacCraith, who provided the resources necessary to complete my experimental work.

Contents

List of Figures

List of Tables

Abbreviations

anti-IgG	Goat **anti-**Mouse **I**mmuno**g**lobulin **G** Antibody
anti-Myo	Mouse **anti-**Human **Myo**globin Antibody
AS	**A**mino**S**ilane
BSA	**B**ovine **S**erum **A**lbumin
CC	**C**orrelation **C**oefficient
cDNA	**c**omplementary **DNA**
CVD	**C**hemical **V**apor-**D**eposited
DNA1P	**DNA**1 **P**robe
DNA1T	**DNA**1 **T**arget
DNA2P	**DNA**2 **P**robe
DNA2T	**DNA**2 **T**arget
IgG	Mouse-**IgG**
LbL	**L**ayer-**b**y-**L**ayer
LP	**L**aser **P**ower
mRNA	**m**essenger **RNA**
Myo	Human **Myo**globin
NSB	**N**on**S**pecific **B**inding
OPD	**O**ptimized **P**oly**D**opamine
OPT	**O**xygen **P**lasma-**T**reated
PAC	**Poly**(**A**crylic **A**cid)
PAH	**P**oly(**A**llylamine **H**ydrochloride)
PBS	**P**hosphate **B**uffered **S**aline
PBST	**PBS** with **T**ween 20
PD	**P**oly**D**opamine
PDMS	**P**oly**D**i**M**ethyl**S**iloxane

PEM	**P**oly**E**lectrolyte **M**ultilayer
PLL	**P**oly-**L**-**L**ysine
PMT	**P**hoto **M**ultiplier **T**ube
PSI	**P**hase-**S**hifting **I**nterferometry
PSS	**P**oly(sodium 4-**S**tyrene**S**ulfonate)
SI	**S**ubstrate-**I**ndependent
SD	**S**tandard **D**eviation
SPR	**S**urface **P**lasmon **R**esonance
SS	**S**ubstrate-**S**pecific
S/N	**S**ignal/**N**oise Ratio

Chapter 1

Overview of Microarray Technology

The development of microarray technology has provided a powerful tool helping researchers to gain a deeper understanding of the chemical processes which enable biological systems such as cells to sustain life[1,2]. Utilization of this technology has made it possible to simultaneously screen for thousands of compounds in an extremely high-throughput and parallel fashion while tremendously reducing the amount of reagents and analysis time required. This ability to rapidly characterize the chemical makeup of biological samples enables the identification biochemical abnormalities which may be caused by disease or environmental contaminates.

The technology itself is based upon the spatial arrangement of multiple distinct receptors, or probes, onto a solid support. The function of these immobilized probes is to bind with analytes, or targets, of interest within a biological sample in order to detect their presence and concentration. Common applications of microarray technology include, but are not limited to, gene expression profiling[3], proteome analysis[4], and toxicological studies[5].

1.1 Types of Microarrays

DNA Microarrays

Microarray technology was initially developed for use with DNA applications. The first example of a DNA-based microarray was utilized for DNA sequencing[6]. This was accomplished by hybridizing a fragmented DNA strand to a set of known oligonucleotides immobilized onto a solid support. Based on the observed hybridization pattern of the fragmented DNA strand, it was possible to reconstruct what its original sequence was. Since that time, the use of DNA microarray technology has rapidly expanded to encompass a variety of applications such as gene expression profiling, genotyping, and splice-variant analysis[7].

Fabrication of DNA microarrays is typically accomplished by spotting multiple distinct DNA fragments onto a suitable surface using a robotic printer[2]. The spotted DNA fragments adhere to the surface via electrostatic adsorption or covalent attachment. Alternatively, DNA oligonucleotides can be synthesized base-by-base directly onto a surface using photolithography and combinatorial chemistry to generate high-density arrays[8]. The process by which DNA oligonucleotides are synthesized onto a surface is illustrated in Figure 1.1. Following microarray fabrication, the DNA probes are exposed to a liquid sample containing target DNA compounds. The immobilized probes hybridize to complementary DNA (cDNA) targets within the sample, enabling their detection through fluorescence or some other means.

A typical cDNA microarray experiment designed to characterize gene expression levels within a cell is illustrated in Figure 1.2. First, a microarray is fabricated using cDNA probes which are complimentary to specific genes of interest within an experimental cell. Generally, the cell under investigation exhibits abnormal gene expression levels due to disease, differential growth conditions, or some other factor which is thought to alter a cell's gene expression. From the experimental cell, messenger RNA (mRNA) is extracted. The mRNA within a cell is the product of gene transcription, and therefore, provides a blueprint of the cell's gene expression profile. The extracted mRNA is then converted into DNA using reverse transcription and simultaneously labeled with a fluorescent dye such as Cy5. The same procedure is also performed using a control cell which exhibits normal gene expression levels, except in this case, a separate fluorescent
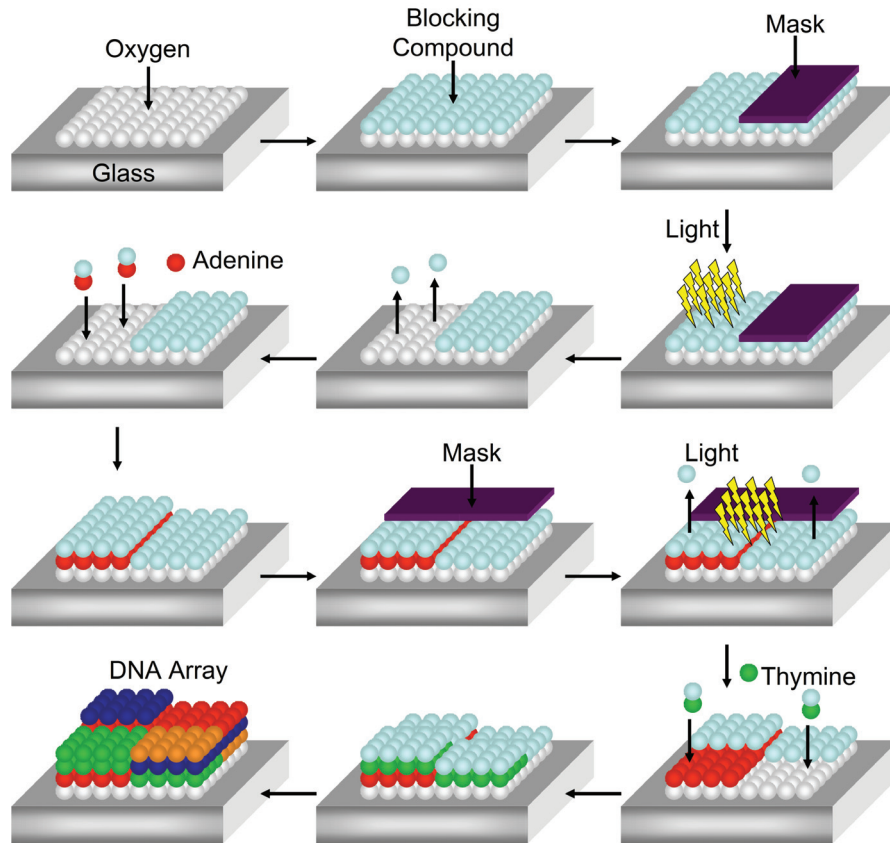
FIGURE 1.1: In situ synthesis of a DNA microarray. A surface such as glass is washed with a blocking agent which can be removed upon exposure to light. Using a photomask, specific areas of the surface are then irradiated in order to remove the blocking agent. Next, the surface is washed with a solution containing a specific nucleotide, such as adenine, which is itself linked to the same blocking compound. The adenine then binds to the area of the surface which was exposed to light while leaving the area blocked again. This process is then repeated using different photomasks and nucleotides until the desired oligonucleotides are formed.

dye, such as Cy3, is used to label the DNA during reverse transcription. Next, equal amounts of the reverse transcribed DNA from the experimental sample and the control sample are mixed together and hybridized to the microarray platform. Based on the observed fluorescence pattern, it is possible to determine which genes are differentially expressed in the experimental cell. For example, if both the experimental cell and the control cell exhibit identical gene expression levels, then a Cy5:Cy3 fluorescence ratio of 1:1 will be observed. However, if the experimental cell exhibits different gene expression levels in comparison to the control cell, changes in the Cy5:Cy3 fluorescence ratio will be observed.
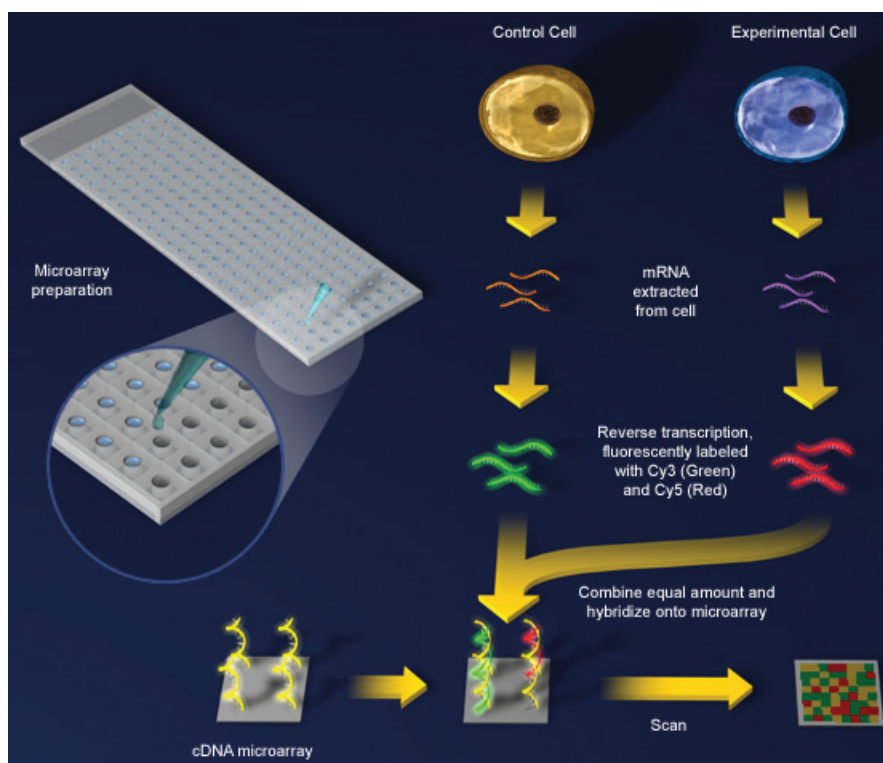
FIGURE 1.2: Illustration outlining a typical cDNA microarray experiment designed to measure gene expression. mRNA is extracted from a control cell and an experimental cell. The mRNA from each sample is then converted into DNA and labeled with separate fluorescent dyes by reverse transcription. The samples are then mixed together and hybridized to a cDNA microarray. The resulting fluorescence pattern is then used to characterize differential gene expression between the control cell and the experimental cell. *Graphic taken from The Science Creative Quarterly (http://www.scq.ubc.ca).*

Protein Microarrays

While the use of microarray technology has primarily been utilized to monitor gene expression, there is a growing interest in examining gene translation at the protein level. To meet this demand, researchers have begun work towards the development of protein microarrays[9,10]. Protein microarrays are similar to their DNA counterparts, except in this case, protein compounds such as antibodies and enzymes are used as probe compounds rather than DNA. One of the first examples of a protein microarray was described by MacBeath and Schreiber[11]. In that work, different protein compounds were arrayed onto glass slides and then exposed to sample solutions containing relevant target compounds. Based on the observed protein-protein interactions it was possible to determine protein function and identify the substrates of protein kinases. Other applications of protein microarray technology include antibody specificity determination[12] and the elucidation of gene function[13].

Other Microarrays

In addition to DNA and protein, microarrays have also been fabricated to examine tissue samples and low molecular weight compounds. Tissue microarrays have been fabricated by arraying hundreds of breast tumor specimens for the characterization of cancer markers[14]. Using these tissue arrays, multiple cancer markers were investigated by analyzing specific DNA, RNA, and protein targets present within each spotted tumor sample. The detection of low molecular weight compounds has also been demonstrated using antibodies bound to narcotic analog coupled proteins arrayed onto thin gold films[15]. Upon exposure to samples containing cocaine, ecstasy, heroin, or amphetamine, displacement of the bound antibodies due to the presence of these narcotics was detectable using surface plasmon resonance (SPR). Additionally, as the application range of microarray technology continues to expand, so too will the platform designs, surface chemistries, and methods of detection.

1.2 Current State-of-the-Art

Platform Designs

While planar glass platforms have been the traditional choice of substrate for microarray applications, the use of alternative materials is becoming more commonplace, as different substrates may provide certain advantages depending upon the desired end goal. For example, platforms possessing thin metallic films have been used to fabricate microarrays which utilize SPR detection[15,16]. Additionally, porous silicon platforms which exhibit high surface areas have been exploited as a means to increase the density of immobilized probes and reduce target detection limits[17]. The utilization of polymer platforms for microarray applications is especially attractive due to their low cost, diverse properties, and ability for integration into microfluidic biochips[18]. For instance, polyimide and poly(ethylene terephthalate) were used as substrates to pattern avidin microarrays capable of binding with biotin-labeled compounds[19]. Additionally, polycarbonate was used to fabricate DNA microarrays within microfluidic channels for the detection of single-nucleotide polymorphisms[20].

Surface Chemistries

In addition to substrate material, surface chemistry plays an important role in determining microarray performance. Typically, microarray surfaces are functionalized via chemical or physical means in order to maximize the density and activity of immobilized probes. In the case of DNA and protein probes, this is often accomplished using amine functional groups, as aminated surfaces have been shown to exhibit strong non-covalent interactions with many nucleic acid and amino acid compounds[21,22]. Additionally, methods to covalently link probe compounds utilizing functional groups such as aldehydes[11] and epoxides[23] have been developed. The use of dendrimers[24] and 3-D hydrogels[25] has also been exploited as a means to increase the surface density of functional groups and enable higher loading capacities for probe compounds.

Generally, the modification methods used to functionalize a surface are dependent upon the platform material. For example, glass and silicon can be functionalized using organosilanes[26], whereas gold is typically functionalized using organothiols[27]. The functionalization of polymer surfaces, on the other hand, is not as straightforward. Because different polymers exhibit a wide range of surface properties, modification methods which work with one polymer may not work with others. Moreover, many polymers exhibit a high resistance towards reaction with nucleophiles, meaning that harsh chemical or physical treatments are often required to introduce functional groups onto their surfaces[28]. Recently, however, methods utilizing polyelectrolyte multilayers[29,30], chemical vapor deposition[31], and self-polymerized dopamine[32] have been developed which are capable of functionalizing a variety of polymer materials without the need of any surface pretreatments.

Detection Methods

Typically, the detection of target compounds which bind to an immobilized receptor is accomplished using fluorescence spectroscopy. However, other methods of detection are also being explored. For example, electrode arrays have been developed which are capable of simultaneously detecting DNA and protein compounds using an electroactive label[33]. Additionally, label-free detection methods have been developed which utilize SPR and mechanical cantilevers. Specifically, SPR detection has been used to examine

the influence of probe density and sequence on the hybridization efficiency of unlabeled DNA targets[34], while nanomechanical cantilever arrays were utilized for the quantitative detection of unlabeled DNA targets[35]. Given the extensive list of platform designs, surface chemistries, and detection methods available, an endless number of combinations can be utilized to develop microarray technology for virtually any desired application.

1.3 Problem

Although microarray data is commonly employed for a variety of research purposes, the technology has yet to find common usage for real-world applications such as medical-care and environmental monitoring. More widespread implementation of microarray technology for practical applications has not been possible as the reliability of this technology was put into question following the publication of key research articles citing poor cross-platform dataset correlation[36]. Specifically, it has been shown that assays performed with the same set of samples generate discordant datasets on different microarray platforms. For example, Kuo et al. examined the gene expression from cancer cell lines using two commercially available microarray platforms: Stanford type cDNA microarrays and Affymetrix and oligonucleotide microarrays[37]. In that work, it was found that assay datasets obtained from the same sample showed poor correlation. This problem relating to low cross-platform dataset correlation has also been reported in other investigations[38,39].

Due to this low cross-platform dataset correlation, the ability to validate assay results between existing and newly developed microarray technologies is often difficult or impossible. The reasons for low cross-platform dataset correlation are often attributed to intrinsic differences in the platforms themselves and a lack of standardized probe designs, assay protocols, and analysis methods between platforms and laboratories[40–42]. In response to these publications, large-scale interlaboratory investigations have been conducted which demonstrate considerable increases in cross-platform dataset correlation when utilizing standardized methodologies[43–45]. For example, Mecham et al. showed that the use of sequence-based matching of probes, as opposed to gene identifier-based matching, produces significantly more consistent cross-platform datasets when analyzing RNA derived from a breast cancer cell line[45]. Additionally, the Toxicogenomics

Research Consortium found significant increases in interlaboratory datasets when using standardized sample preparation methods, assay protocols, and analysis techniques[38].

Despite the use of standardized probe designs, assay protocols, and analysis methods, however, the ability to generate concordant cross-platform datasets remains limited due to intrinsic differences in the microarray platforms themselves. In particular, dissimilar cross-platform surface properties result in differential probe immobilization densities, probe/target affinities, and target nonspecific binding[9,46,47]. These differences in surface properties represent a primary source of cross-platform dataset discordance which cannot be overcome by the standardization of methodologies such as assay protocol and analysis technique.

1.4   Objective

The primary objective of the work presented in this thesis was to develop a method which would enable the production of truly concordant cross-platform microarray datasets. Achievement of this goal requires the ability to eliminate differences in surface properties between microarray platforms in order to generate similar probe immobilization densities, probe/target affinities, and nonspecific binding of target compounds. One possible solution to overcome differences in cross-platform surface properties would be to adopt a common microarray platform to perform specific applications. The adoption of a common platform is an impractical option, however, as it would stagnate future development and advancement of microarray technology in terms of platform design, surface chemistry, and detection method. With that said, any feasible solution to the defined problem must be able to satisfy the following criteria:

- Ability to render the surface properties of any platform identical

- Ability to tailor and optimize those surface properties to suit specific microarray applications

- Ability to replicate the surface property optimizations onto any existing or newly developed platform with identical results

Satisfaction of these criteria would enable the ability to generate more concordant cross-platform datasets while still facilitating sustainable development of the technology

in terms of platform design, surface chemistry, probe design, assay protocol, detection method, and analysis technique. To meet these criteria, the development and use of multifunctional substrate-independent (SI) surface coatings was explored as a potential method to eliminate the initial differences in surface properties and obtain truly concordant cross-platform microarray assay datasets.

Chapter 2

Multifunctional SI Surface Coatings

2.1 Introduction

As discussed in Chapter 1, the only way to obtain truly concordant cross-platform microarray datasets is to render the surface properties of different platforms identical. To meet this objective, the use of SI surface coatings was investigated. Here, characteristics which a SI surface coating must possess in order to serve as an effective cross-platform interface for microarray applications are examined. Furthermore, the development of a SI surface coating which meets the necessary requirements to serve as an effective coating for microarray applications is described. Aspects of the surface coating thickness, morphology, uniformity, density, and surface energy are characterized, and how these characteristics are relevant to the development of microarray technology is discussed.

2.2 Materials and Methods

2.2.1 Materials

Glass microscope slides were obtained from Sigma-Aldrich (Dublin, Ireland); mica substrates from SPI Supplies (West Chester, PA, USA); silicon wafers from Silicon Inc.

(Boise, ID); and Zeonor cycloolefin polymer slides from Åmic (Uppsala, Sweden). Poly(-allylamine hydrochloride) (PAH, $M_w = 70K$) and poly(sodium 4-styrenesulfonate) (PSS, $M_w = 70K$) were obtained from Sigma-Aldrich. DY547 NHS-ester was obtained from Dyomics GmbH(Jena, Germany). All other chemicals and reagents were obtained from Sigma-Aldrich.

2.2.2 Substrate Preparation

Gold slides were prepared by electron-beam evaporation of gold onto glass slides using an Edwards Auto 306 high vacuum system (West Sussex, U.K.). All substrates were initially cleaned by rinsing with distilled water, then ethanol, and dried with a gentle steam of air. Some substrate materials were oxygen plasma-treated (OPT) by exposure to an oxygen plasma using an Oxford Instruments PlasmaLab 80Plus (Abindon, Oxfordshire, UK) at 5 sccm O_2, 40 mTorr pressure, and 50 W power for 2 min.

2.2.3 Labeling of PAH

PAH was labeled with DY547 fluorescent dye by dissolving 200 mg of PAH in 8 mL of water, giving a final concentration of 25 mg/mL PAH. This solution was then added to 100 mg of DY547 and allowed to react for 2 hours. Unconjugated dye was separated from the DY547-labeled PAH by dialysis in water.

2.3 Surface Modification Methods

Prior to the development of a SI surface coating, a few considerations must be made regarding the requirements which should be met for a surface coating to serve as a useful cross-platform interface for microarray applications. Firstly, the coating should be compatible with most materials to enable transferability of the technique onto any existing or newly developed platform. Based on this requirement, the use of chemical modification methods such as silane or thiol chemistry can immediately be eliminated, as these techniques are limited to specific oxide and metallic compounds, respectively. Second, it should be possible to deposit the coating onto substrates with complex geometries to enable transferability of the technique onto any existing or newly developed platform

designs. This requirement rules out the use of techniques such as Langmuir-Blodgett and spin coating, as these methods are limited to planar surfaces and cannot be used to obtain uniform coatings on 3-dimensional geometries such as microchannels.

Of the currently available surface modification techniques, only a few meet these two criteria. One possible method is the use of chemical vapor-deposited (CVD) reactive polymer coatings. Certain types of CVD polymer coatings have been shown to deposit stably onto a wide range of materials with simple or complex geometries[48], satisfying both requirements to serve as a common cross-platform surface coating. Additionally, it has been shown that CVD polymer coatings are capable of further functionalization following deposition onto a substrate surface. Of particular relevance to this thesis, Thevenet et al. demonstrated the use of these polymer coatings to fabricate DNA arrays with similar results on different substrate materials[49]. This ability to functionalize and fine-tune the surface properties of the coating to perform specific applications satisfies an additional criterion necessary for the coating to serve as a potential cross-platform interface for the development of microarray technology.

CVD polymer coatings also allow for precise control over the layer thickness and can be used to achieve film thicknesses down to just a few nanometers. The ability to control layer thickness at the nanoscale represents a significant advantage with the use of CVD polymer films. For example, the use of thick layers (>10nm) is undesirable as they could interfere with desirable intrinsic properties of the platform material. In particular, platforms utilizing an optically based detection method may require the use of a platform material exhibiting a specific transparency or reflectivity. In this case, thicker surface coatings may interfere with these intrinsic properties of the material, resulting in a decrease in the platform's performance. Alternatively, too thin a layer may not be sufficient enough to mask the surface properties of the underlying material. In this case, the underlying substrate material will influence subsequent functionalization of the platform surface with other chemical groups or biomolecules. If the underlying material effects the ability to functionalize the surface, the coating will be unsuitable to serve as a common cross-platform interface as dissimilar platforms will yield different results. For these reasons, a SI surface coating must be thick enough to mask the surface properties of the underlying material, yet thin enough to sufficiently minimize interference with the intrinsic properties of the substrate material which may be of importance to the platform's functional design.

While the use of CVD polymer films satisfies all of the criteria required to serve as a common cross-platform surface coating, the method does not come without its limitations. In particular, the technique cannot be utilized to coat substrates larger than the instrument's plasma chamber. Nor can it be used to coat the surface of objects such as nanoparticles, limiting the potential application range of this method. Furthermore, CVD requires the use of expensive instrumentation which is not available for use by all researchers and laboratories.

The use polyelectrolyte multilayer (PEM) films, on the other hand, presents an alternative surface modification technique which can be used to overcome many of the limitations encountered with CVD polymer coatings[50]. Similar to CVD coatings, PEMs have also been shown to stably deposit onto a wide range of substrates with simple or complex geometries. Unlike CVD coatings though, PEMs can be utilized to coat objects of any size, including nanoparticles[51]. Additionally, polyelectrolyte (PE) compounds are relatively inexpensive and their deposition does not require the use any sophisticated equipment, making their use readily available to all researchers and laboratories. Based on these advantages, attention was focused towards the development of a SI surface coating based on the use of PEMs.

2.4 PEMs

PEM films are assembled onto solid surfaces via the alternate adsorption of cationic and anionic polymers from solution. Typically, the mechanism behind PEM formation is electrostatic self-assembly, where each PE layer adsorbed results in a charge inversion, priming the surface for subsequent deposition of an oppositely-charged PE[52].

Because the films are assembled layer-by-layer (LbL), the use of PEMs offer control over the layer thicknesses at the nanometer scale. It should be noted, though, that the deposition of PEM films is not limited to electrostatic assembly. Recently, it has been shown that other forces such as hydrophobic interactions[29], hydrogen-bonding[53,54], and covalent linkage[55] can be exploited to initiate multilayer buildup on a broad range of materials.

The use of electrostatically-assembled PEMs was originally described by Decher et al. in the early 1990s[56–58]. Since that time, their use has proven to be an extremely

simple and versatile method to pattern and fine-tune a variety of functionalities onto the surface of many different materials[50,59]. Furthermore, the multifunctional characteristics of PEM coatings have been exploited to perform a diverse range of applications ranging from nanoparticle functionalization[60] to microfluidic channel modification[61], and of particular relevance to this thesis, the fabrication of DNA and protein microarrays[62,63].
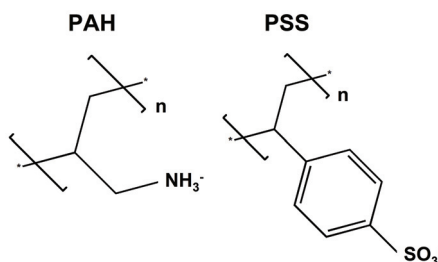
FIGURE 2.1: Chemical structures of the PEs used to assemble the multilayer system described in this investigation.

In this work, the deposition of a PEM system based on the alternate assembly of PAH and PSS was characterized on a variety of materials. The chemical structure of these two PEs is provided in Figure 2.1. PAH is a cationic polymer possessing amine groups along its backbone, while PSS is an anionic polymer with sulfonate groups along its backbone. The use of a PAH/PSS based multilayer system was chosen as this combination of PEs has been well characterized in the literature and proven to be quite versatile in terms of functionality and stability[52,64].

2.4.1 PEM Deposition

Platforms

Deposition of the PEM surface coating was characterized on five different platform materials: glass, gold, mica, polymer, and silicon. The polymer used in this investigation was Zeonor, which is a commercial cyclo-olefin polymer with high optical transparency. The use of such a diverse set of substrates was deliberately chosen in order to establish the range of materials capable of initiating buildup of the PAH/PSS-based PEM surface coating. Buildup of the PEM coating was monitored on both native and OPT substrates. Oxygen plasma is commonly used to oxidize surfaces and increase charge density[65,66]. OPT substrates were included in this investigation to determine whether an increase in

surface charge density has an impact upon PEM deposition, especially for the polymer substrate, which has a neutral charge in its native state. The OPT substrates were prepared by exposing each material to an oxygen plasma using an Oxford Instruments PlasmaLab 80Plus at 5sccm O_2, 40 mTorr pressure, and 50 W power for 2 minutes.

LbL PEM Assembly

The PEM assembly process is illustrated in Figure 2.2. Prior to deposition of the PAH/PSS multilayer system, all substrates were cleaned with water and ethanol then dried using a slide centrifuge. Next, the substrates were incubated in 2mg/mL PAH (MW 70K) in water (pH 7.4) containing 0.1 M sodium chloride for 10 minutes. Following the incubation period, each substrate was washed with 5 exchanges of water to remove any unbound PAH and dried using the slide centrifuge. The PAH-coated substrates were then incubated in 2mg/mL PSS (MW 70K) in phosphate-buffered saline (PBS) (pH 7.4) for 10 minutes. Following incubation in the PSS solution, the substrates were washed and dried again. This deposition cycle was repeated until the desired number of PE layers was achieved. Assuming that multilayer formation occurs, the PEM coating can ultimately be capped with either PSS to provide a negative sulfonated surface or PAH to provide a positive aminated surface.

2.4.2 PEM Thickness and Morphology

The PEM thickness and surface roughness were characterized on native glass and polymer substrates using phase-shifting interferometry (PSI). The thickness was characterized to provide information regarding the growth rate and surface area of the PEM coating on each material.

Prior to multilayer assembly, a drop of polydimethylsiloxane (PDMS) was polymerized on the glass and polymer substrates. A PEM system composed of PAH(PSS/PAH)$_5$ was then assembled onto both substrates according to the procedure described in Section 2.4.1. Following deposition of the PEM coating, the PDMS drops were removed to create a defined step between the PEM coating and the substrate surfaces. The surfaces were then imaged using a Wyko NT1100 optical profiling system to generate the PSI images shown in Figure 2.3.
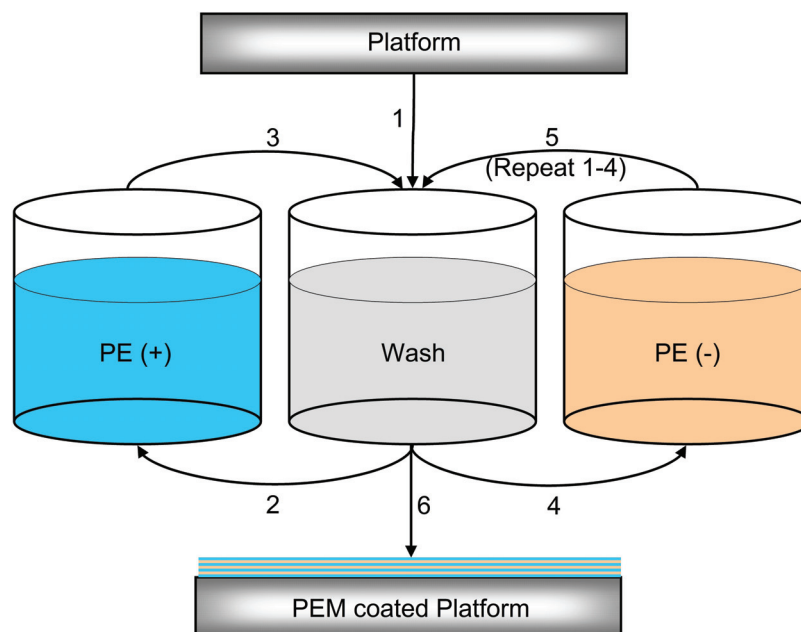
FIGURE 2.2: Stepwise assembly of PEMs. Prior to multilayer assembly, a solid substrate is washed (1). The substrate is then incubated in a positively charged PE (2) and then washed in water to remove any unbound or loosely bound PE from the surface (3). Next, the substrate is incubated in a negatively charged PE (4). Steps 1-4 are repeated (5) until the desired number of layers is achieved (6).

In Figure 2.3, the blue region represents the substrate surface, while the green region represent the PEM surface. As shown by the green regions, the PEM surface is higher than the substrate surface, indicating that growth of the PEM coating occurred on both glass and polymer. Because the surface properties of glass and polymer are significantly different, it was expected to observe very different PEM growth rates on each material. However, the final PEM thicknesses, as calculated by the Wyko software, were very similar on each substrate (8±1nm on glass and 9±2nm on polymer), indicating similar growth rates of the PSS/PAH multilayer system on both materials. Growth of the PEM system on both glass and polymer demonstrates the ability to initiate multilayer buildup on two very different materials. Specifically, the glass is a relatively hydrophilic and negatively-charged oxide material, whereas the polymer is a hydrophobic and uncharged organic material.

In addition to similar PEM growth rates on different substrates, it is desirable to obtain uniform surface roughnesses on different substrates following the deposition of the PEM coating. Platforms with different surface roughnesses will also exhibit differences in surface area. In regard to microarray development, differences in cross-platform
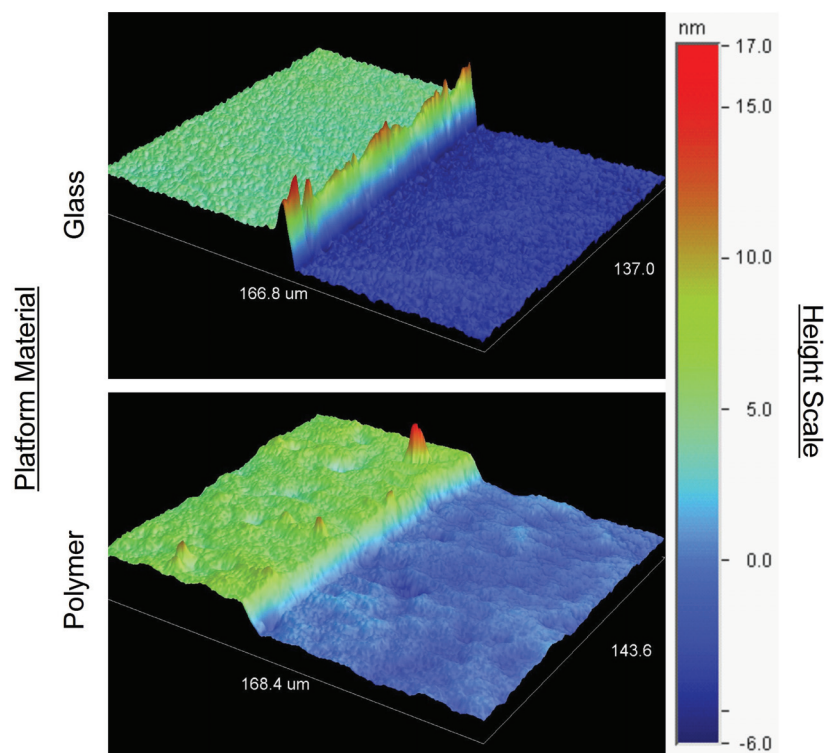
FIGURE 2.3: PSI images of the PEM coating on native glass and polymer. In each image, the blue area represents the substrate surface and the green area represents the PEM surface. The step between the substrate surface and PEM surface was created by the removal of a polymerized PDMS drop.

surface roughness can introduce a significant source of dataset discordance. Specifically, platforms with rougher surfaces will provide a larger surface area, which will result in increased probe densities relative to platforms with smoother surfaces. Differences in cross-platform probe densities will ultimately yield dissimilar target responses when performing assays from the same sample.

As shown in Figure 2.3, the surface roughness of the PEM coating on glass is much smoother than the PEM coating on polymer, indicating significant differences in surface roughness between the two platforms. It should be noted, however, that the surface of the polymer substrate itself is significantly rougher than the glass surface, as shown by the blue regions in each image. Therefore, the surface roughness differences observed in Figure 2.3 are most likely not a limitation with the PEM coating, but rather, a consequence of initial surface roughness differences between the substrates themselves. Therefore, it should be possible to overcome this apparent limitation with the use of platforms exhibiting similar initial surface roughnesses.

2.4.3 PEM Surface Energy

While the images in Figure 2.3 provide information regarding the thickness and surface morphology of the PEM coating, they do not supply any information regarding the surface properties. To investigate the surface properties of the PEM coating, water contact angles were measured throughout the assembly process. Specifically, the contact angle (θ_C) is the angle at which a liquid/gas interface meets a solid[67], as illustrated in Figure 2.4.
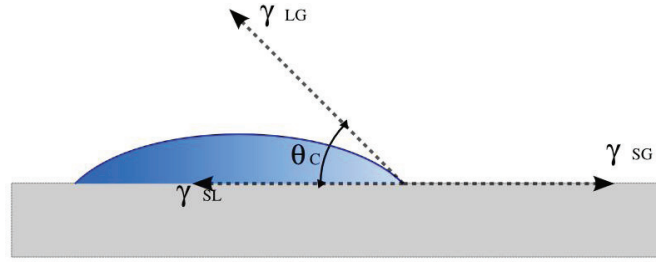
FIGURE 2.4: The contact angle (θ_C) at a liquid/gas/solid interface. The value of θ_C on a surface will be dependent upon the interfacial energies between the solid/gas (γ_{SG}), solid/liquid (γ_{SL}), and liquid/gas phases (γ_{LG}).

The contact angle is dependent upon the interfacial energies between the solid/gas phase (γ_{SG}), the solid/liquid phase (γ_{SL}), and the liquid/gas phase (γ_{LG}) according to the Young Equation:

$$0 = \gamma_{SG} - \gamma_{SL} - \gamma_{LG} \cos \theta_C \qquad (2.1)$$

In this experimental design, the liquid (water) and the vapor (ambient atmosphere) were considered to be constant, and therefore, changes in the contact angles represent changes in the surface energy of the platforms as deposition of the PEM coating progresses. Using a FTA200 dynamic contact angle analyzer, water contact angles were recorded on native and OPT glass, gold, mica, polymer, and silicon following the deposition of each PE layer. The contact angles recorded from these measurements are plotted in Figure 2.5.

Looking at the leftmost datapoints in Figure 2.5, a broad range of contact angles is observed across the materials prior to deposition of PEs. For example, the OPT glass, mica, and silicon substrates exhibit contact angles close to 0°, while the native polymer

substrate exhibits a contact angle approaching $100°$. All other substrates exhibit contact angles somewhere in between $0°$ and $100°$, representing a diverse set of platforms in terms of surface energies, and therefore, surface properties.
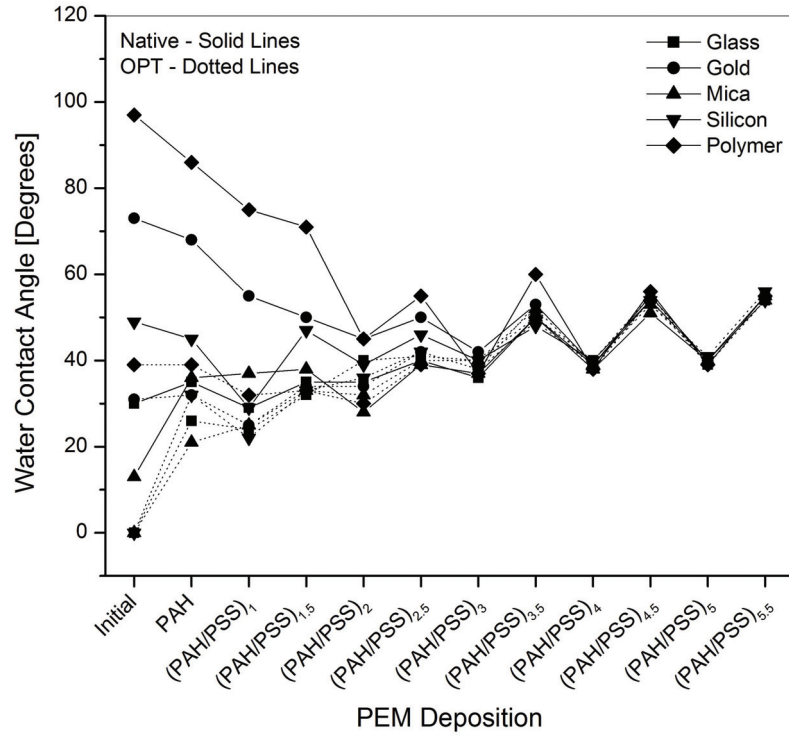
FIGURE 2.5: Water contact angles measured throughout the PEM deposition process. Solid lines represent native materials and dotted lines represent OPT materials.

As PEM assembly progresses, however, the contact angles begin to change on each material. For example, the contact angles of the OPT glass, mica, and silicon platforms jump from $0°$ to over $20°$ following deposition of the first PAH layer. The increased contact angle observed on these materials suggests a change in their surface energies due to the adsorption of PAH. A significant change in contact angle due to PAH adsorption is also observed on the native polymer substrate, despite its surface being uncharged and hydrophobic. In this case, the contact angle drops from $100°$ to below $90°$. The ability to deposit PAH onto an uncharged polymer substrate suggests that forces other than electrostatic are exploited to initiate multilayer buildup of the PAH/PSS system.

Further analysis of Figure 2.5 reveals a clear trend in the contact angle readings between each material as PEM assembly progresses. Specifically, after deposition of the third PSS/PAH bilayer, the contact angles measured on each substrate begin to converge. By the fourth bilayer, the contact angles are nearly identical and begin to exhibit similar

contact angle changes with each subsequent PE layer deposited, switching back and forth from 40° to 60°, depending on whether the PEM system is capped with PSS or PAH, respectively. This convergence of the contact angles suggests that by the forth PSS/PAH bilayer deposited, the surface energies of each material become equivalent and further PE assembly onto their surfaces yields similar results, even on materials which exhibited significantly different initial surface properties.

2.4.4 PEM Density

Assuming that the surface energies of different materials become equivalent following deposition of the PEM coating, it might be expected that subsequent functionalities introduced onto their surfaces would yield similar results in terms of density and thickness. To test this assumption, PEM deposition was characterized further utilizing a fluorescent dye-labeled PE. The total fluorescence intensity generated by a fluorescent dye-labeled PE deposited onto a surface will provide information regarding the density of the dye on the surface, and therefore, the density of the PE to which it is conjugated.

Here, PAH was labeled with DY547 fluorescent dye by dissolving 200mg of PAH in 4mL of water to give a final concentration of 50mg/ml PAH. To this solution, 100mg of DY547 was added and allowed to react in the dark. Following a two hour reaction time, unconjugated dye was separated from the DY547-labeled PAH by dialysis against water.

Using the DY547-labeled PAH, PEM assembly was monitored on native glass and polymer substrates again. Prior to deposition of the DY547-labeled PAH, a base coating of PAH(PSS/PAH)$_2$ was deposited on the substrates to serve as a primer for subsequent deposition of the dye-labeled PAH. Following deposition of the PAH(PSS/PAH)$_2$ primer layers, bilayers of PSS and DY547-labeled PAH were assembled. After the deposition of each dye-labeled PAH layer, the fluorescence intensity was measured over a 0.75x1.50cm area on the glass and polymer substrates using a Perkin Elmer ScanArray G$_x$ microarray scanner. Both substrates were scanned with an excitation wavelength of 543nm using a laser power (LP) of 100% and a fixed photomultiplier tube (PMT) setting of 50%. The fluorescence intensities generated on both substrates following the assembly of each PSS/DY547-labeled PAH bilayer are plotted in Figure 2.6.
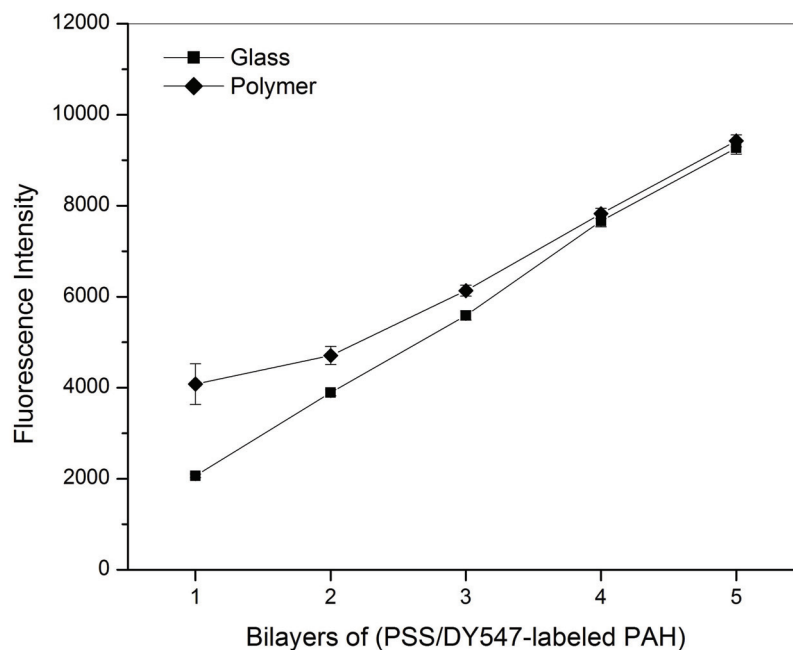
FIGURE 2.6: Quantified fluorescence intensities generated by bilayers of PSS and DY547-labeled PAH assembled onto PAH(PSS/PAH)$_2$-coated glass and polymer.

As shown in Figure 2.6, the first PSS/DY547-labeled PAH bilayer generates significantly different fluorescence intensities on the PAH(PSS/PAH)$_2$-coated glass and polymer substrates, suggesting that the dye-labeled PAH initially assembles onto each surface at different densities. Specifically, the glass platform generated a fluorescence intensity of around 2000, while the polymer substrate generated an intensity of around 4000. Additionally, going from the first to the second bilayer, the rate of fluorescence increase is significantly different on each material, increasing from 2000 to almost 4000 on glass, while only increasing from 4000 to 4500 on polymer. This difference in the rate of fluorescence increase observed between the glass and polymer substrates indicates that the PE layers are depositing at different densities on the two surfaces, which also indicates that the surface properties between each substrate are still significantly different. After deposition of the third bilayer, however, both the fluorescence intensity and the rate of fluorescence increase begin to converge on each material. Additionally, by the fourth and fifth bilayer, both the fluorescence intensity and the rate of fluorescence increase are nearly identical, suggesting that the dye-labeled PAH begins to deposit at equal densities and that the surface properties are similar on each platform at that stage of the PEM assembly process.

The standard deviation (SD) bars in Figure 2.6, which represent the variation in the fluorescence intensity over the scanned areas, can be used to compare the relative uniformity of the dye-labeled PAH layers on the glass and polymer surfaces. For example, the SD bars of the glass datapoints are relatively small for each bilayer of PSS and DY547-labeled PAH assembled, indicating uniform fluorescence, and therefore, density of the PAH throughout the assembly process. The polymer substrate, on the other hand, has a comparatively large SD bar following deposition of the first PSS/DY547-labeled PAH bilayer, indicating that the fluorescence uniformity is significantly lower on the polymer substrate in comparison to the glass surface. With the deposition of each subsequent bilayer, though, the SD bars on the polymer datapoints get smaller and smaller, indicating that as the assembly process continues, the uniformity of the multilayer system improves. This observation also corroborates with previous research articles claiming that surface heterogenieties encountered during PEM deposition are self-correcting as the assembly process continues[52].

2.4.5 Disadvantages of PEMs

As is the case with CVD coatings, the use of PEMs also comes with certain limitations and disadvantages. Of particular concern is stability. Because PEMs are typically held together through electrostatic interactions, they will ultimately become unstable at some threshold pH or salinity, depending upon the specific PEs used. Therefore, the application range of a particular PEM system will be limited to the environmental conditions at which it remains stable. Another disadvantage with PEMs is the deposition procedure itself, which is a multi-step process. Because PEMs require sequential deposition of multiple layers, the process can be rather lengthy and prone to error if not using an automated procedure.

Recently though, investigations into the use catechol-modified PEs have demonstrated the ability to reduce the number of layers required to completely suppress the surface properties of the underlying material down to only three bilayers, as opposed to five, representing a significant simplification of the deposition process[68]. These catechol-modified PEs also exhibit wider stability ranges and were shown to serve as effective "universal" primer layers, capable of initiating PEM multilayer buildup even on highly adhesion-resistant materials such as poly(tetrafluoroethylene) (PTFE).

2.5 Polydopamine Coating

The conjugation of PEs with cathecol groups for SI PEM deposition derives from another recently developed surface coating based on the self-polymerization of dopamine[32]. Polydopamine (PD) is a multifunctional biomimetic film originally inspired by mussels, which show a natural ability to adhere strongly onto organic and inorganic surfaces, even under wet conditions. It is thought that the high content of 3,4-dihydroxy-L-phenylalanine (catechol) and lysine (amine) residues, present in the amino acid composition of proteins which mussels excrete, contribute to this ability. In a marine environment (pH 8.5), these catechol and amine groups exhibit latent reactivity, slowly forming strong covalent and noncovalent interactions with each other and with surfaces. As shown by its chemical structure in Figure 2.7, dopamine contains both a catechol and an amine group, enabling it to undergo self-polymerization onto a broad range of materials.
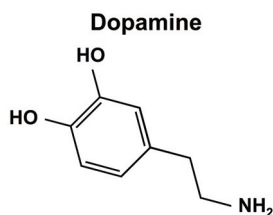
FIGURE 2.7: Chemical structure of dopamine.

Because polymerization occurs slowly, it is possible to control the film thickness at the nanometer scale. Additionally, the resultant surface possesses both catechol and amine groups, providing a multifunctional coating capable of further chemical modification. Based on these abilities, the PD coating was examined alongside the PEM coating as a potential SI surface coating to perform complex multianalyte microarray applications.

2.5.1 PD Deposition

The PD coating was deposited by immersing solid substrates into a 2mg/ml solution of dopamine in 10mM tris (pH 8.5) for 24 hours, as illustrated in Figure 2.8. Using this method, Lee et al. reported a final film thickness of around 50nm[32], whereas here, a thickness of only 2nm was obtained, as measured by PSI on glass on polymer substrates.

This discrepancy in the final film thicknesses may have been due to differences in the buffer preparation method or unmentioned variables in the Lee article, such as deposition temperature. Aside from PSI measurements, further characterization of the PD coating was not performed as it has been thoroughly described in the literature[69].
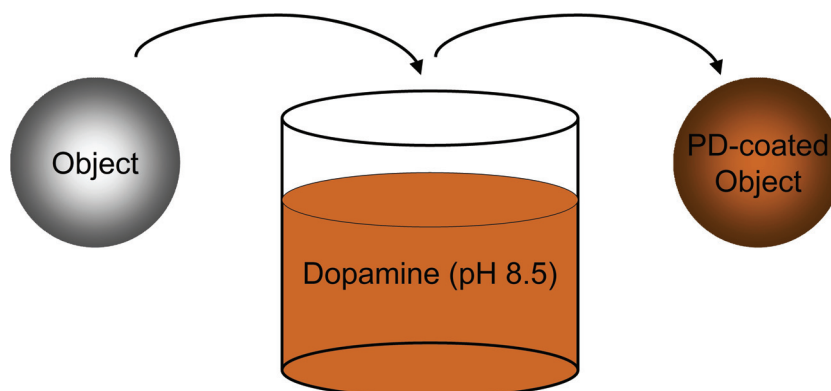
FIGURE 2.8: Illustration depicting the PD deposition process. An object is placed into a solution of dopamine at alkaline conditions, allowing time for the dopamine to self-polymerize on the object's surface.

The nature of the PD deposition process has certain advantages and disadvantages to the use of PEMs. One advantage is that the deposition process is a single step, meaning it is simpler and less prone to error. Additionally, because the coating is chemically cross-linked, it should exhibit a wider stability range, and therefore, broader application range than most electrostatically assembled PEM systems. One potential drawback with the use of PD, however, is its color. Specifically, oxidation of the catechol group to a quinone during the polymerization process yields visibly brown films whose transparency is reduced as the coating's thickness increases. The opacity of the PD film may interfere with some types of optical-based detection methods, depending on the platform design. Due to the advantages and disadvantages associated with each type of SI surface coating, the optimum coating will ultimately depend on the application and the platform design under investigation.

SI Surface Coating Summary

In this chapter, the development of a PEM-based SI surface coating was described. PSI images revealed that a PEM system composed of PAH(PSS/PAH)$_5$, assembled according to the protocol described in Section 2.4.1, generated similar film thicknesses of less than

10nm on native glass and polymer substrates, indicating that the PEM growth rate is similar on both materials.

Contact angle measurements revealed that the PEM coating was capable of assembling onto organic (polymer), inorganic (glass and mica), metallic (gold), and semi-conducting (silicon) materials without the need for any preliminary surface treatments. Additionally, the nature of the LbL assembly process enables deposition of the PEM coating onto substrates of most sizes and dimensions. Further analysis of the contact angles suggested that as PEM assembly proceeds, the PEM coating serves to mask the surface properties of the underlying substrate and convert them into the properties of the PEM coating itself. This was evident from the convergence of the water contact angles recorded across each substrate material following the deposition of four PAH/PSS bilayers. In terms of microarray development, these observations are significant as they indicate that it may be possible to exploit the PEM coating as a method to eliminate differences in surface properties on any platform, and therefore, generate more concordant cross-platform microarray datasets following a sample assay.

Analysis of the dye-labeled PAH fluorescence intensities in Figure 2.6 revealed that after the deposition of a sufficient number of PE layers, subsequent layers begin to deposit at equal densities onto different substrate materials, providing further evidence that the surface properties of different materials become similar as the PEM assembly proceeds. Although PAH is a component of the PEM system itself, the dye-labeled PAH can be considered a functionality on its own, as this compound serves to integrate fluorophores into the PEM and switch the outer functional groups from sulfonate to amine. Additionally, assembly of PAH onto the PSS-capped multilayer results in a charge inversion and a change in the surface energy, generating a surface which exhibits an entirely different functionality.

Because it was possible to assemble one functionality onto the surface of different materials with nearly identical results, the same may hold true for any functionality assembled onto these surfaces, including biomolecules such as DNA and protein. This assumption will be investigated in subsequent chapters of this thesis, where biomolecule functionalities will be patterned onto the PEM coating, alongside the PD coating, and used to perform complex multianalyte microarray assays on different platforms.

Chapter 3

Multianalyte Microarray Development

3.1 Introduction

In this chapter, the development and analysis of a multianalyte microarray application utilizing both DNA and protein compounds is described. The purpose of the experimental work was to establish the performance of the microarray design on the SI surface coatings versus conventionally used microarray platform surface coatings. Critical aspects regarding microarray fabrication, sample assay, and data analysis methodologies which influence performance parameters are reviewed in order to address current issues and obstacles with the development of microarray technology. In particular, platform-dependent variables which limit the extent of cross-platform comparability are identified and their impact upon microarray development is thoroughly discussed. Additionally, results of the experimental work described in this chapter will provide a baseline reference point to compare microarray fabrication and sample assay developments introduced in subsequent chapters of this thesis.

3.2 Materials and Methods

3.2.1 Materials

Poly-L-lysine (PLL, M_w = 150K-300K) and (3-aminopropyl)triethoxysilane (AS) were obtained from Sigma-Aldrich. Mouse IgG (IgG), goat anti-mouse IgG (whole molecule) antibody (anti-IgG), and bovine serum albumin (BSA) were obtained from Sigma-Aldrich. Human myoglobin (Myo) and mouse anti-human myoglobin antibody (anti-Myo) were obtained from Hytest Ltd. (Turku, Finland). All Cy3-labeled DNA probes and Cy5-labeled DNA targets were obtained from TIB MOLBIOL (Berlin, Germany). Cy3 monoreactive dye, Cy5 monoreactive dye, and PD-10 columns were obtained from GE Healthcare (Buckinghamshire, U.K.). All other chemicals and reagents were obtained from Sigma-Aldrich.

3.2.2 Substrate Preparation

AS- and PLL-coated glass platforms were prepared to serve as reference substrates. For this, glass substrates were rinsed with distilled water, then ethanol, and dried with a gentle steam of air. The glass substrates were then exposed to an oxygen plasma using an Oxford Instruments PlasmaLab 80Plus at 5sccm O_2, 40mTorr pressure, and 50W power for 2 minutes. The oxygen plasma treatment was used to increase the negative charge density of the glass surface and promote adhesion of the AS and PLL. Following oxygen plasma treatment, AS was deposited by incubating glass platforms in a 1% (v/v) solution of AS in ethanol for 10 minutes, while PLL was deposited by incubating in a 0.01% (w/v) solution of PLL in water for 10 minutes. After incubation in the AS and PLL solutions, the platforms were washed with 5 exchanges of water and dried using a slide centrifuge.

3.2.3 Labeling of Protein Compounds

The anti-IgG probe was conjugated with Cy3 according to the manufacturers instructions. Briefly, 1 mL of 0.1 M sodium carbonate buffer at pH 9.3 was added to 1 mg of anti-IgG to obtain a final concentration of 1 mg/mL. The anti-IgG solution was then added to a vial of Cy3 monoreactive dye, inverted several times for mixing, and allowed

to react for 30 min in the dark at room temperature. Following the reaction, the Cy3-labeled anti-IgG was separated from unconjugated dye and buffer exchanged into 1x PBS at pH 7.4 using a PD-10 column according to the manufacturers instructions. The same conjugation procedure was also used to label the anti-Myo probe with Cy3 and the IgG and Myo targets with Cy5.

3.3 Microarray Fabrication

Platform

The experimental design reported in this chapter utilizes a common microarray platform to enable the comparison of different surface coating types on the same platform. For this comparison, plain glass microscope slides were chosen as this substrate is known to be compatible with all the surface coatings investigated. Additionally, glass microscope slides are inexpensive and readily available.

Surface Coatings

The PEM and PD surface coatings were examined for their potential suitability for multianalyte microarray applications. Deposition of these SI surface coatings was described previously in Chapter 2. Additionally, AS- and PLL-coated glass slides were prepared to serve as references with which to compare assay performance on the SI surface coatings. AS and PLL were chosen as references since these surface coatings are commonly employed for the fabrication of both DNA and protein microarrays. Each of these coatings provide highly aminated surfaces and have been shown to be effective for the immobilization of DNA and protein compounds[21,22].

Probe Design

All probes used in this experimental design were labeled with Cy3 fluorescent dye in order allow performance comparisons between the surface coatings in terms of probe immobilization density and spot integrity. A total of four probe compounds were used in the array design: two DNA strands, designated DNA1P and DNA2P, and two proteins,

anti-Myo and anti-IgG. The DNA1P and DNA2P probes were both single-stranded oligonucleotides with the sequences 5'-TTATCATCTCTTATTACCTCTAA and 5'-T-TgTCTCTgCggTggTTggCATT, respectively. The use of multiple probes with such differing chemical natures was deliberately chosen in order to assess the compatibility of dissimilar probe/target pairs with each other and with each surface coating in a multianalyte assay format.

Probe Deposition

To generate a single array, the Cy3-labeled probe solutions were diluted to 2000nM in water and four replicate spots of each were deposited according to the layout shown in Figure 3.1. The probes were spotted using a Scienion AG sciFLEXARRAYER piezo-dispenser, which prints small droplets at a volume of around 500pL. Four replicate spots were utilized to enabled the calculation of mean fluorescence signals with SDs so that intra- and inter-platform performance variability could be determined.
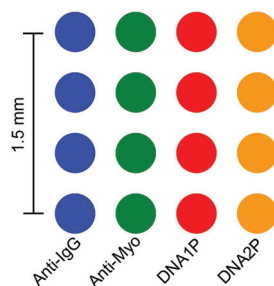
FIGURE 3.1: Layout of the printed microarrays used in the multianalyte assay design. Four replicates of each Cy3-labeled probe compound (Anti-IgG, Anti-Myo, DNA1P, and DNA2P) were spotted at a concentration of 2000 nM with a spacing of 500 μm between spots.

Platform Washing

Following probe deposition, it is typically required to wash the microarray platform surface in order to remove unbound or loosely bound probes which could interfere with subsequent steps of the sample assay procedure. This is generally done with a buffer solution containing surfactant. Here, the microarray platforms were washed in PBS containing 0.05% Tween 20 (PBST) at a pH of 7.4. Washing was performed manually by plunging the printing microarrays into a beaker containing PBST and wafting the

platforms back and forth for approximately 10 seconds. The platforms were then allowed to sit in the PBST solution for 10 minutes prior to blocking.

Platform Blocking

Blocking is a critical step when performing sample assays on microarray platforms. Generally, microarray platforms are designed to promote the immobilization of biomolecular probes at a high density in order to provide a large number of localized receptor sites for target compounds in a sample. Following probe deposition, however, the opposite is desirable: a surface which minimizes the adsorption, or nonspecific binding (NSB), of biomolecular target compounds in a sample. NSB of target compounds can have profound negative effects on microarray performance. For example, surfaces which exhibit high levels of target NSB will generate an elevated background fluorescence and reduce the signal to noise (S/N) ratio. Furthermore, surfaces which exhibit high NSB with target compounds can capture them from the sample before they have the opportunity to find and bind with their respective probe partner.

To minimize problems associated with NSB, a compound which exhibits low affinity with the target analyte is typically adsorbed onto the microarray surface prior to the sample assay. For a single analyte assay, this is simply a matter of blocking the surface with a compound which is known to minimize NSB of the target of interest. In the case of multianalyte assays, however, the process becomes much more complex as dissimilar targets will exhibit different chemical natures, resulting in differential NSB depending on the targets themselves and the chemical properties of the platform surface. In other words, a surface which blocks relatively well against the adsorption of one target may actually increase the adsorption of other targets, and vice versa. This differential target NSB represents a significant obstacle with the development of higher complexity multianalyte microarray platforms.

Here, microarray platforms were blocked in PBS containing 2% BSA for 30 minutes. BSA is commonly used to block surfaces for protein microarray applications and has also been shown to be effective at reducing NSB of nucleic acid targets[21,70]. After blocking in BSA for 30 minutes, the microarrays were again washed in PBST to remove excess BSA, then briefly rinsed with water and dried using a slide centrifuge.

3.4 Multianalyte Assay Design

Target Analytes

All target compounds were labeled with Cy5 fluorescent dye to enable characterization of assay performance in terms of target response and NSB. The target and probe compounds were labeled with different dyes so that analysis of the targets could be carried out separately from the probes. Two DNA targets, designated DNA1T and DNA2T, and two protein targets, mouse IgG (IgG) and human myoglobin (Myo), were used to perform sample assays. The two DNA targets were single-stranded DNA oligonucleotides complementary to the spotted DNA probes, while the two protein targets, IgG and Myo, specifically bind with the anti-IgG and anti-Myo probes. IgG was used as a model protein compound while Myo (pI 7.1) is a commonly used cardiac marker[71].

Sample Compositions

Microarray performance in a single analyte format was investigated using single target sample solutions. Specifically, samples containing only one target compound at a concentration of 100nM were prepared in a solution of PBS containing 2% BSA. In addition to blocking, BSA is commonly used as an additive in target sample solutions as it has been shown to reduce NSB of many target analytes to the microarray platform. NSB is reduced due to the presence of another compound which competes with the target for adsorption onto the platform surface. Normally, the BSA is introduced at a higher concentration relative to other analytes so competition favors adsorption of BSA over the target compounds.

To investigate microarray performance in a multianalyte format, another sample was prepared which contained a mixture of all four targets, each at a concentration of 100nM. The mixed target sample was used to examine the compatibility of the four probe/targets pairs with each other in a mulitanalyte format and determine whether the compatibility of the probe/target pairs is influenced by the surface properties of the platform. Furthermore, a blank sample was prepared which contained no target compounds to serve as a negative control.

Sample Assays

In order to perform sample assays, each microarray platform was fitted with hybridization chambers to isolate each array from its neighbors and prevent the mixing of target samples during the assay. Each array was then exposed to 100μL of a sample solution for a 30 minute incubation period. Following the incubation period, the platforms were washed with PBST, given a brief rinse with water, and dried using a slide centrifuge.

3.5   Microarray Assay Analysis

Fluorescence intensities were measured by scanning the microarray platforms with a Perkin Elmer ScanArray G_x. Each platform was scanned at a fixed LP and PMT setting so that the fluorescence signals could be directly compared between platforms.

Photomultiplier Tube Calibration

Prior to scanning, the PMT setting was adjusted to achieve the largest possible signal response without obtaining any saturated signals. For this, each platform was given a preliminary scan using a LP of 100% and the minimum PMT setting of 35% to identify the largest fluorescent signal across all the platforms. Once the largest signal was identified, the PMT setting was adjusted until it was just below saturation. The calibration procedure was performed at wavelengths of 543nm and 633nm to excite the Cy3-labeled probes and the Cy5-labeled targets, respectively. The calibrated PMT settings found were 50% at 543nm and 55% at 633nm.

Fluorescence Scans

Following PMT adjustment, each platform was rescanned at both wavelengths using a LP of 100% and the selected PMT settings. The microarray images obtained from these scans are shown in Figure 3.2. The images in the upper block represent the probe fluorescence signals obtained by exciting the Cy3 fluorophores at 543nm, while the images in the lower block represent the target fluorescence signals obtained by exciting the Cy5 fluorophores at 633nm. The images are further sorted by surface coating (rows)
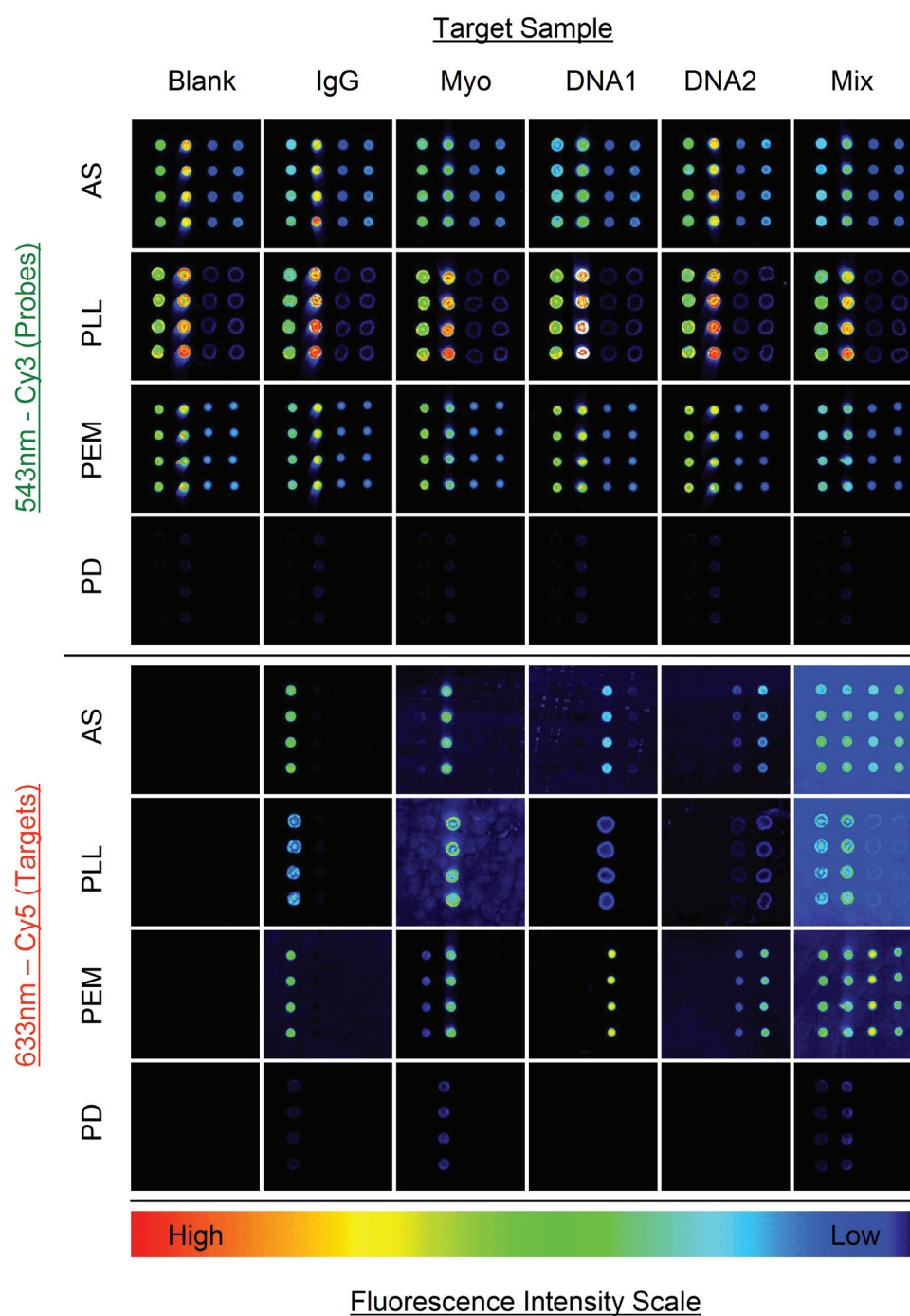
FIGURE 3.2: Fluorescent images used to characterize the microarray assay performance. Images in the upper block represent arrays scanned using a wavelength of 543nm to visualize the immobilized Cy3-labeled probes, while images in the lower block represent arrays scanned using a wavelength of 633nm to visualize the bound Cy5-labeled targets. The array images are further sorted by the target sample solution to which they were exposed (columns) and the surface coating onto which the arrays were printed (rows). The fluorescence intensity scale (rainbow bar) is provided below the image sets for comparison of the fluorescence signals generated by each array.

and target sample (columns). Using the rainbow color palette shown at the bottom of Figure 3.2, the fluorescence intensities can be compared between images, where red indicates high fluorescence intensities and blue indicates low. These images were utilized to generate all data sets used to characterize the mutlianalyte assay performance.

Interpretation of Fluorescence Intensities

When analyzing the images in Figure 3.2, it should be noted that the absolute number of probe and target molecules within a given spot cannot be determined from the measured fluorescence signals because the fluorescent-dye labeling and emission efficiency is unknown. For example, in the upper left image of Figure 3.2, which represents the 543nm-excited fluorescence from an array exposed to the blank sample on the AS-coated platform, the fluorescence intensity of the antibody probes is significantly higher than that of the DNA probes, suggesting that the antibody probes are at a higher density. However, differences in the labeling efficiency between the probe compounds may have resulted in antibody probes which possess significantly more fluorophores per molecule than the DNA probes, thereby producing higher fluorescence intensities for the antibody probes even when immobilized at a lower density than the DNA probes. In fact, a higher labeling efficiency with the antibody probes in comparison to the DNA probes is a likely scenario given that they are much larger and possess more amine functional groups available for reaction with the Cy dyes.

Despite the larger fluorescence intensities produced by the antibody probes, though, it is more likely that the density of the DNA probes is higher than the density of antibody probes due to size issues. Because the size of the antibody probes are much larger in comparison to the DNA probes, each antibody probe requires more surface area, meaning fewer molecules can fit into the same area. However, a higher DNA density is not necessarily true, assuming that the surface has a much higher affinity for the antibody probes than the DNA probes. This situation turned out to be the case on the PD coating, where no DNA probe could be detected, indicating that the PD coating has a very low affinity for the DNA probes used.

Although the absolute density of the probes and targets cannot be determined from the fluorescence images in Figure 3.2, it is possible to compare the relative densities between platforms. For example, looking at the arrays exposed to the DNA1 target in

the lower image block (633nm, Cy5 channel), the largest signal intensities are observed on the PEM-coated platform, followed by the AS, then PLL, and finally PD, which shows no presence of bound DNA1 target. While the exact number of bound DNA1T on each platform is unknown, it can be said that the PEM coating bound more DNA1 targets than did the other platforms. This ability to characterize the relative amounts of probe and target between each platform enables the comparison of performance parameters such as probe immobilization density, target response, binding affinity, specificity, NSB, and S/N.

Image Analysis

Analysis of each spot in Figure 3.2 was performed using the software package ScanArray Express by Perkin Elmer. The software analyzes spots based on a user defined template which provides the placement and layout of the arrays. Here, analysis was performed using an adaptive circle method. The adaptive circle method uses an algorithm to first identify each spot and then adjusts the spot diameter to match the size of the spot. The mean spot intensity and background intensity is then quantified individually for each spot identified. Figure 3.3 provides an illustration showing how the software defines the region to calculate both the signal (green region) and background (red region) intensity. The mean spot intensity is obtained by averaging the intensities of each pixel within the spot circle. Similarly, the mean background intensity is obtained by averaging the intensities of each pixel inside an annulus of a defined outer and inner diameter outside of the spot.
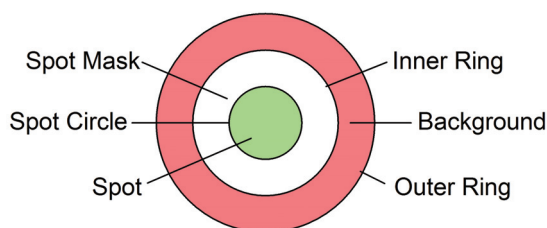
FIGURE 3.3: Illustration depicting the regions used by the analysis software from which to calculate the spot signal intensities and spot background intensities from the images shown in Figure 3.2. The spot signal intensity is defined as the mean of the intensities of each pixel within the spot circle (green region), while the spot background intensity is defined as the mean of the intensities of each pixel within a ring outside the spot circle (red region).

3.6 Multianalyte Assay Performance Characterization

Following analysis of the images in Figure 3.2, characterization of microarray performance on each surface coating was carried out using the signal intensities, background intensities, and background intensity SDs, plotted in Figure 3.4. It should be noted that only two variables were introduced into the experimental design: surface coatings and target samples. All other experimental factors (i.e. microarray fabrication, assay protocol and data analysis) were constant, and can thus be considered standardized for this analysis. Therefore, comparisons made and conclusions drawn throughout this chapter are in the context of performance differences due to the surface coatings and/or target samples.

Each datapoint in Figure 3.4 was obtained by averaging the values of the four replicate spots within an array for a given probe/target pair to obtain a mean value and SD. For example, the leftmost □ datapoint in Figure 3.4A represents the mean probe signal intensity (543nm, Cy3 channel) obtained from the four replicate Cy3-labeled DNA1 spots on the AS-coated glass platform exposed to the blank sample. Similarly, the leftmost □, □, and □ datapoints represent the mean probe signal intensities of the Cy3-labeled DNA2, anti-IgG, and anti-Myo probes within that same array, respectively. For visual comparison, the array from which these first four datapoints were calculated can be seen in the upper left image in Figure 3.2. The second group of four colored datapoints from the left in Figure 3.4A represent the mean probe signal intensities obtained on the array exposed to the sample containing 100nM of Cy5-labeled DNA1 target, and so forth. Moving down to Figures 3.4B and C, the probe background intensity and probe background intensity SD corresponding to each data point shown in Figure 3.4A are also plotted.

The graphs shown in the right column (633nm, Cy5 channel) of Figure 3.4 correspond to the graphs in the left column, except that here each datapoint represents the fluorescence intensities of the Cy5-labeled targets. For example, the first set of colored datapoints (□, □, □, and □) in Figure 3.4D represent the target signal responses generated on the array exposed to the blank sample on the AS-coated platform. In this case, each probe generated a fluorescence signal close to zero, which was an expected result as no target compounds were present in the sample solution. The array exposed to the target sample containing 100nm of Cy5-labeled DNA1 target, on the other hand,
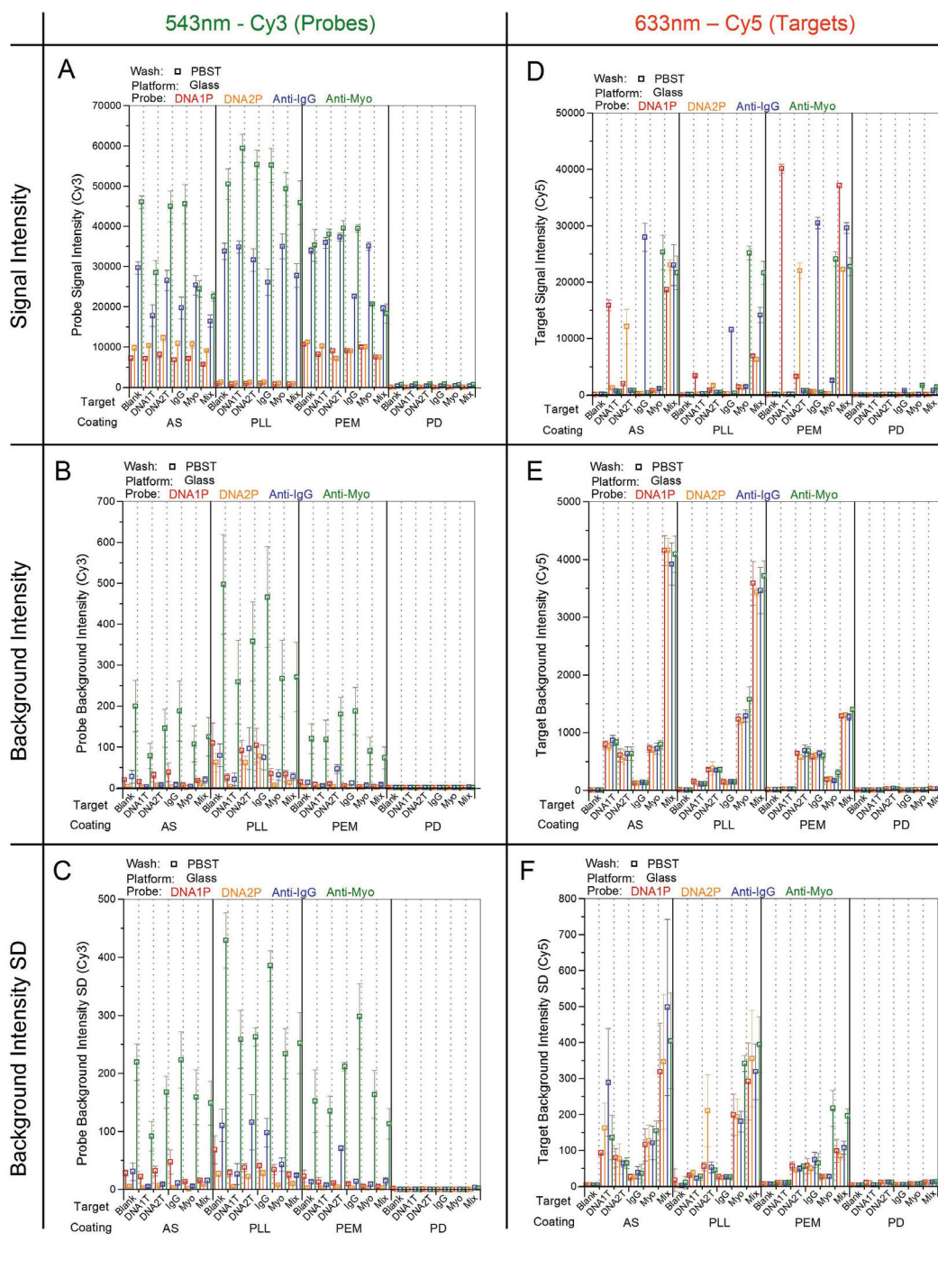
FIGURE 3.4: Total dataset obtained from the analysis of the images in Figure 3.2. Graphs A-C (left column) represent the probe data, while graphs D-F (right column) represent the target data. The probe and target datasets are further sorted (rows) by fluorescence signal intensity, background intensity, and background intensity SD. Each datapoint within a graph represents the mean of the four replicates of a specific probe spot within an array. The probe compounds are color coded for quick reference: DNA1P, DNA2P, Anti-IgG, Anti-Myo

generated a mean intensity value of 15000 on the DNA1 probe spots, as shown by the second □ datapoint from the left in Figure 3.4D, while relatively low signal intensities were generated on the three other probe compounds (DNA2P, anti-IgG, and anti-myo) which were not specific to the DNA1 target.

It should be noted that Figure 3.4 represents the entire dataset used to analyze microarray performance throughout this chapter. Because the dataset shown in Figure 3.4 is so large, each graph will be systematically broken down into smaller pieces to extract meaningful information and simplify interpretation in terms of platform performance and dataset comparability.

3.6.1   Probe Characterization

3.6.1.1   Probe Signal Intensity

In order to generate a target response on a microarray platform, it must be possible to deposit capture molecules (probes) onto its surface. Ideally, the surface should be capable of immobilizing a high density of active probe molecules in order to provide a large number of binding sites for target compounds present in a given sample solution. Here, the probe immobilization densities are investigated on each surface coating using the signal intensities which were plotted in Figure 3.4A.

As explained in Section 3.5, it is impossible to determine the absolute probe density from the measured fluorescence intensities because the labeling efficiency of the Cy3 fluorescent dye is unknown. Furthermore, because labeling efficiencies are typically different with dissimilar compounds, it is impossible to compare the relative immobilization density between different probes. It is possible, however, to compare the relative immobilization density of the same probe on different surface coatings to determine which coating provides the highest immobilization density for that specific probe.

The probe signal intensities of each probe compound were obtained by averaging the signal intensities of 24 probe replicates (4 spots per array × 6 arrays per platform = 24 replicates). For example, the first □ data point on the left in Figure 3.5 represents the mean DNA1 probe signal intensity calculated by averaging the fluorescence intensities of 24 spot replicates printed onto the AS-coated platform. This mean value is grouped with

the mean DNA1 probe signal intensities obtained on the other surface coatings in order to compare the relative immobilization density of the DNA1 probe on each coating.
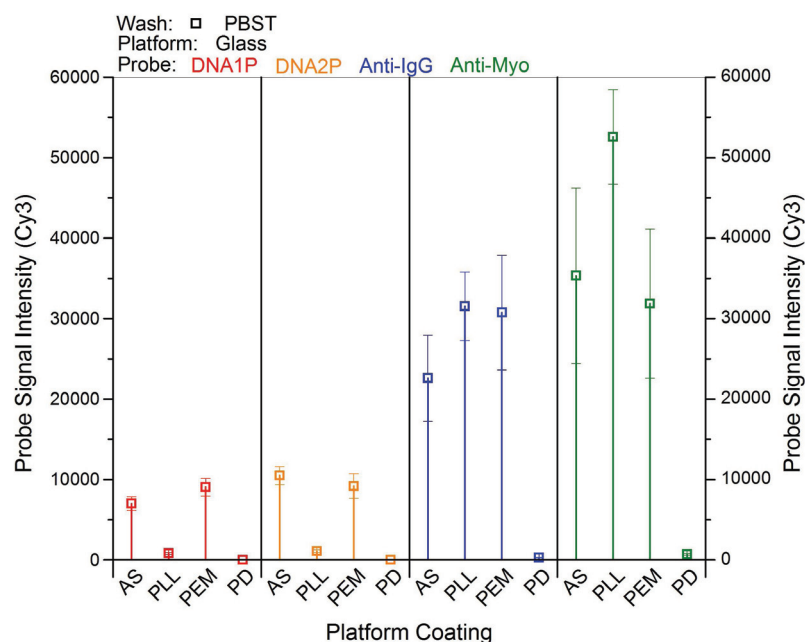
FIGURE 3.5: Probe signal intensities generated on each surface coating. Each datapoint was obtained from the mean of 24 Cy3-labeled probe replicates (4 spots per array × 6 arrays per platform = 24 replicates). Datapoints are grouped by probe compound then sorted by surface coating to compare the relative immobilization density of each probe on each surface coating.

In Figure 3.5, the DNA1 probe shows the highest immobilization density on the PEM coating followed by the AS coating, which provides an immobilization density of around 80% of that obtained on the PEM coating. In comparison, the PLL coating shows a rather low immobilization density of the DNA1 probe while PD shows virtually none, illustrating how the same probe compound will typically immobilize at different densities on platforms exhibiting dissimilar surface properties. These differences in probe immobilization density represent the first example of a platform-dependent source of discordance which serves to limit the extent of comparability between assay datasets obtained on different platforms.

Similar immobilization density trends on each surface coating were observed with the DNA2 probe, except in this case, the AS coating showed a slightly higher immobilization density than the PEM coating. This observation demonstrates how the relative immobilization density between different probes (i.e. DNA1P and DNA2P) can change depending on the surface properties of the platform used. In this case, the PEM coating

is better suited for the immobilization of the DNA1 probe whereas the AS coating is better suited for the DNA2 probe.

Based on these differential probe immobilization densities observed between each platform, it can be concluded that the density at which a probe immobilizes onto a surface is dependent upon the chemical properties of both the probe and the platform surface. Therefore, it can be difficult to predict how the inclusion of new probe compounds will perform relative to established probes on a given microarray platform. Furthermore, it will be even more complicated to predict how each probe in a given microarray application will perform if attempting to transfer them onto a newly developed platform. Because microarray platforms are rapidly evolving in terms of design and surface chemistry, the transferability of established probes may not be possible in many cases, introducing another obstacle which limits the extent of cross-platform comparability and the rate of developmental progress, even when standardized probes, assay methodologies, and analysis methods are utilized.

Considering now the protein probes in Figure 3.5, both the anti-IgG and the anti-Myo exhibited the highest immobilization densities on the PLL coating, with the AS and PEM coatings not much lower. The PD coating showed very poor protein probe immobilization densities, as it did with the DNA probes, indicating that this surface coating may not be suitable for either DNA or protein microarray applications. Overall, the AS and PEM coatings performed relatively well with all 4 probe compounds, indicating that these surfaces may be suitable for single analyte assays using either DNA or protein probes, and possibly even multianalyte assays which utilize both. In regard to the antibody probes, the PLL coating showed the highest immobilization densities, suggesting that this surface may provide the highest performance in terms of target response signals for protein microarray applications. However, because the immobilization density of the DNA probes was rather low, the PLL coating may not be the most suitable for DNA microarray applications in comparison to the AS and PEM coatings.

3.6.1.2   Probe Background Intensity

The probe background intensities and background intensity SDs were used to investigate the spot integrity of each probe compound on the different surface coatings. Mean values of these two parameters were calculated from 24 replicate spots in the same manner

used to calculate the mean probe signal intensities in Figure 3.5, as described in Section 3.6.1.1. The values obtained from this analysis are shown in Figures3.6A and B.
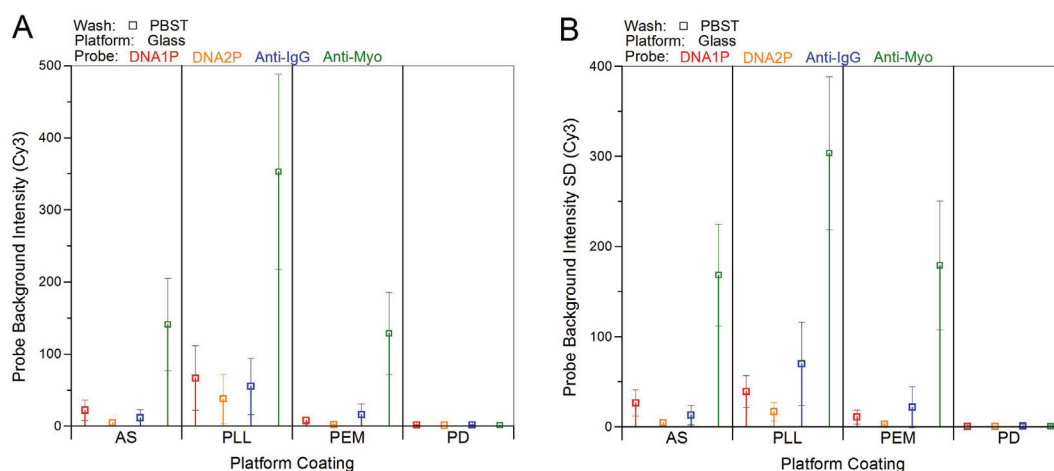
FIGURE 3.6: Probe background intensity (graph A) and probe background intensity SD (graph B) generated on each surface coating. Each datapoint was obtained from the same 24 probe replicates used to generate the probe signal intensity datapoints plotted in Figure 3.5. The datapoints are first grouped by surface coating and then probe compound to compare the background intensity and background intensity SD between each surface coating.

It should be noted that the SDs plotted in Figure 3.6B do not derive from the SD bars shown in Figure 3.6A, which represent the SD of the mean background intensities between the 24 probe replicates (interspot background SD). Rather, the SDs plotted in Figure 3.6B represent the mean SD of the background intensities around an individual spot (intraspot background SD). As explained in Section 3.5, the analysis software calculates the local background intensity around an individual spot by averaging the intensities of each pixel within a ring around that spot, as illustrated in Figure 3.3, thus allowing for the determination of intraspot background and background SD.

Ideally, probe molecules are confined within the spot circle as defined by the analysis software. Assuming this is the case, the expected result would show a background intensity equal to the intrinsic background produced by the microarray platform itself, indicating that no Cy3-labeled probes are present outside the spot circle. Additionally, the background intensity around different probe compounds (i.e. DNA1 and anti-IgG) would be equivalent on the same platform. This, however, was not the observed result seen in Figure 3.6A. For example, the AS-coated platform generated significantly different background intensities around each probe compound, as shown by the leftmost set

of four colored datapoints (□, □, □, and □). In particular, the anti-Myo probe showed an exceptionally high background intensity compared to the other 3 probe compounds. Similarly high anti-IgG probe background intensities were also observed on the PLL and PEM surface coatings. The PD coating, on the other hand, produced virtually no background fluorescence intensity around any probe compound. In the case of the PD coating, however, this was an expected result, since this coating showed low levels of probe immobilization in general, as determined from Figure 3.5.

The differential probe background intensities observed in Figure 3.6A are an indication of probe spot streaking, which may have occurred during microarray fabrication. Specifically, the wash step performed after probe spotting may have caused unbound or loosely bound probes on the surface to desorb and then quickly readsorb outside the spot circle as defined by the analysis software. This occurrence is a common problem encountered during microarray fabrication and is often referred to as "comet tails" in the literature, due to the visual resemblance when observed on fluorescence scan images.

Comet tails can have profound negative effects upon microarray performance by introducing target receptor sites outside the probe spot circle. During the sample assay, fluorescent dye-labeled targets will specifically bind to these receptors outside the spot circle, causing a higher background intensity. Additionally, because the target compounds are presented with receptor sites outside the spot circle, the target response due to specific binding between the probe and target will be diffused over a larger area, which in turn reduces the theoretical detection limit.

Another drawback created by comet tails is that they typically streak in one direction, resulting in high background intensities on one side of the spot, but not the other. This creates a non-uniform background intensity which then translates into a higher background intensity SD. When comparing Figures 3.6A and B, probes which produced higher background intensities correlated with probes which produced higher background intensity SDs. This correlation is further indication that that the different levels of background intensity between different probes is due to the presence of comet tails, with some probes, in particular anti-Myo, streaking more than others.

Source of Probe Background Intensity

To confirm whether comet tail formation occurred during microarray fabrication, each platform was rescanned at the maximum PMT setting of 100% in order to increase the fluorescence sensitivity. Figure 3.7 shows images of microarrays printed onto each surface coating and scanned using the maximum PMT. For comparison, the original images which were obtained at a PMT setting of 45% are also shown.
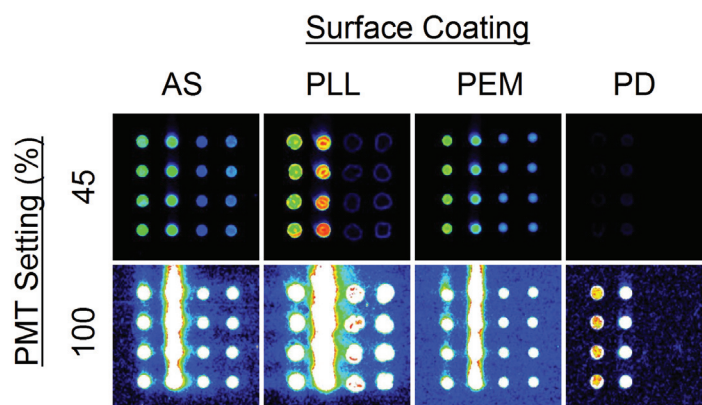
FIGURE 3.7: Evidence of probe streaking. The fluorescent images depict typical arrays printed onto each surface coating (columns) and scanned using a wavelength of 543nm at a PMT setting of 45% (top row) and 100% (bottom row). Images scanned at the higher PMT setting reveal significant probe streaking, or comet tails, on each coating.

In Figure 3.7, the presence of comet tails cannot be seen in the images scanned using a PMT setting of 45%. However, significant streaking of probes is revealed when scanned at a PMT setting of 100%, verifying that the presence of comet tails on the surface and explaining the differences in background intensity and background intensity SDs observed in Figures 3.6A and B, respectively. Additionally, looking at the image of the PD coating scanned at a PMT setting of 100%, some extent of antibody probe immobilization is seen. However, there is no presence of either DNA probe, providing further indication that this SI surface coating may not be compatible with DNA microarray applications.

3.6.2 Target Characterization

Using the images shown in the lower block of Figure 3.2, binding of the Cy5-labeled targets onto the microarray platform surfaces were analyzed to determine the performance of each coating in terms of target response, probe specificity, NSB, and S/N.

Additionally, the effect of the sample composition on these assay performance parameters were assessed by comparing the intensity values obtained from samples containing a single target versus multiple targets. Also, using the probe intensities examined earlier and target intensities examined here, it is possible to determine whether the platforms' surface properties have an impact upon the binding affinity between the probe/target pairs tested.

3.6.2.1 Target Signal Intensity

The target responses on each platform were compared using the datapoints plotted in Figure 3.4D, which represent the mean target signal intensity generated by Cy5-labeled targets bound to the four replicate probe spots within an array. These datapoints were grouped by the target sample solution to generate Figure 3.8. Graphs A-D in Figure 3.8 represent the Cy5 fluorescence signal intensities generated by the single target sample solutions containing 100nM of DNA1T, DNA2T, IgG, or Myo, respectively. Graph E represents the signal intensities generated by a mixed target sample containing 100nM of each target, and graph F represents those generated by a blank sample containing no targets.

Figure 3.8A shows the target responses generated on each surface coating after 30 minutes exposure to a sample containing 100nM of Cy5-labeled DNA1T. In this case, fluorescence signals were generated by the DNA1 probe spots (□ datapoints) on the AS, PLL, and PEM coating, indicating a specific and detectable interaction between the DNA1 probe/target pair on these surfaces. Similarly, specific fluorescence signals were also observed with the other single target samples (DNA2T, IgG, and Myo), as shown in graphs B-D. In most cases, each target generates a fluorescence signal only on its probe partner, and not on the other three probes within the array.

In a single analyte format, the largest fluorescence responses for both DNA targets and the IgG target was observed on the PEM coating, followed by the AS coating, and then the PLL coating, as shown in Figures 3.8A, B, and C. In regard to the Myo target, whose target response is shown in Figure 3.8D, the fluorescence intensities were significantly different to those observed in Figures3.8A-C. Specifically, the AS coating slightly outperformed the PLL which slightly outperformed the PEM. The poorest performing surface in terms of target signal response was the PD coating, which did not generate
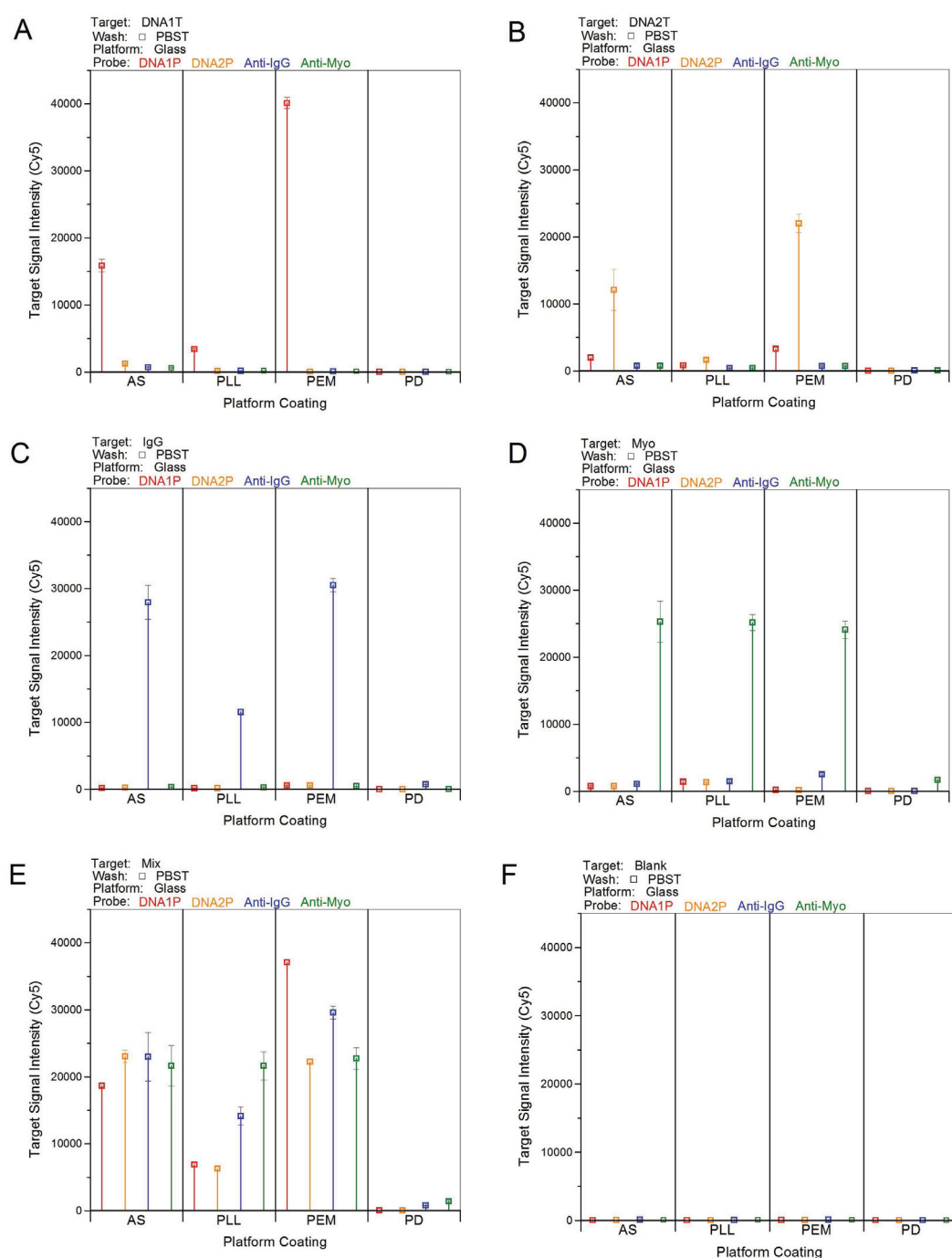
FIGURE 3.8: Target signal intensities generated by each target sample solution. Graphs A-D represent the target responses generated by the 100nM Cy5-labeled single target samples DNA1T, DNA2T, IgG, and Myo, respectively; graph E represents the target responses generated by the mixed sample containing 100nM of each Cy5-labeled target; and graph F represents the target responses generated by a blank sample containing no target compounds. Each datapoint was obtained from the mean signal intensity of the four probe replicates within an array exposed to the respective target sample solution. Within each graph, the datapoints are grouped by surface coating to compare the specific and nonspecific interaction of each target with each probe.

any detectable fluorescence intensities for either DNA target and relatively small fluorescence intensities with both protein targets, IgG and Myo. This was an expected result, however, as the probe immobilization densities were relatively low on the PD coating, as shown by the probe fluorescence intensities in Figure 3.5 and the images in Figure 3.7.

When analyzing assay performance in a multianalyte format, the PEM coating generated the largest overall target fluorescence responses when utilizing the mixed target sample, as shown in Figure 3.8E. Also, the performance of the AS coating in a multianalyte format was relatively good in comparison to the PEM, with the exception of the DNA1 target, which generated a considerably lower fluorescence response on the AS coating. The PLL and PD coatings, on the other hand, performed rather poorly with this multianalyte format, generating significantly lower target responses in comparison to the AS and PEM coatings.

Although the PEM coating provided the highest performance in terms of target signal response in this multianalyte design, it should be noted that other aspects of assay performance, such as specificity and NSB, may be highly influential upon the overall performance. Therefore, thorough analysis of these additional aspects must be taken into consideration before definitive conclusions can be made regarding the overall analytical performance of each surface coating with this particular application.

In terms of cross-platform comparability, Figure 3.8 reveals a significant limitation regarding the ability to integrate a common cross-platform reference. For example, because all probes were spotted at the same concentration on each platform and underwent identical post processing steps such as washing, blocking, and sample assay, a common reference could be defined as the ratio of the DNA1 to DNA2 target signal intensities when exposed to a reference solution, such as the mixed target sample. In this case, the AS coating generated a DNA1/DNA2 signal ratio of 0.8, calculated from the intensity values plotted in Figure 3.8E. Therefore, it would be expected to see a similar DNA1/DNA2 ratio on the PLL and PEM coating in order to validate the datasets obtained on those platforms. However, the DNA1/DNA2 ratios generated on the PLL and PEM coatings were significantly different to that obtained on the AS coating. Specifically, the PLL coating generated a DNA1/DNA2 ratio of 1.1, while the PEM coating

generated a ratio of 1.7. Furthermore, the target signal intensity ratios generated between any combination of probe/target pairs are significantly different from platform to platform, indicating that it may be impossible to define an accurate cross-platform reference in this assay design. This inability to integrate a common cross-platform reference represents perhaps the most significant limitation in terms of cross-platform microarray comparability and dataset validation.

3.6.2.2 Target Specificity

Ideally, an immobilized probe interacts only with its target partner and not with other analytes present in a sample. A probe which interacts with other analytes can lead to a false negative or false positive reading during assay analysis. A false negative could occur if a sample constituent interacts with a probe or a target in such a manner that it prevents or inhibits specific binding between a probe/target pair. Alternatively, interaction between a labeled target and a probe which is specific to a different target could result in a false positive. Therefore, specificity between probes and targets is a critical parameter to consider when developing multianalyte microarrays.

In this section, specificity between the probes and targets is analyzed using the fluorescence intensities plotted in Figures 3.8A-D, which represented the target signal intensities obtained on each probe compound using single target sample solutions. For example, further analysis of Figure 3.8A reveals that almost no fluorescence signal was generated by the Cy5-labeled DNA1T on the DNA2, Anti-IgG, or Anti-Myo probes, indicating that the DNA1 target is highly specific with its binding partner and not the other probes used in the microarray design. The Cy5-labeled DNA2 target, on the other hand, generated a significant fluorescence signal on the DNA1 probe spots on both the AS and PEM coatings, as shown in Figure 3.8B. This observation suggests that there may be cross-reactivity between the DNA1 probe and the DNA2 target on these surfaces. Ultimately, this cross-reactivity can have profound negative effects upon assay analysis, possibly resulting in a false positive detection of the DNA1 target even if it is not present in the sample solution.

Cross-reactivity is also observed in Figure 3.8D, which represents the target signal intensities generated by the Cy5-labeled Myo. Here, a significant fluorescence signal was generated on the anti-IgG probe spots on the PEM coating, indicating cross-reactivity

between the anti-IgG probe and the Myo target. It should be noted, though, that the same cross-reactivity was not observed on the AS or PLL coating, suggesting that this interaction between the anti-IgG probe and the Myo target may be an adverse effect generated specifically by the PEM coating. For instance, it is possible that the surface properties of the PEM coating may induce a change in the orientation or conformation of the anti-IgG probe which results in a higher affinity between it and the Myo target. Although the exact mechanism is unknown, this specificity change appears to be influenced by the surface properties of the microarray platform, as the platforms' surface properties represent the only variable in this case. This platform-dependent change in specificity represents another source of cross-platform discordance which limits the extent of comparability between datasets obtained on different microarray platforms.

The platform-dependent change in specificity between the anti-IgG probe and Myo target also raises the issue that a performance compromise must be made based on the desired application and end goal. For example, in some applications it may be desirable to utilize the PEM coating as it provides the best overall performance in terms of target signal response in a multianalyte format. However, utilization of the PEM coating may induce an unwanted cross-reactivity between the anti-IgG and the Myo, which is not observed on the other coatings. Alternatively, it may be desirable to minimize this cross-reactivity, in which case, the AS coating would be the better choice. Utilization of the AS coating, however, means that performance will be lost in regard to the DNA1 target response.

3.6.2.3 Probe/Target Affinity

Further analysis within and between the graphs in Figure 3.8 reveals some interesting and unexpected observations in terms of the relative target signal intensities obtained between different probes and surface coatings. For example, in reference to Figure 3.5, it was shown that the PLL surface immobilized the highest density of the anti-IgG probe relative to the other coatings. Based on that result, it was predicted that the PLL coating would provide the largest target response when exposed to the Cy5-labeled IgG. As shown in Figure 3.8C, however, the IgG target signal response generated on the PLL surface was significantly lower in comparison to the response obtained on the AS and PEM coatings. This result indicates that the binding affinity between anti-IgG and IgG

changes depending on the surface properties of the platform used. Specifically, the anti-IgG/IgG pair affinity on the PLL coating is significantly reduced in comparison to the affinities observed on the AS and PEM coatings. This change in probe affinity is more than likely caused by differences in the probe orientation and/or conformation between platforms.

A more detailed comparison of the binding affinity between the probes and targets on each surface coatings is presented in Figure 3.9. The datapoints in Figure 3.9 were obtained using the ratio of the target signal intensity (Cy5) to probe signal intensity (Cy3) between a specific probe/target pair within a microarray exposed to a given sample. For example, the first □ datapoint on the left was generated by averaging the Cy5/Cy3 signal intensity ratios of the four replicate DNA1 probe spots on the AS coating which were exposed to a single target sample containing 100nM of the DNA1 target. Similarly, the first ⊠ datapoint on the left, slightly above the □ datapoint, represents the Cy5/Cy3 signal intensity generated by the DNA1 probes on the AS coating following exposure to the mixed target sample solution containing 100nM of all four target compounds. These two datapoints were overlaid to determine whether the sample composition has any effect upon the probe/target affinities.

As shown by the ⊠ datapoints, which represent the affinity of the DNA1 probe/target pair with the mixed target sample, differences in affinity are observed depending on the surface coating used. Specifically, the PLL and PEM coating both generated an affinity value near 5, whereas the AS coating generated an affinity value of only 2.5. This result indicates that the surface properties of the AS-coated platform act to reduce the affinity of the DNA1 probe/target pair more so than the PLL and PEM-coated platforms. Also, it should be noted that the PLL coating provided the highest affinity for the DNA1 probe/target pair. However, as shown earlier in Figures 3.5 and 3.8, the PLL coating performed relatively poorly in comparison to the AS and PEM coated platforms in terms of probe immobilization density and target response with the DNA1 target/probe pair, respectively. This observation exemplifies a situation where a particular surface coating provides high performance for one assay performance parameter but low performance for other parameters. This situation represents another scenario where a compromise may need to be made depending on the desired application and end goal. For instance, if all three performance parameters (probe density, target response, and target/probe affinity) are of importance for the development of a microarray assay incorporating the
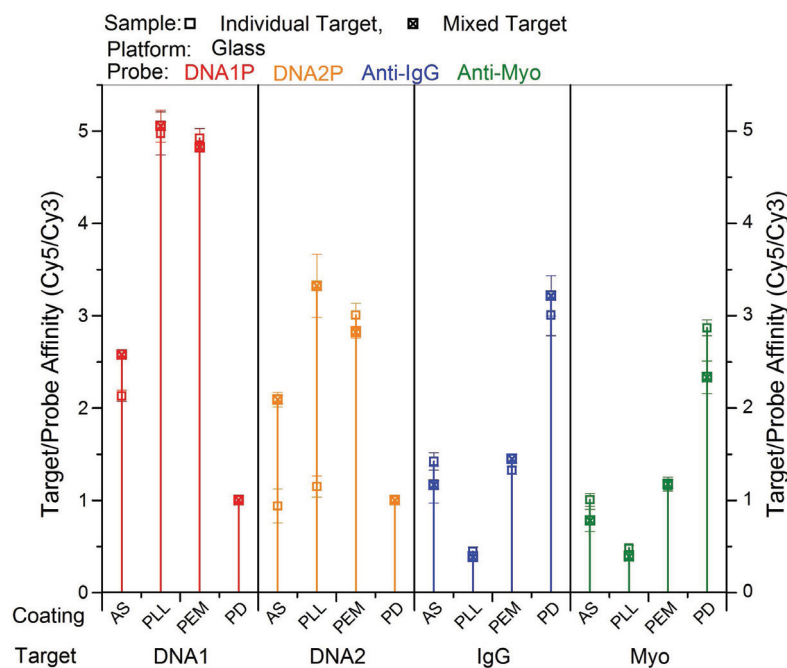
FIGURE 3.9: Probe/target affinities generated on each surface coating. The affinity of each probe/target pair was calculated using the ratio of the target signal intensity to the probe signal intensity (Cy5/Cy3). Each datapoint represents the mean of the of the four replicate probe spots within an array exposed to their respective target sample solution. Additionally, the affinities generated when utilizing the single target samples (□ datapoints) are overlaid onto the affinities generated when utilizing the mixed target sample (⊠ datapoints) to compare the effect of sample composition on the affinity of each probe/target pair.

DNA1 probe/target pair, then the PEM coating would probably be the best choice, as it provided relatively high performances for each of those parameters. However, this may not always be the case for other probe/target pairs, since different probes and targets will interact differentially with each other on dissimilar platforms.

When comparing between different surface coatings in Figure 3.9, similar affinity changes are observed between the DNA1 and DNA2 probe/target pairs. However, the DNA2 pair exhibited lower overall affinities on each coating relative to DNA1 pair, illustrating how different DNA probes can exhibit higher or lower affinities depending on their sequence, or probe design. Considering now the protein probe/target pairs in Figure 3.9, IgG and Myo also showed differential affinities depending on the surface coating. In this case, however, the highest IgG and Myo affinities were observed on the PD coating, which produced an affinity value of about 3, whereas the AS and PEM coatings produced values closer to 1. Interestingly, the PLL coating generated the lowest

affinities for the protein compounds, which is in stark contrast with the DNA affinities, which were highest on the PLL coating.

In terms of multianalyte assay development, these differential cross-platform affinities introduce more platform-dependent variables which must be considered when trying to define which surface is most ideal for a specific application. Because different applications have different end goals, the ideal surface will ultimately vary. Therefore, it can never be said which microarray surface coating is "best" without first defining the end goal. For example, assuming the end goal is the development of an assay capable of detecting amino-acid compounds while completely preventing interference from nucleic-acid compounds, then the PD coating may very well be the best choice, as this coating generated the highest affinities between the protein probe/target pairs and was resistant to DNA adsorption.

In general, the sample composition, whether single target or a mixture of all four targets, had little influence on the probe/target affinities, with the exception of the DNA2 probe/target pair on the AS and PLL coating. On these two coatings, the DNA2 affinities were significantly higher in the mixed target sample than in the single target sample which contained only the DNA2 target. The reason for this apparent sample-dependent affinity change is unknown. However, one possible explanation is that some other target or targets in the mixed sample solution interacted with the DNA2 target in such a manner that its affinity with the DNA2 probe spots was increased. This hypothesis is unlikely, though, as an interaction between the DNA2 target with other targets would have also been observed on the PEM coating and not just the AS and PLL coating. This suggests that the affinity change is not caused by an interaction between the target compounds but, rather, the result of a platform-dependent change in the interaction between the probes and the sample constituents. For instance, the surface properties of the AS and PLL coating may have altered the conformation of the DNA2 probe, which inadvertently increased its specificity towards other target compounds. There are, however, alternative possibilities which could explain this phenomena, prompting the need for further experimental investigations before a definitive explanation can be provided.

The platform-dependent changes in probe/target affinity observed in Figure 3.9 represent another significant source of cross-platform microarray dataset discordance generated by intrinsic differences in surface properties on different platforms. Additionally,

this source of dataset discordance is further compounded by differences in the chemical nature of the specific probe/target pairs utilized in the microarray design. Because the probe/target affinities are dependent upon both the surface properties of the platform and the chemical properties of the probe, it is difficult to predict how newly integrated probes will behave in a multianalyte format relative to established probes. In terms of microarray development, these drawbacks represent another obstacle which limits cross-platform comparability and impedes more rapid validation of new technologies. Furthermore, the rate of developmental progress is significantly limited since advances made on one platform are typically not transferable to newly developed platforms.

3.6.2.4 Effect of Sample Composition on Target Response

To investigate the effect of sample composition further, the target signal responses generated by samples containing a single target were compared to those generated by the mixed target sample, which contained all the target samples (Figure 3.10). For an accurate comparison to be made, it is important to consider the target response due to cross-reactivity with Cy5-labeled targets which are not specific to a given probe. Therefore, the signal responses generated by each single target sample and the blank sample were summed in order to account for the total target response generated by each single target sample on a specific probe. This value was then compared to the signal response generated by the mixed target sample to determine whether the sample composition influences the target signal response. For example, the first □ datapoint on the left in Figure 3.10 was obtained by summing the DNA1 target responses generated on the AS coating by the four single target sample solutions (□ datapoints, Figure 3.8A-D) and the blank sample solution (□ datapoint, Figure 3.8F). The resulting value was then overlaid onto the target signal response generated by the DNA1 probe on the AS coating using the mixed sample solution (□ datapoint, Figure 3.8E), which contained all four targets. This procedure was then repeated for the other probe spots on each surface coating to generate Figure 3.10, where the □ datapoints represent the sum of the single target samples and blank sample signal responses, while the ⊠ datapoints represent the mixed target sample signal responses.

Upon initial analysis of the datapoints in Figure 3.10, no significant trends can be observed regarding the effect of sample composition on the target signal responses. For
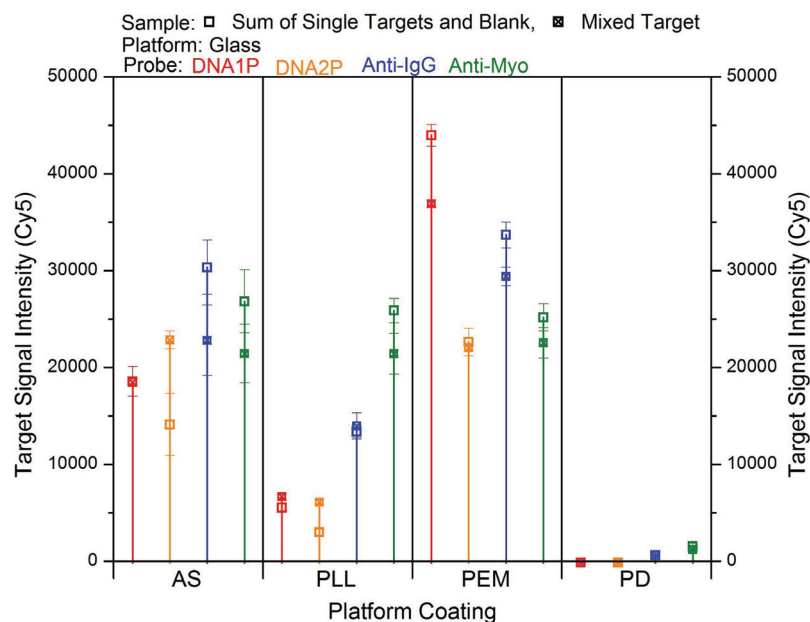
FIGURE 3.10: Influence of sample composition on the target signal response generated by each probe compound on each coating. The □ datapoints represent the sum of the mean target signal intensities generated on a specific probe compound by each single target sample and the blank sample, while the ⊠ datapoints represent the mean target signal intensities generated on a specific probe compound by the mixed target sample. The sum of the target responses generated by the single target samples and the blank are overlaid onto the target responses generated by the mixed target sample to compare the effect of sample composition on the overall target response on each surface coating.

example, on the AS coating no signal differences were observed between the mixed and single target samples with the DNA1 probe/target pair. The DNA2 probe/target pair, on the other hand, generated a significantly higher target response with the mixed target sample in comparison to the single target sample solutions on the AS and PLL-coated platforms. This sample-dependent change in the DNA2 target signal, however, was not observed on the PEM coating, where target signal intensities were similar regardless of using the mixed or single target samples. Aside from the DNA2 probe/target pair on the AS and PLL coatings, however, the sample-dependent changes in the target signal responses were typically small, indicating that the sample composition had little effect upon the overall signal responses generated.

Because no significant trends can be observed in Figure 3.10, few conclusions can be drawn regarding the effect of sample composition on the target response. However, the influence of sample composition should still be given special consideration when developing microarray platforms and analysis of datasets obtained on them. Although

the sample composition appears to have little effect on the target signal response in this microarray design, effects may be seen with alternative designs which utilize different platforms, probes, target samples. Furthermore, it is also possible that the sample composition may have significant effects upon other aspects of the assay performance, such as NSB. Taking these factors into consideration, the use of integrated reference probes and target samples is highly stressed in order to examine effects on signal intensity caused by differences in the sample composition. Failure to integrate accurate references can prevent the ability to discriminate between true target response signals and signals caused by interference of other sample constituents, possibly resulting in a false positive or negative detection.

3.6.2.5   Target Background Intensity

Ideally, the surface properties of a given microarray platform show a high resistance towards NSB of target compounds present in a sample. Surfaces which adsorb target compounds can have profound negative effects on the assay performance due to an increase in the background fluorescence relative to the signal fluorescence, resulting in a lower S/N ratio. Furthermore, surfaces which have a high affinity for targets can reduce the theoretical detection limit by stripping the targets from the sample solution before they have an opportunity to find and bind with their probe partner, preventing the detection of targets present at lower concentrations which would otherwise be detectable.

The target background intensities generated by each sample solution were compared between surface coatings using the datapoints plotted earlier in Figure 3.4E, which represented the fluorescence intensity generated by the presence of Cy5-labeled targets in the background region around the probe spot, as illustrated in Figure 3.3. These datapoints were grouped by the target sample solution and are replotted in Figure 3.11 to compare the interaction of each target with each surface coating. Graphs A-D in Figure 3.11 represent the target background intensities generated on each surface coating by the single target samples containing 100nM of either DNA1T, DNA2T, IgG, or Myo, respectively. Graph E represents the target background intensities generated by the mixed target sample, and graph F represents the target background intensities generated by the blank sample.
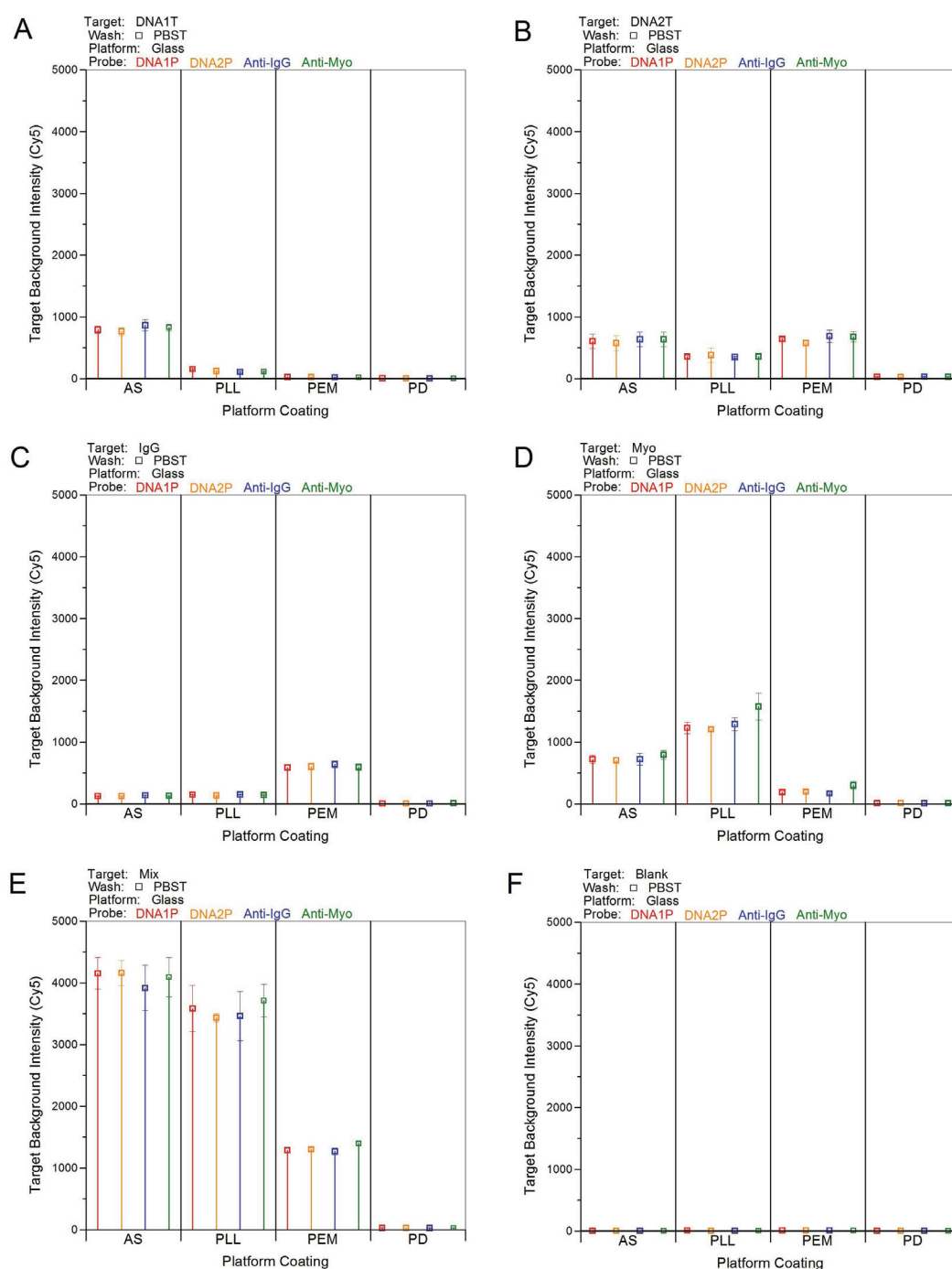
FIGURE 3.11: Target background intensities generated by each target sample as a result on NSB. Graphs A-D represent the target background intensities generated by the 100nM Cy5-labeled single target samples DNA1T, DNA2T, IgG, and Myo, respectively; graph E represents the target background intensities generated by the mixed sample containing 100nM of each Cy5-labeled target; and graph F represents the target background intensities generated by a blank sample containing no target compounds. Each datapoint was obtained using the mean background intensity of the four replicate spots for a given probe compound exposed to a particular target sample. Within each graph, the datapoints are grouped by surface coating so the extent of NSB can be compared between each surface coating.

In Figure 3.11A, the first noteworthy observation is the background intensity generated on the AS coating by a sample containing 100nM of the Cy5-labeled DNA1 target. Specifically, the fluorescence signal due to NSB of the DNA1 target was measured near 1000 around each probe compound (DNA1P, DNA2P, Anti-IgG, and Anti-Myo). The differences in the magnitude of the fluorescence intensities generated by each probe compound on the AS coating can be used as a measure of the uniformity of the surface properties over the array area. Assuming an ideal microarray platform which exhibits perfectly uniform surface properties, the background intensity generated around each probe spot would be identical. In Figure 3.11A, relatively small differences are observed in the DNA1 target background intensity around each probe compound, indicating that the surface properties of the AS coating are relatively uniform over the array area. Furthermore, based on the background intensities observed in graphs B-E of Figure 3.11, the surface properties of each coating seem relatively uniform, with perhaps the exception of the PLL coating shown in Figure 3.11D, which represents the background intensity generated by the Cy5-labeled Myo target. Specifically, the anti-Myo probes generated a significantly higher background intensity compared to the DNA1P, DNA2P, and anti-IgG probes, indicating an increase in NSB of the Myo target around the anti-Myo probes relative to the three other probes. The increased fluorescence intensity around the anti-Myo probes, however, is most likely not a result of NSB, but rather, a specific interaction between the Myo target and the anti-Myo comet tails, which were observed earlier in Figure 3.7. As shown by the images in Figure 3.7, comet tails were most prominent around the anti-Myo probes on the PLL surface. These anti-Myo comet tails introduced receptor sites for the Cy5-labeled Myo target outside the spot circle, explaining the increased background intensity observed around the anti-Myo probes when exposed to the Myo target.

Another noteworthy observation seen Figure 3.11A is the extent of background fluorescence generated by the DNA1 target on the AS coating compared to the other coatings. In this case, the background fluorescence due to NSB of the DNA1 target is significantly higher on the AS coating relative to the PLL, PEM, and PD coatings. In terms of cross-platform comparability, this result represents a scenario where the same target compound exhibits differential levels of NSB depending upon the surface properties of the microarray platform. This platform-dependent change in target NSB brings forth yet another source of cross-platform discordance which limits the extent

of comparability between datasets obtained on different platforms, even when utilizing standardized assay and analysis methods. In terms of performance, the AS coating provides the least desirable surface coating in regard to NSB of the DNA1 target. This negative performance observed specifically on the AS coating, however, was not observed with all targets. For example, Figure 3.11B represents the background fluorescence generated by the DNA2 target on each surface. In this case, significant background intensities were generated on the AS, PLL, and PEM coatings. This is in stark contrast to the background intensities observed between these coatings with the DNA1 target. Whereas the DNA1 target preferentially adsorbs onto the AS coating only, the DNA2 target exhibits significant adsorption onto the AS, PLL, and PEM coatings. Differential NSB between surface coatings was also observed with the protein targets. For example, the datapoints in Figure 3.11C show significant background intensities due to NSB of the IgG target on the PEM coating, but not the other three coatings, whereas the Myo target generated significant background intensities on both the AS and PLL coatings, but not the PEM coating, as shown in Figure 3.11D.

The background intensities observed within and between graphs A-D in Figures 3.11 demonstrate how different target compounds will exhibit differential NSB on dissimilar platforms. Differential NSB on dissimilar platforms introduces another complexity which negates the ability to accurately compare cross-platform datasets, especially in the case of a multianalyte design. For instance, the datasets generated from a hypothetical dual analyte assay which utilizes the DNA1 and IgG targets would be rather difficult to compare between the AS and PEM coatings. The reason for this difficulty can be inferred from the datapoints in Figures 3.11A and C, which represent the background intensities generated by these two targets on each surface coating. In this case, detection of the IgG target on the AS coating would be highly influenced by the presence of DNA1 target, as the DNA1 target exhibits significant NSB onto the AS coating, as shown in Figure 3.11A. NSB of the DNA1 target will increase the overall background intensity, resulting in a lower IgG S/N ratio. Furthermore, the magnitude of the IgG S/N ratio will fluctuate depending on the concentration of the DNA1 target in the sample. Specifically, high concentrations of the DNA1 target would result in a lower IgG S/N ratio, while lower concentrations of the DNA1 target would result in a higher S/N ratio. Vice versa, detection of the DNA1 target on the PEM coating would be highly influenced by the presence of IgG target in the sample solution, since IgG exhibits significant NSB onto the PEM

coating, as shown in Figure 3.11C. Ultimately, this platform-dependent and sample-dependent differential NSB make it difficult or impossible to compare cross-platform assay results, especially when utilizing real-world samples of unknown composition.

3.6.2.6   Effect of Sample Composition on NSB

Previously in Figure 3.10, the effects of sample composition on the target signal responses were compared between samples containing a single target versus a sample containing all four targets. There, it was determined that the target signal intensities of the probe/target pairs were largely unaffected by the sample composition. In this section, the effect of sample composition on the target background intensity is examined to determine whether sample composition has an influence on the extent of target NSB (Figure 3.12).

Similar to Figure 3.10, the background intensities generated by each single target sample and the blank were summed in order to account for the background intensities generated by each single target sample. For example, the first □ datapoint on the left in Figure 3.12 was obtained by summing the target background intensities around the DNA1 probe spots on the AS coating generated by each single target sample (leftmost □ datapoints in Figures 3.11A-D) and the blank sample (leftmost □ datapoint in Figure 3.11F). The resulting value was then overlaid onto the target background intensity generated by the mixed sample (leftmost □ datapoint in Figure 3.11E), which contained all 4 targets. This procedure was then repeated for the other probe spots and coatings to generate Figure 3.12, where the □ datapoints represent the sum of background intensities generated by the single target samples and the blank sample, while the ⊠ datapoints represent the background intensities generated by the mixed target sample.

Analysis of the background intensities obtained on the AS coating in Figure 3.12 indicate that the background fluorescence due to NSB of target compounds is highly influenced by the sample composition. For example, the sum of the background intensities generated by the four single target samples on the AS coating was slightly above 2000 around each probe compound, as shown by the □ datapoints in Figure 3.12. Based on that result, it would be expected to see a similar background fluorescence intensity generated by the mixed target sample on the AS coating. This was not the observed
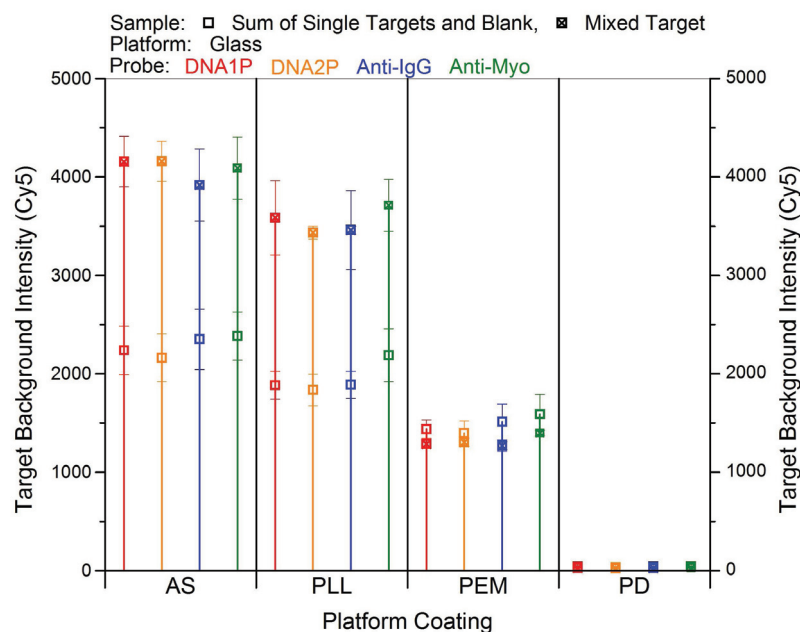
FIGURE 3.12: Influence of sample composition on the target background intensity generated on each coating. The □ datapoints represent the sum of the mean target background intensities generated around a specific probe by each single target sample and the blank sample, while the ⊠ datapoints represent the mean target background intensities generated around a specific probe by the mixed target sample. The sum of the target background intensities generated by the single target samples and the blank sample are overlaid onto the target background intensities generated by the mixed target sample to compare the effect of sample composition on the overall NSB of target compounds on each coating.

result, however, as shown with the ⊠ datapoints. Rather, the mixed target sample generated a background intensity roughly double that which was generated by the sum of the single target samples, indicating that the level of NSB on the AS coating is, to some extent, compounded by the presence of other sample constituents. This same effect was also observed on the PLL coating, where the background intensity is nearly double when using the mixed target sample in comparison to the sum of the single target samples. These elevated levels of target NSB exhibited by the mixed target sample on the AS and PLL coatings can be visually observed in Figure 3.2 as the images with a uniform blue background, which indicate a higher background fluorescence intensity.

One possible explanation for the increased background fluorescence generated by the mixed target sample may be an interaction between target compounds which have bound to the platform surface and target compounds still in solution. For instance, binding of the DNA1 target onto the AS-coated platform will have two effects. Firstly, there

will be an increase in the background intensity due to NSB of the Cy5-labeled DNA1T. Second, there will be a change in the surface properties of the microarray platform due to the presence of these DNA1 targets on the surface. Because the surface properties of the platform are now different, subsequent adsorption of other target compounds in the sample solution may either be increased or decreased, depending upon the chemical nature of the surface itself and the targets present. In the case that subsequent adsorption of other target compounds is induced, a second round of NSB occurs, resulting in a further increase in background intensity and another change in surface properties, which may or may not induce a third round of NSB and so forth. This scenario may provide an explanation as to why the background intensity is compounded depending on the composition of the sample. In terms of microarray development, this situation represents another obstacle which complicates analysis of multianalyte assay datasets, in that the extent of background fluorescence will fluctuate depending on the composition of the sample solution. This sample-dependent fluctuation in NSB can be especially problematic when using real-world samples of unknown composition.

Unlike the AS and PLL coatings, however, the PEM coating did not show any significant fluctuation in the background intensity due to the sample composition. In this case, the mixed target sample and the sum of the single target samples both generated a background intensity near 1500. Additionally, the overall background intensity generated on the PEM coating was slightly lower than the background intensities on the AS and PLL coatings. In terms of assay performance, this result represents a significant advantage with the PEM coating in that it generates a lower background intensity and appears largely unaffected by the sample composition, with this specific assay design at least. It is possible that these advantages are specific to this combination of probe/target pairs and not a general advantage for any assay design, prompting the need for further investigation with other multianalyte systems.

In terms of cross-platform dataset comparability, the effect of sample composition on target NSB reveals an additional platform-dependent source of discordance. Specifically, the AS and PLL-coated platforms exhibit twice as much NSB when using the mixed target sample versus the single target samples; whereas the PEM-coated platform exhibits similar NSB regardless of the sample composition. Therefore, it is likely that other microarray platforms will also exhibit differential NSB depending on the platform's surface properties and the chemical nature of the targets present in the sample.

3.6.2.7   S/N

The final performance parameter characterized for this multianalyte microarray design was the S/N, which was calculated using the target signal intensity (S), target background intensity (B), and target background intensity SD (BSD) according to the formula[72]:

$$S/N = [(S - B)/BSD].$$ (3.1)

The values obtained using Equation 3.1 are plotted in Figure 3.13. It should be noted that the Y-axis scales of each graph in Figure 3.13 are adjusted due to large differences in the S/N ratios generated by different sample solutions. For example, the largest S/N ratio generated by the DNA1 target sample was 4500, which was observed on the PEM coating as shown in Figure 3.13A. In Figure 3.13B, however, the largest S/N generated by the DNA2 target was only 500, also observed on the PEM coating. Plotting these two graphs on the same scale would have complicated the ability to make intra-graph comparisons, especially in graphs which showed lower overall S/N ratios. Therefore, the scales were adjusted to enable comparison within and between each graph.

In Figure 3.13A, a relatively large DNA1 target S/N ratio was generated on the PEM coating in comparison to the other coatings, and in particular, the AS coating, which generated a S/N ratio almost negligible to that obtained on the PEM coating. This was an unexpected result, as it was shown earlier in Figure 3.8A that the AS coating generated a DNA1 target signal response nearly half that obtained on the PEM coating. Therefore, it was expected to see a comparatively similar DNA1 target S/N ratio between the AS and PEM coatings. The low S/N ratio generated on the AS coating can be explained, though, when taking into account the background intensity and background intensity SD generated by the DNA1 target. Specifically, going back to Figure 3.11A in Section 3.6.2.5, which represented the background intensities due to NSB of the DNA1 target, the AS coating generated a significantly higher background intensity relative to the PEM coating. Because the target background intensity is subtracted from the target signal intensity when calculating the S/N, a reduction in the numerator of Equation 3.1 is seen, resulting in a lower S/N ratio.
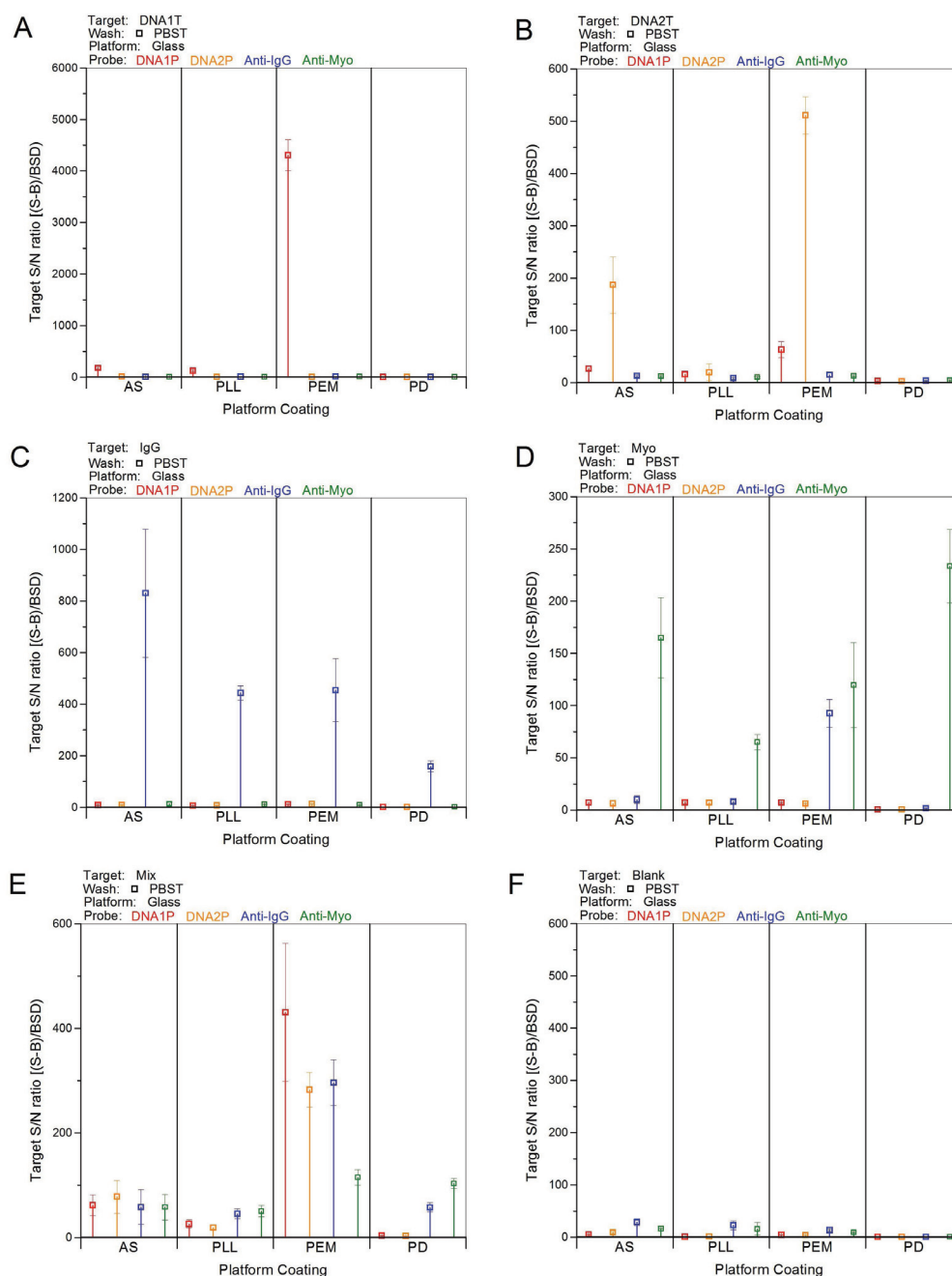
FIGURE 3.13: Target S/N ratios calculated using Equation 3.1. Graphs A-D represent the S/N ratios generated by the 100nM Cy5-labeled single target samples DNA1T, DNA2T, IgG, and Myo, respectively; graph E represents the S/N ratios generated by the mixed sample containing 100nM of each Cy5-labeled target; and graph F represents the S/N ratios generated by a blank sample containing no target compounds. Each datapoint was obtained from the mean S/N ratios of the four probe replicates within an array exposed to the respective target sample solution. Within each graph, the datapoints are grouped by surface coating to compare the S/N ratios of each target compound between the surface coatings.

An even more significant factor contributing to the low DNA1 S/N ratio obtained on the AS is the background intensity SD, which alone represents the denominator of Equation 3.1. Going back to Figure 3.4F in Section 3.6, the □ datapoint representing the target background intensity SD generated by the DNA1 target sample on the AS coating was measured at around 100, whereas the corresponding target background intensity SD generated on the PEM coating was closer to zero. The increased background intensity SD observed on the AS coating compared to the PEM coating explains the significantly lower DNA1 S/N ratio on the AS coating in comparison to the PEM coating.

It should be noted additionally, that the reduced DNA1 S/N ratio observed on the AS coating is primarily due to the high levels of NSB of the DNA1 target onto that surface, contributing to both the increased background and background SD. This impact of target NSB upon the S/N ratios can also be seen in Figure 3.13B, which represents the S/N ratios obtained with the DNA2 target sample. In this case, the DNA2 target showed significant NSB onto the AS, PLL, and PEM coatings, resulting in relatively low S/N ratios on all three surfaces. This correlation between high NSB and low S/N ratios is also observed with the mixed target sample, as shown in Figure 3.13E. Here, the overall S/N ratios are significantly lower than those obtained using the single target sample solutions, due to the significantly higher background intensities generated with the mixed target sample in comparison to the single target samples, as shown previously in Figure 3.12. It should also be noted in Figure 3.13E that the S/N ratios obtained on the PEM coating are significantly higher than those obtained on either the AS or PLL coating. This result is again a consequence of the PEM coating showing significantly lower target NSB than the AS and PLL coatings when using the mixed target sample, as shown in Figure 3.12E.

In terms of performance, the PEM provides a significant advantage over the other surface coatings in terms of S/N ratios in a single analyte format with the DNA targets and in a multianalyte format with the mixed target sample, as determined from Figures 3.13 A, B, and E. On the other hand, the AS coating provides the best performance with the IgG target sample, while the PD coating is best with the Myo target sample, as shown in Figures 3.13 C and D, respectively. In terms of cross-platform comparability, virtually none is seen. Each coating generates vastly different S/N ratios and there are no evident trends within or between graphs.

Earlier, in Section 3.6.2.2, cross-reactivity between a probe with unspecific targets was discussed. There, analysis of the fluorescence intensities showed significant target signal responses due to cross-reactivity on the PEM coating. For example, the Myo target was found to generate a significant target response on the anti-IgG probe spots, as shown in Figure 3.8D. In Figure 3.13B, the effects of cross-reactivity between the anti-IgG and the Myo upon the S/N ratio can be seen. Specifically, a relatively large S/N ratio is observed on the anti-IgG probe on the PEM coating when exposed to the Myo sample, as shown by the □ datapoint. This observation correlates with the cross-reactivity which occurred on the PEM coating between the Myo target and anti-IgG probe. In this case, however, the S/N ratio of the anti-IgG probe is nearly the same in magnitude as the anti-Myo probe, even though no Cy5-labeled IgG target is present.

The adverse effect upon the S/N ratio due to cross-reactivity represents a significant disadvantage with the use of the PEM coating for this particular assay design. During assay analysis, the detection limit of a compound is typically defined as a certain threshold value of the S/N. Therefore, presence of the Myo target may raise the S/N of the anti-IgG probe above the detection threshold, resulting in a false positive detection of the IgG target, even if there is no IgG present in the sample solution.

3.7   Summary of Multianalyte Microarray

An in-depth analysis of the datasets shown in Figure 3.4 provided significant information regarding the cross-platform performance and comparability of a multianalyte assay on glass microarray platforms when introducing two variables into the experimental design: different surface coatings and different sample solutions. The use of different surface coatings enabled the identification of coatings which provide the best performance for the probe/target pairs used in this microarray design. It was found that no single surface provided the best performance for all the probe/target pairs. Rather, certain coatings performed relatively well with some probe/target pairs, but not necessarily with other probe/target pairs. Based on this finding, it was concluded that the ideal surface coating will vary depending upon the desired application and end goal.

In terms of cross-platform comparability, the use of different surface coatings enabled the identification of platform-dependent sources of variability which limit the extent of

comparability between datasets generated on different platforms. Specifically, it was determined that differences in the surface properties of different platforms will have a profound influence upon virtually every aspect of the assay performance examined: probe immobilization density, target response, target specificity, probe/target affinity, NSB, and S/N. Furthermore, it was discussed how these platform-dependent performance differences prevent the ability to integrate a common cross-platform control, representing perhaps the greatest limitation negating the ability to accurately compare and validate datasets obtained on different microarray platforms.

The use of different sample solutions in the assay design enabled the identification of performance parameters which are influenced by the sample composition. Datasets obtained when using different samples indicated that sample composition affects some aspects of assay performance but not others. For instance, the sample composition was found to have little influence over the target signal responses, but had a significant impact upon the levels of target NSB. Specifically, it was found that the mixed target sample served to compound the extent of NSB on the AS and PLL coating, but not on the PEM coating. These sample-dependent and platform-dependent complexities encountered in a multianalyte format represent another limitation upon development and validation of microarray technologies, in which real-world samples of unknown composition will generate differential NSB on different microarray platforms.

In terms of meeting the thesis objectives, this chapter establishes a fundamental reference point in terms assay performance and cross-platform comparability. Using the datasets obtained here, it should be possible to investigate how the introduction of new variables into the microarray design will effect the overall assay performance and cross-platform comparability.

Chapter 4

Modification of the Multianalyte Microarray Design

4.1 Introduction

During microarray development, new variables can be introduced into virtually any aspect of an experimental design: platform, probe/target pairs, assay protocol, detection method, etc. Any change introduced into the experimental design can have a positive or negative impact upon the assay performance. For example, modification of a platform's surface chemistry may increase the target signal response for one compound, but reduce it for another. An example of this scenario was observed earlier in Figures 3.8C and D. Specifically, the IgG target signal response was higher on the PEM coating in comparison to the AS coating, whereas the Myo response was higher on the AS coating versus the PEM coating. Alternatively, a change introduced into the experimental design may improve one performance parameter for a specific probe/target pair, but reduce some other performance parameter. For instance, modifying a platforms surface chemistry may increase a targets signal intensity, but it may also increase the background intensity due to NSB of that target. This situation was observed with the IgG target on the PEM coating. Specifically, the PEM coating generated the highest IgG signal intensities, but it also generated the highest IgG background intensities, as shown in Figure 3.8C and 3.11C, respectively.

In the previous chapter, multianalyte microarrays were fabricated onto surface-modified glass platforms in order to characterize and compare the assay performance using a given set of variables (platform surface chemistries and sample compositions) and a defined set of constants (probe/target pairs, microarray fabrication, sample assays, and analysis methods). In this chapter, new experimental variables are introduced to determine whether it is possible to improve assay performance and tailor the surface chemistry of SI surface coatings for multianalyte microarray applications.

4.2 Materials and Methods

4.2.1 Materials

Poly(acrylic acid) (PAC, $M_w = 100K$) was obtained from Sigma-Aldrich.

4.2.2 Elimination of Probe Comet Tails

The experimental design used in Chapter 3 resulted in the formation of probe comet tails on the AS, PLL, and PEM coatings, as shown in the images in Figure 3.7. The presence of these comet tails translated into significantly increased background intensities and background intensity SDs, which further translated into reduced S/N ratios. As discussed in Section 3.6.1.2, probe comet tails are created during the wash step performed immediately after probe spotting, where unbound probe desorbs from the platform surface and quickly readsorbs in the spot vicinity. A typical countermeasure used to reduce the extent of comet tails is to lower the concentration of the probe spotting solution in order to minimize the amount of unbound or loosely bound probe on the microarray platform surface prior to the wash step. However, because the concentration of the spotting solution is reduced, this approach also reduces the probe immobilization density as well.

To overcome this compromise between comet tails and probe immobilization density, it was desirable to develop a method which reduces comet tail formation without having to lower the spotting concentration. Previous experimental work in this area showed that this is possible by introducing a negatively-charged PE compound into the wash solution used after probe spotting[30]. Specifically, the inclusion of PAC in the PBST

wash solution was found to significantly reduce comet tails of antibody probes on the PEM coating.

In that work, it was found that the PAC serves to introduce a competition with the antibody probes for adsorption onto the PEM surface during the wash step, when unbound or loosely bound antibody probe is released from the platform surface. Because the amine-rich surface of the PEM coating is positively-charged, it exhibits a high affinity for the negatively-charged PAC, whose chemical structure is shown in Figure 4.1.
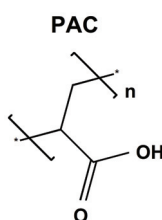
FIGURE 4.1: Chemical structure of PAC.

Once adsorbed, the carboxyl-functionalized PAC provides a barrier which reduces the extent of re-adsorption of antibody probes which are lifted from the platform surface during the wash step. Based on this mechanism, it was hypothesized that the negatively-charged PAC might also provide effective suppression of DNA probe comet tails, as DNA is also negatively-charged. Additionally, it was hypothesized that the inclusion of PAC into the wash solution might suppress probe comet tails on other positively-charged surfaces, such as the AS and PLL-coated glass platforms.

To test these assumptions, the microarray fabrication procedure was modified to include PAC in the PBST wash solution. Here, rather than washing the printed microarrays with PBST as described in Chapter 3, the microarrays were washed with PBST containing 2mg/ml PAC (MW 70K) according to the procedure described in Section 3.3. Inclusion of the PAC wash represents the first new variable introduced into this experimental design.

4.2.3 Reduction of Target NSB

As discussed in Chapter 3, NSB is typically reduced by blocking the surface of the microarray platform with a compound known to resist the adsorption of target compounds from a sample solution. In the previous assay design, this was accomplished by blocking

the platforms with BSA according to the procedure described in Section 3.3. Analysis of the target background intensities in section 3.6.2.5, however, revealed significant and differential levels of NSB depending on the surface coating, target compound, and sample composition. These differential levels of target NSB represented a significant aspect of assay performance which could potentially be improved upon.

Several approaches may be taken when attempting to reduce NSB. For instance, the length of the blocking step can be increased to provide more time for the blocking agent (BSA) to adsorb onto the surface and provide a more effective barrier against NSB. Alternatively, the surface may be blocked with an entirely different blocking agent, such as poly(ethylene glycol), which has also been shown to effectively reduce NSB of many biomolecule compounds [22,47].

In this multianalyte microarray design, both DNA and protein targets were used. It has recently been shown that PAC-coated surfaces show a high resistance against NSB of DNA [73] and protein [74] compounds. As discussed is Section 4.2.2, the microarray fabrication procedure in this chapter is modified to incorporate a PAC wash following probe deposition. During that wash step, the microarray platforms are allowed to sit in the PAC wash solution for 10 minutes, providing ample time for the assembly of a PAC monolayer onto the surface. Therefore, it was anticipated that the PAC layer adsorbed during the wash step could be utilized to fulfill two functions: the elimination of probe comet tails and a reduction in the overall NSB of target compounds during the sample assay.

4.2.4 Modification of the PD Coating

As mentioned in Chapter 1, in order for a SI surface coating to serve as a useful cross-platform interface for microarray development, it must be possible to modify and tailor its surface properties to perform specific applications. Of the two SI surface coatings examined, the PD coating showed a rather poor performance relative to the other coatings examined. Specifically, it was found that the native PD coating immobilized relatively low densities of the protein probes anti-IgG and anti-Myo, resulting in poor signal responses with their respective target partners, as shown in Figure 3.8. Furthermore, the PD coating was incapable of performing DNA microarray applications due to its

inability to immobilize sufficient amounts of DNA probe to generate a detectable target response.

In this chapter, experimental data are presented concerning modification of the PD coating in order to determine whether its multifunctional characteristics can be tailored to perform the multianalyte design used in Chapter 3. Because the PD coating was only recently developed, few methods of functionalizing its surface with biomolecules have been reported[69]. Previously in Chapter 2, it was reported that LbL-assembly of the PSS/PAH multilayer system could be utilized to functionalize the surface of many materials, including a hydrophobic polymer. Additionally, the PSS/PAH multilayer system proved highly effective for the immobilization of biomolecules. Therefore, rather than develop a method from scratch, LbL-assembly of PSS and PAH was utilized for modification of the PD surface. Use of this optimized PD (OPD) coating represents the second and final new variable introduced into the experimental design.

Here, a three layer PEM system composed of PAH(PSS/PAH) was assembled onto the PD surface according to the procedure described in Section 2.4.1. It should be mentioned that assembly of the PSS/PAH multilayer system is not simply a case of dropping one SI surface coating onto another SI surface coating. Rather, the three layer PAH(PSS/PAH) multilayer system is merely a means to functionalize the surface of the PD coating by increasing the amount of amine groups on its surface. Furthermore, because only three PE layers are assembled, the multilayer system is not thick enough to completely suppress the surface properties of the underlying PD coating, therefore, the surface properties of the OPD coating are significantly different to those of the SI PEM coating composed of a PAH(PSS/PAH)$_5$ multilayer system.

4.3 Multianalyte Microarray Analysis

Aside from the PAC wash and the OPD coating, all other aspects of the experimental design were kept consistent to those reported in Chapter 3, including the microarray scan parameters and analysis methods. Therefore, any changes observed in the multianalyte assay performance can be attributed to either the PAC wash or the OPD modification. Figure 4.2 shows the microarray images obtained when using the experimental design described in this chapter. Because the arrays were scanned using the

same wavelengths, LP settings, and PMT settings used to obtain the images in Figure 3.2, a direct comparison between both image sets can be made.

Comparing between the images in Figures 3.2 and 4.2, some preliminary observations can be made regarding the effect of the PAC wash and the OPD coating on the assay performance. For example, when utilizing the PBST wash, the PLL coating provided the highest protein probe immobilization densities, as shown by the images in the upper block of Figure 3.2. When utilizing the PAC wash, however, the PLL coating shows the lowest protein probe immobilization densities, as shown by the corresponding images in Figure 4.2. Furthermore, the protein probe spots on the PAC-washed PLL coating are highly irregular in shape, indicating that the surface properties of the PLL-coated glass platform are not uniform. This observation suggests that the PAC wash may have stripped some PLL from the surface, resulting in an inhomogeneous glass/PLL surface.

Another significant observation can be made regarding the probe fluorescence intensities on the PD coating versus the OPD coating. Specifically, very low probe fluorescence intensities were observed on the PD coating, as shown previously in Figure 3.2. In Figure 4.2, however, significant probe fluorescence intensities are observed with both the protein and DNA compounds on the OPD surface, suggesting that this coating may be suitable for multianalyte microarray assays. This assumption is corroborated by the target fluorescence intensities generated on the OPD coating, as shown by the images in the lower block of Figure 4.2.

The images in the lower block of Figure 4.2 also provide significant information regarding the effect of the PAC wash on target NSB. For example, the mixed target sample generated significant background fluorescence on the PBST-washed AS and PLL coatings, as shown by the blue images in Figure 3.2. The PAC-washed platforms, on the other hand, generated significantly lower background fluorescence, as shown by the corresponding images in Figure 4.2. This observation suggests that the PAC wash is highly effective for reducing the NSB of target compounds in multianalyte assays which employ both DNA and protein targets.
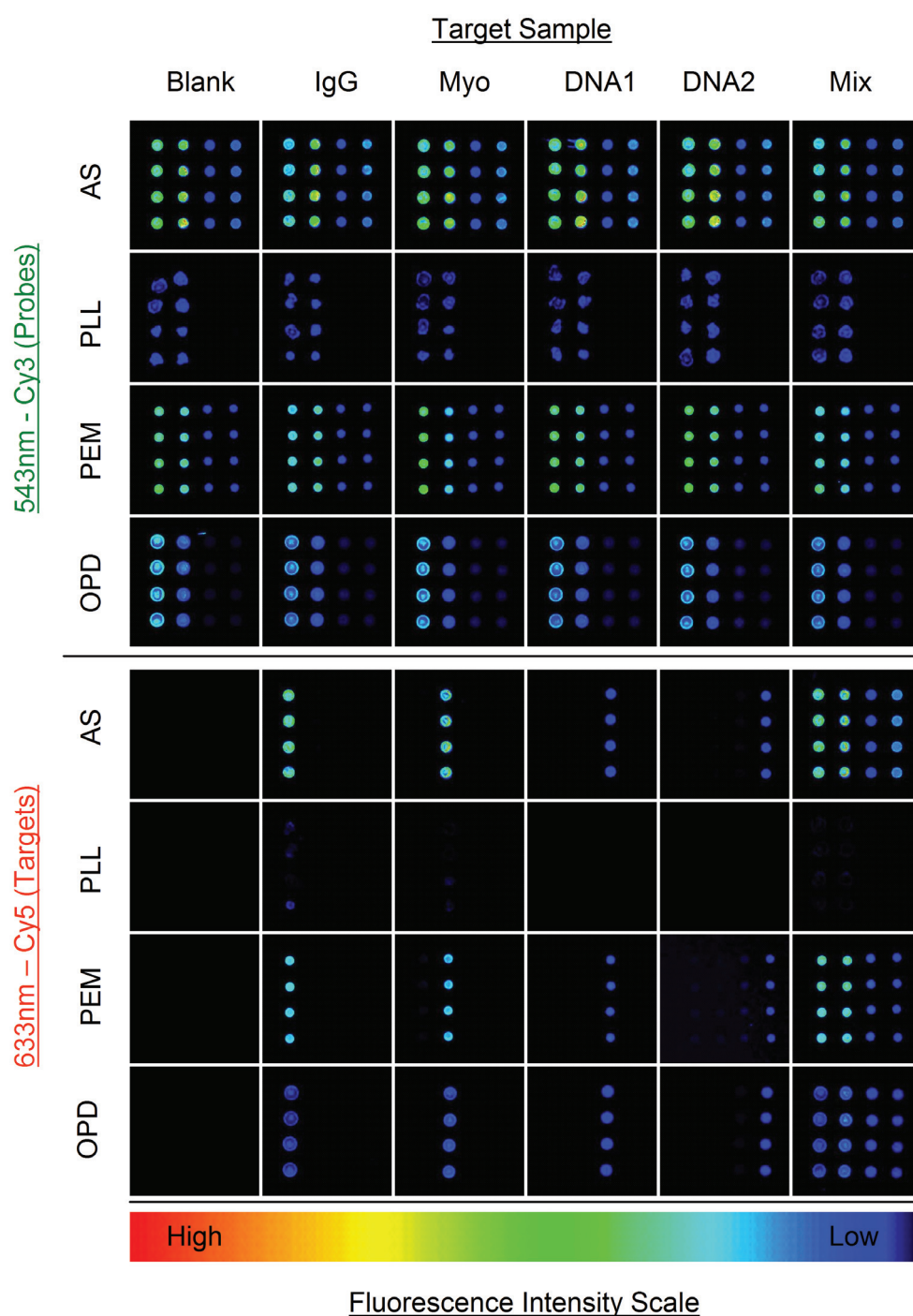
FIGURE 4.2: Fluorescent images obtained when utilizing the PAC wash and the OPD coating in the microarray design. Images in the upper block represent arrays scanned using a wavelength of 543nm to visualize the immobilized Cy3-labeled probes, while images in the lower block represent arrays scanned using a wavelength of 633nm to visualize the bound Cy5-labeled targets. The array images are further sorted by the target sample solution to which they were exposed (columns) and the surface coating to which the arrays were printed onto (rows). The fluorescence intensity scale (rainbow bar) is provided below the image sets for comparison of the fluorescence signals generated by each array.

4.4 Effect of New Variables on Multianalyte Assay Performance

To fully characterize the effect of the PAC wash and the OPD coating on the multianalyte assay performance, the fluorescence intensities of the image set in Figure 4.2 were analyzed in terms of signal, background, and background SD. Analysis of the image set was performed according to the procedure described in Section3.5 and then plotted in Figure 4.3. The graphs shown in Figure 4.3 were generated and arranged in the same manner used to obtain the graphs in Figure 3.4, explained previously in Section 3.6. It should be noted that the datapoints plotted in Figure 3.4 are included in Figure 4.3 to simplify comparison between the PBST-washed platforms and the PAC-washed platforms.

In Figure 4.3, significant differences in the fluorescence intensities are observed between the PAC-washed platforms and the PBST-washed platforms. For example, the PAC-washed platforms typically generated lower probe and target signal intensities in comparison to the PBST-washed platforms, as shown in Figures 4.3A and D. Similarly, the PAC-washed platforms also generated lower background intensities and background intensity SDs, as shown in Figures 4.3B, E, C, and F. For example, the PBST-washed platforms show differential levels of background and background SD, depending on the platform and probe/target pair. Utilization of the PAC wash, however, reduces the background and background SD to nearly undetectable levels on each platform and with all probe/target pairs. These fluorescence differences observed between the PBST and PAC-washed platforms will have a significant impact upon many assay performance parameters analyzed.

Figure 4.3 represents the entire dataset used to characterize and compare the multianalyte assay performance throughout this chapter. From this dataset, the effect of the PAC wash and the OPD coating on aspects of assay performance such as probe immobilization density, target response, specificity, affinity, NSB, and S/N were investigated and the results are reported below.
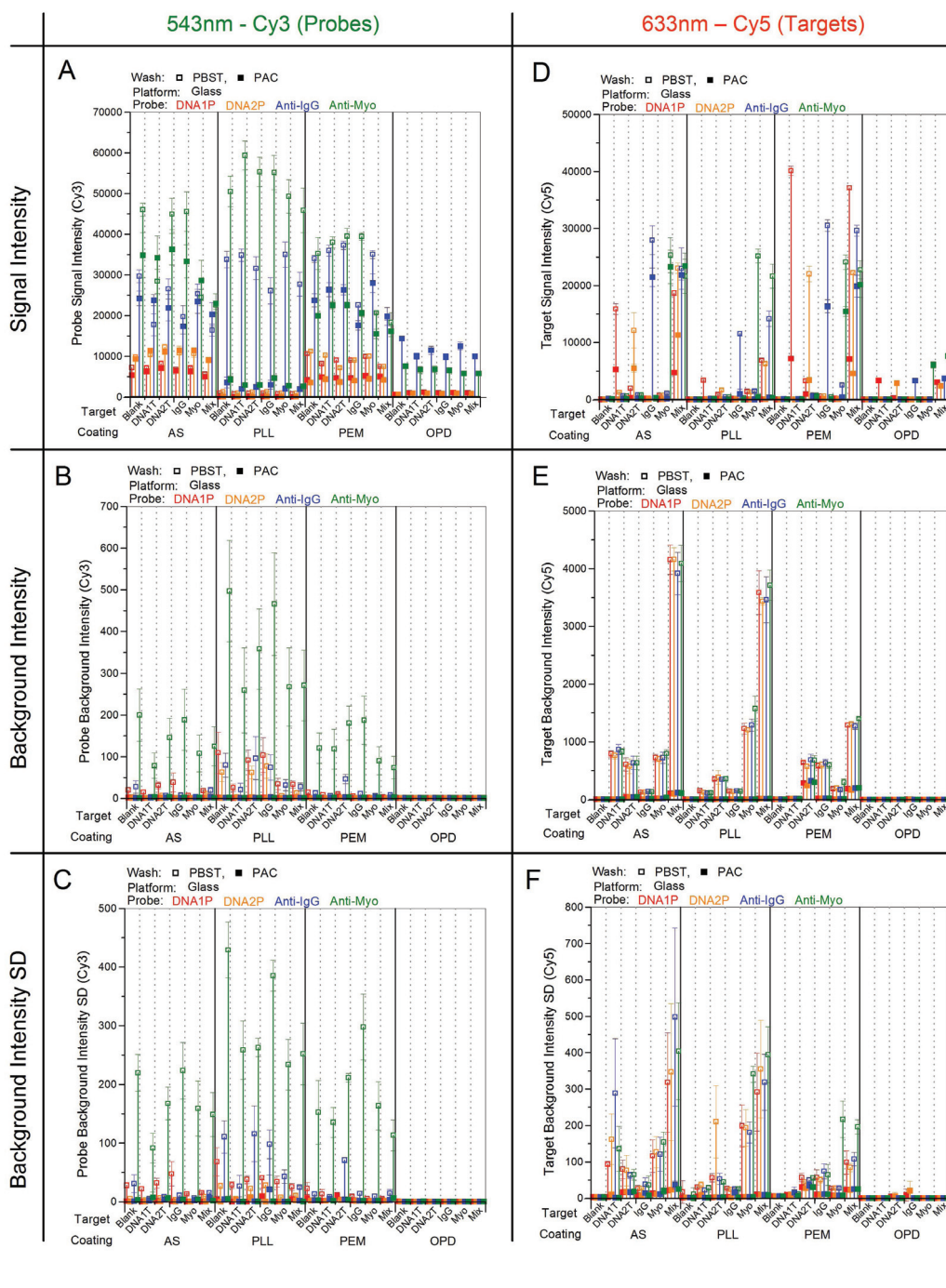
FIGURE 4.3: Total dataset obtained from the analysis of the images in Figure 3.2 (PBST-washed platforms) and 4.2 (PAC-washed platforms). In each graph, the □ datapoints represent values obtained on the PBST-washed platforms, while the ■ datapoints represent those obtained on the PAC-washed platforms. Graphs A-C (left column) represent the probe data, while graphs D-F (right column) represent the target data. The datasets are further sorted by fluorescence signal intensity (top row), background intensity (middle row), and background intensity SD (bottom row). Each datapoint within a graph represents the mean of four replicate spots for a specific probe compound within an array. Each probe compound is color-coded for quick reference: DNA1P, DNA2P, Anti-IgG, Anti-Myo

4.4.1 Probe Analysis

4.4.1.1 Probe Signal Intensity

Although microarray washing is performed following the deposition of the probe compounds, the inclusion of additives such as PAC can have negative effects on the probe immobilization density. Each surface coating in this experimental design provides a positively-charged, amine-rich surface which will exhibit an uncertain affinity for the negatively-charged, carboxylic groups of the PAC. If the surface properties of a given platform exhibits a higher affinity for PAC than the spotted probe compounds, the PAC may act to strip probe molecules from the surface, resulting in lower probe immobilization densities. To determine whether the PAC wash had any effect upon the probe immobilization densities, the probe signal intensities generated by the PAC-washed platforms were compared to those generated by the PBST-washed platforms. To enable a direct comparison, the probe signal intensities generated on the PAC-washed platforms were calculated in the same manner used to calculate those obtained on the PBST-washed platforms, explained previously in Section 3.6.1.1. To simplify comparison between the two datasets, the probe signal intensities calculated from the PAC-washed platforms were overlaid directly onto those obtained from the PBST-washed platforms to generate Figure 4.4.

As expected, the extent of probe stripping due to the PAC wash is significantly different depending on the probe compound and surface coating. For example, the leftmost red datapoints in Figure 4.4 represent the DNA1 probe immobilization densities on the AS coating. In this case, the □ datapoint (PBST wash) is only slightly higher than the ■ datapoint (PAC wash), indicating that the PAC wash had very little impact upon the DNA1 probe immobilization density on the AS coating. On the PEM coating, however, the DNA1 probe immobilization density is significantly lower when using the PAC wash in comparison to the PBST wash. Specifically, the PBST wash generated a DNA1P signal intensity of around 10,000, whereas the PAC wash generated a signal of roughly half that, indicating that the PAC wash strips significantly more DNA1 probe from the PEM surface than does the PBST wash. The PAC wash also causes significant stripping of the DNA1 probe from the PLL surface. When using the PBST wash, some extent of DNA1 probe was observed on the PLL coating. The inclusion of PAC into the
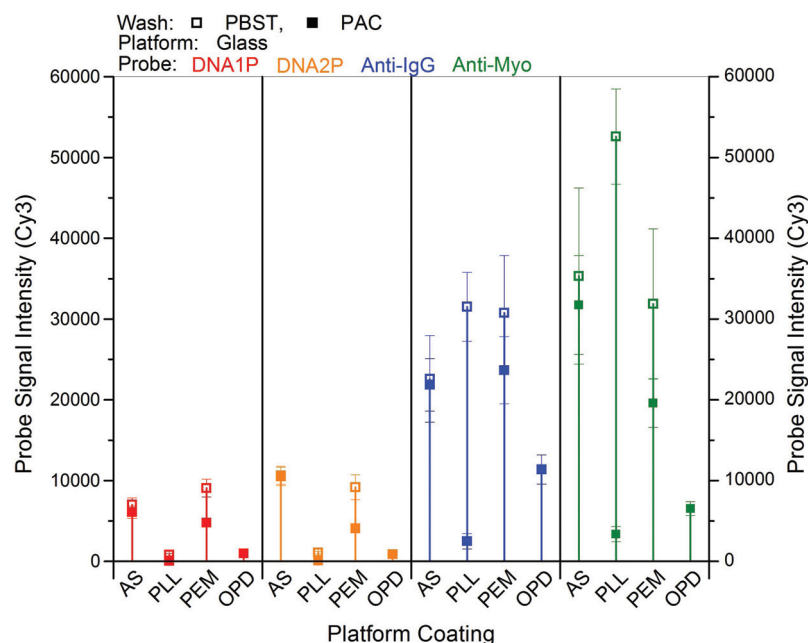
FIGURE 4.4: Effect of the PAC wash and OPD coating on the probe signal intensities. The □ datapoints represent values obtained on the PBST-washed platforms, while the ■ datapoints represent those obtained on the PAC-washed platforms.

wash solution, however, results in a DNA1 probe signal intensity close to zero, indicating that very little DNA1 probe is present on the PLL surface.

Similar immobilization trends between each coating are observed with the DNA2 probe. In this case, virtually no DNA stripping was observed on the AS surface, but significant stripping is seen on the PEM surface. The differences in the extent of DNA probe stripping observed between the AS and PEM coating could be due to differences between the affinity of the DNA probes with the AS and PEM coating. For example, very little DNA was stripped from the AS surface, suggesting a strong affinity between DNA and the AS surface. On the PEM coating, however, significant DNA stripping was observed, indicating a much weaker affinity between the DNA and PEM surface. Alternatively, the differences in the extent of DNA probe stripping may have been caused by differences in the affinity between the PAC with the AS and PEM coatings, rather that differences in the affinity between the DNA with the AS and PEM coating. For instance, it is possible that the affinity of the DNA is equal on both the AS and PEM surfaces, but the affinity of the PAC is much stronger on the PEM surface relative to the AS surface. Assuming this to be the case, the PAC may act to displace DNA probes immobilized onto the PEM coating but not the AS coating. Because there are two

possible mechanisms causing the observed probe stripping, further experimental work in this area is required to identify the true mechanism causing probe stripping on each surface.

Considering now the ■ and ■ datapoints in Figure 4.4, the effect of the PAC wash on the protein probe immobilization densities can be seen. Similar to the DNA probes, the protein probes show a high resistance against stripping on the AS surface when using the PAC wash, generating probe signal intensities similar to that obtained with the PBST wash. The PLL coating, on the other hand, shows significant stripping of the protein probes. In the previous experimental design, the PLL coating provided the highest immobilization densities for both the anti-IgG and anti-Myo probes when using the PBST wash. When utilizing the PAC wash, however, the PLL surface shows the lowest antibody probe immobilization densities in comparison to the other surface coatings examined, suggesting that use of the PAC wash may not be compatible with the PLL-coated glass platform.

Protein probe stripping was also observed on the PEM coating. However, the relative extent of stripping on the PEM coating was not as large as it was with the DNA probes. This observation provides significant information regarding the affinities of the DNA and protein probes with the PEM surface. Specifically, the PAC wash stripped a greater percentage of DNA probes in comparison to the protein probes on the PEM surface, indicating that the PEM coating has a weaker affinity with the DNA probes than it does with the antibody probes. In terms of microarray assay development, this result suggests that the experimental design used here may be more compatible with protein microarray applications than DNA microarray applications, as the protein probe immobilization densities were largely unaffected by the inclusion of PAC in the wash solution.

In terms of assay performance, the reductions in probe density created by the PAC wash will have profound negative effect upon both the target signal response and detection range. For instance, assuming that a probe spot with a specific diameter contains a total of 100 receptors, then the theoretical detection range could potentially be between 1 and 100 target molecules. On the other hand, a probe spot of the same diameter which only has 10 receptors would have a theoretical target detection range between 1 and 10. As shown in Figure 4.4, the PAC wash had an overall negative impact upon the probe immobilization densities. In most cases, the PAC served to strip probe molecules

from the surface, however, differential extents of probe stripping were observed depended upon the probe compound and the surface coating, suggesting that the compatibility of the PAC wash will vary depending on the microarray platform and assay design.

It should be noted that a PBST wash was not performed on the OPD coating. Therefore, the extent of probe stripping due to the PAC wash cannot be determined from the datapoints in Figure 4.4. It is possible, however, to compare the probe signal intensities generated on the PAC-washed OPD coating to those generated on the PBST-washed PD coating to determine whether the OPD coating provides any improvement upon the native PD coating in terms of probe immobilization density. Assuming multilayer assembly occurred on the PD coating, the OPD surface should possess significantly more amine groups than the native PD coating and provide a viable surface for the immobilization of protein and DNA probes. To investigate this, the probe signal intensities generated on the OPD coating (Figure 4.4) were compared to those on the PD coating (Figure 3.5). Previously, it was determined that the PD was incapable of DNA immobilization, as indicated by the probe signal intensities plotted in Figure 3.5. In Figure 4.4, though, some extent of DNA probe immobilization can be seen on the OPD coating. Although relatively low DNA probe signal intensities were generated on the OPD coating, this result indicates a significant improvement upon the native PD coating, which showed no DNA probe immobilization. An even greater improvement is seen on the OPD coating in regard to the protein probe immobilization densities. Going back to Figure 3.5, the PD coating showed very low immobilization densities with both the anti-IgG and anti-Myo probes. The OPD coating, on the other hand, generated relatively large signal responses of over 10,000 and 5,000 for the anti-IgG and anti-Myo probes, respectively. This result demonstrates the ability to optimize and fine-tune the surface properties of a multifunctional SI surface coating to suit a specific application, satisfying a key objective established in the Chapter 1.

4.4.1.2   Probe Background Intensity

Previously in Section 3.6.1.2, analysis of the probe background intensities and probe background intensity SDs shown in Figures 3.6A and B respectively, revealed a significant extent of fluorescence due to the presence of probe compounds outside the spot circle. Also, the extent of background intensity and background intensity SD was significantly

different depending on the surface coating and probe compound examined. Ultimately, it was determined from the images in Figure 3.7 that the source of this background fluorescence was due to the presence of probe comet tails which were created during the wash step performed immediately after probe spotting. To combat this problem, PAC was introduced into the wash solution with the hope that it would minimize the extent of comet tails.

To determine whether the PAC wash had any effect upon comet tails, the probe background intensities and background intensity SDs generated on the PAC-washed platforms were compared to those generated on the PBST-washed platforms. In order to make a direct comparison between the two experimental designs, the probe background intensities and background intensity SDs generated on the PAC-washed platforms were calculated in the same manner used to calculate those obtained on the PBST-washed platforms, explained previously in Section 3.6.1.2. In Figure 4.5A and B, the intensity values generated on the PAC-washed platforms were overlaid directly onto those obtained with the PBST-washed platforms to simplify comparison between the two experimental designs.
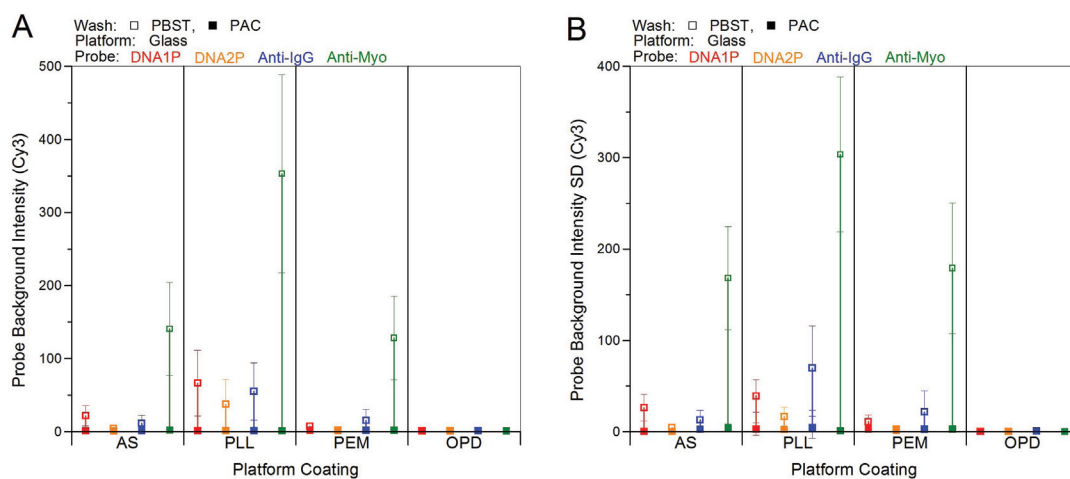
FIGURE 4.5: Effect of the PAC wash and OPD coating on the probe background intensity (graph A) and probe background intensity SD (graph B) generated on each surface coating. The □ datapoints represent values obtained on the PBST-washed platforms, while the ■ datapoints represent those obtained on the PAC-washed platforms.

As shown in Figures 4.5A and B, the PBST wash generated significantly different levels of background and background SDs between surface coatings and probe compounds, as shown by the □ datapoints. As shown by the ■ datapoints, on the other

hand, the inclusion of PAC into the wash solution eliminates virtually all background intensity and background intensity SD on each coating and with all probes, indicating little or no presence of Cy3-labeled probes outside the spot circles. This result suggests that the inclusion of PAC into the wash solution significantly reduces the extent of comet tail formation during microarray fabrication.

4.4.1.3 Effect of PAC Wash on Comet Tails

To verify whether the reduced probe background intensities and background intensity SDs observed in Figure 4.5 A and B were due to a reduction in the probe comet tails, each PAC-washed platform was rescanned at the maximum PMT setting of 100 in order to increase the fluorescence sensitivity. The images in Figure 4.6 show typical microarrays printed onto each surface coating and washed with the PAC solution. For comparison, microarrays washed with the PBST solution are also shown.
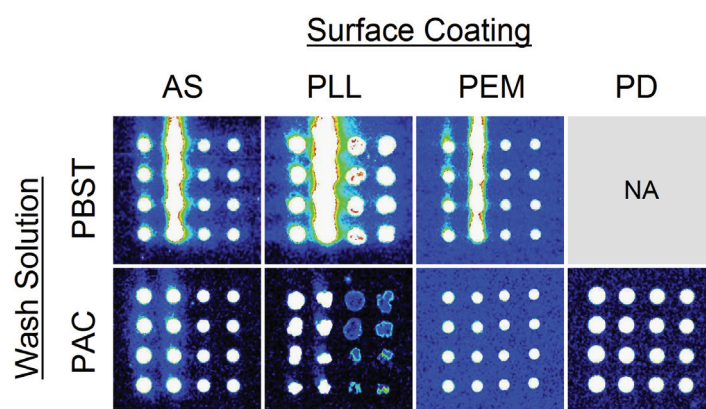
FIGURE 4.6: Effect of the PAC wash on probe comet tails. Fluorescent images of typical arrays printed onto each surface coating (columns) then scanned using a wavelength of 543nm at a PMT setting of 100%. The PBST-washed platforms are shown in the top row, while the PAC washed platforms are shown in the bottom row.

In Figure 4.6, a significant reduction in probe comet tails is observed on the PAC-washed platforms in comparison to the PBST-washed platforms. Specifically, images which depict the PBST-washed platforms show high fluorescence intensities around the probe spots in comparison to the intrinsic background fluorescence generated by the platforms themselves. When utilizing the PAC wash, however, the fluorescence intensities around the probe spots are significantly reduced or eliminated altogether, resulting

in a background fluorescence closer to the intrinsic background fluorescence generated by the platforms.

In terms of assay performance, this result exemplifies a situation where a new experimental variable decreases performance of one assay parameter but improves another. For example, it was determined in Section 4.4.1.1 that the inclusion of PAC into the wash solution typically results in reduced probe immobilization densities, which will ultimately generate lower target signal responses. However, the PAC wash also serves to reduce the extent of comet tail formation, which will result in significantly increased target S/N ratios.

4.4.2 Target Analysis

4.4.2.1 Target Signal Intensity

Figure 4.7 shows the effect of the PAC wash on the target responses. The datapoints plotted in Figure 4.7 were obtained from Figure 4.3D, which represented the target fluorescence intensities generated by the Cy5-labeled compounds. To simplify analysis, the datapoints were grouped and sorted in the same manner used to generate Figure 3.8, described previously in Section 3.6.2.1.

Graphs A-D in Figure 4.7 represent the Cy5 fluorescence signal intensities generated by the single target sample solutions containing 100nM of either DNA1T, DNA2T, IgG, or Myo, respectively. Graph E represents the signal intensities generated by a mixed target sample containing 100nM of each target, and graph F shows the response generated by a blank sample containing no targets. In each graph, the □ datapoints represent the PBST-washed platforms while the ■ datapoints represent the PAC-washed platforms.

Previously in Figure 4.4, it was revealed that the PAC wash typically stripped probe from the surface, resulting in lower probe densities. Because lower probe densities were observed on the PAC-washed platforms, it was expected to see decreases in the target signal response as well. As shown in Figure 4.7, this was indeed the case. In Figures 4.7A-E, the PAC-washed platforms show lower overall target signal intensities in comparison to the PBST-washed platforms. For example, looking at the leftmost
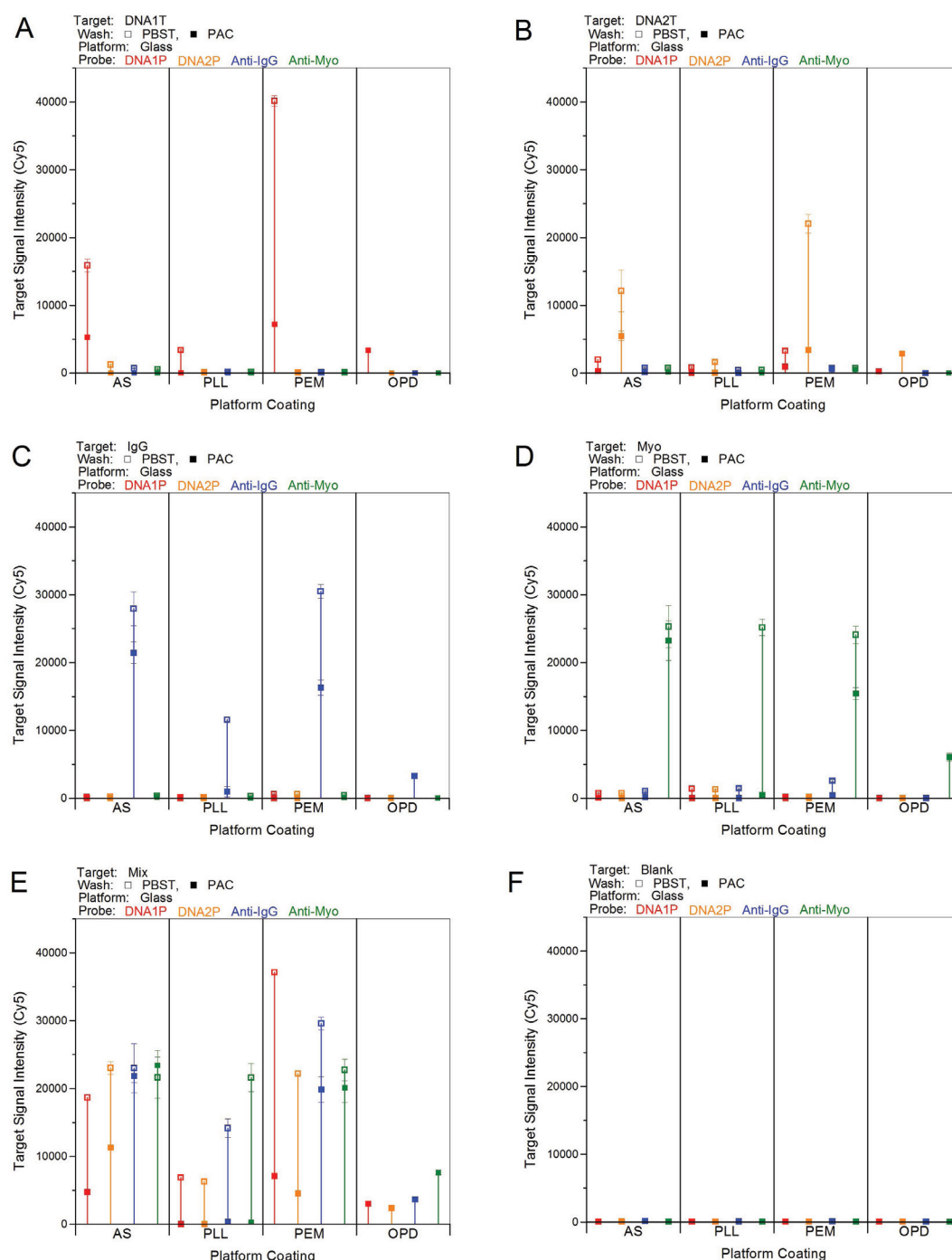
FIGURE 4.7: Effect of the PAC wash and OPD coating on the target signal intensities generated by each target sample solution. The □ datapoints represent values obtained on the PBST-washed platforms, while the ■ datapoints represent those obtained on the PAC-washed platforms. Graphs A-D represent the target responses generated by the 100nM Cy5-labeled single target samples DNA1T, DNA2T, IgG, and Myo, respectively; graph E represents the target responses generated by the mixed sample containing 100nM of each Cy5-labeled target; and graph F represents the target responses generated by a blank sample containing no target compounds.

□ and ■ datapoints in Figure 4.7A, the fluorescence signal response generated by the DNA1 target sample on the AS-coated platform can be seen. In this case, the PBST-washed platform generated a signal response just over 15,000. When utilizing the PAC wash, however, the target signal response drops to a value of about 5000, roughly 66% lower. In terms of performance, this reduction of the target signal intensities represents a significant drawback with the inclusion of the PAC wash in the assay design.

In Figure 4.7A, reduction of the DNA1 probe signal response due to the PAC wash was also observed on the PEM coating. In this case, however, the signal reduction was significantly larger. Specifically, the PBST-washed platform generated a DNA1 target response of around 40,000, whereas the PAC-washed platform generated a target response of around 7,500, roughly 81% lower. This result suggests that the effect of PAC upon the target signal responses is highly influenced by a platforms surface properties. In this case, a significantly larger reduction in the DNA1 target response was observed on the PEM coating in comparison to the AS coating.

In addition to platform-dependent factors, reduction of the target signal responses was also found to be dependent upon the probe/target pair. For example, the PAC-washed AS coating was found to generate a DNA1 target response 66% lower than on the PBST-washed AS coating. When looking at the IgG target responses in Figure 4.7C, though, a smaller reduction is seen on the PAC-washed AS coating. In this case, the IgG target signal response was only reduced by 23%. This result indicates that different probe/target pairs on the same platform will react differently to new variables introduced into the experimental design. The differential reduction in the target signal responses due to both platform-dependent and probe/target pair-dependent factors illustrate a further complexity which must be considered when developing, comparing, and validating new microarray technologies.

Figure 4.7 also provides significant information regarding the effect of the OPD coating on the target signal intensities. Previously in Figure 3.8, it was found that the PBST-washed PD coating did not generate any detectable DNA target response. Furthermore, the protein target responses on the PD coating were rather poor in comparison to the other coatings. On the PAC-washed OPD coating, however, detectable signal intensities were generated by both the DNA and protein targets, as shown in Figure 4.7. In comparison to the PAC-washed AS and PEM coatings, however, the OPD

coating typically generated significantly lower target signal responses.

Despite the comparatively low target signal responses on the OPD coating, though, this result clearly demonstrates the ability to modify the PD surface properties and significantly improve assay performance for both DNA and protein microarray applications. Additionally, because the PD coating is a multifunctional surface, sustainable development and optimization of its surface properties for multianalyte microarray applications should be possible through alternative modification methods, satisfying a key objective established in Chapter 1. More importantly, developments made on platforms which utilize the PD coating should be transferable onto a range of other platforms, as the PD is a SI surface coating. This ability will be investigated later in Chapter 5.

4.4.2.2 Effect of PAC Wash on Target Specificity

In the previous experimental design, significant cross-reactivity was observed between the DNA1 probe and the DNA2 target on the AS and PEM-coated platforms when using the PBST wash, as shown in Figure 3.8. Here, the effect of the PAC wash on this cross-reactivity will be examined.

Here, specificity will be defined as the ratio of a target's signal response on a different probe (unspecific receptor) to the target signal response generated on its probe partner (specific receptor). Ideally, the value of this ratio is close to zero, which would indicate little or no cross-reactivity. To examine specificity, the unspecific/specific target signal response ratios were analyzed from the target signal responses plotted in Figure 4.7. For example, calculated from the leftmost □ and □ datapoints in Figure 4.7B, the DNA2 target generated a DNA1P/DNA2P signal response ratio of 0.16 on the PBST-washed AS-coated platform, indicating that the DNA2 target generates a signal response on the DNA1 probe 16% in magnitude of what it generates on its binding partner, the DNA2 probe. On the PAC-washed AS-coated platform, calculated from the leftmost ■ and ■ datapoints, the same ratio was only 0.05, indicating that the DNA2 target generates a signal response on the DNA1 probe 5% in magnitude of what it generates on its binding partner, the DNA2 probe. This result suggests that the inclusion of PAC into the wash solution improves the specificity of the DNA1 probe on the AS surface, reducing the cross-reactivity signal response with the DNA2 target from 16% to 5%.

While specificity of the DNA1 probe was significantly improved by the PAC wash on the AS coating, the same improvement was not observed on the PEM coating. In this case, the DNA2 target generated a DNA1P/DNA2P spot fluorescence ratio of 0.14 when using the PBST wash. When utilizing the PAC wash, however, the DNA1P/DNA2P spot fluorescence ratio nearly doubles to a value of 0.27, indicating that the PAC wash has a profound negative impact upon the specificity of the DNA1 probe on the PEM coating.

These findings indicates that the PAC wash increases the DNA1 probe specificity on one platform but decreases it on another, demonstrating how a newly introduced variable can have a significantly different impact upon a specific performance parameter depending on the platform used. This result illustrates how microarray assay improvements reported in the literature may often be specific to the platform investigated and not a general improvement applicable to other platforms. In terms of microarray development, this result represents another factor which impedes the ability to transfer and build upon previously reported findings, thereby limiting the developmental rate of microarray technology.

4.4.2.3 Probe/Target Affinity

When comparing the probe signal intensities in Figure 4.4 to the target signal responses in Figure 4.7, some unexpected observations can be seen. For example, the signal intensities of the DNA1 probe on the AS coating, represented by the leftmost □ and ■ datapoints in Figure 4.4, were very similar on both the PBST and PAC-washed platforms, indicating that that PAC wash stripped very little DNA1 probe from the AS-coated platform. Based on that observation, it was expected to see very similar DNA1 target responses as well. As shown in Figure 4.7, however, the DNA1 target response on the AS coating is significantly lower on the PAC-washed platform in comparison to the PBST-washed platform, suggesting a reduction in the DNA1 probe/target affinity due to the PAC wash. To investigate this observation further, the effect of the PAC wash on the probe/target affinities was analyzed.

Previously, in Section 3.6.2.3, the probe/target affinities were compared on the PBST-washed platforms using their Cy5/Cy3 signal ratios. Additionally, the effect of the sample composition on the probe/target affinities was investigated by comparing

the affinities generated when using a single target sample versus a mixed target sample. From that investigation, it was found that the sample composition had little effect upon the probe affinities on the PBST-washed platforms, as shown by the □ datapoints (individual target samples) and the ⊠ datapoints (mixed target sample) in Figure 3.9. These affinity values are replotted in Figure 4.8, along with the affinity values obtained on the PAC-washed platforms, to determine the effect of the PAC wash on this performance parameter.
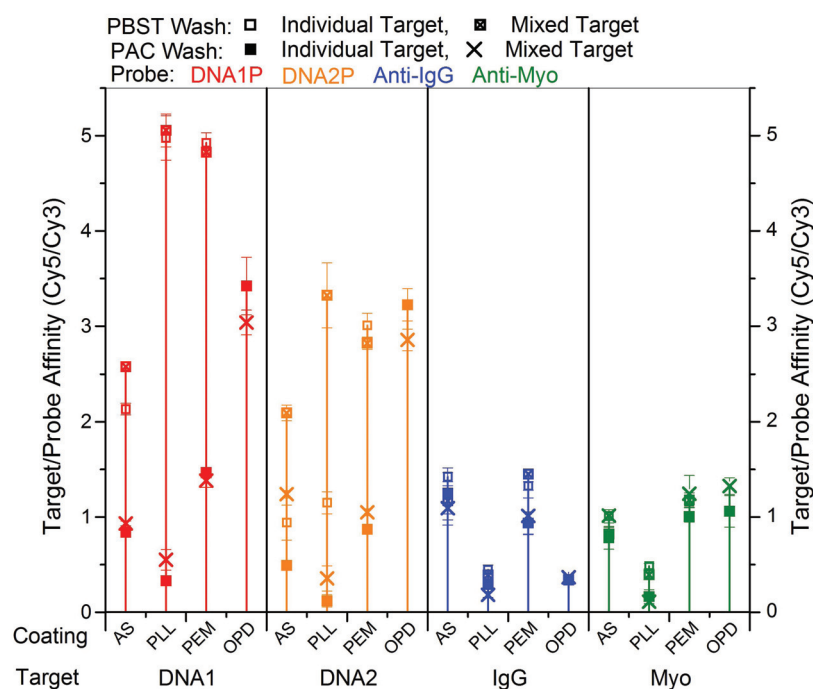
FIGURE 4.8: Effect of the PAC wash and OPD coating on the probe/target affinities generated on each surface coating. The affinity of each probe/target pair was calculated using the ratio of the target signal intensity to the probe signal intensity (Cy5/Cy3). The □ datapoints represent the affinities generated with the single target sample on the PBST-platforms, while the ⊠ datapoints represent the affinities generated with the mixed target sample on the PBST-washed platforms. The ■ datapoints represent the affinities generated by the single target samples on the PAC-washed platforms, while the × datapoints represent the affinities generated by the mixed target sample on the PAC-washed platforms.

Similar to the PBST-washed platforms, the PAC-washed platforms show relatively small changes in affinity due to differences in the sample composition, as shown by the ■ datapoints (individual target samples) and the × datapoints (mixed target sample). When comparing the affinities between the PBST and PAC-washed platforms, however, significant affinity changes are observed with some probe/target pairs, but not others. Specifically, the PAC wash generated significantly lower affinities for both DNA probe/

target pairs (■ and ■ datapoints) on the AS, PLL, and PEM coated platforms. On the other hand, the affinities of the protein probe/target pairs on the PAC-washed platforms (■ and ■ datapoints) showed little or no change with respect to those generated on the PBST-washed platforms. This result illustrates another example of the differential effect a newly introduced variable will have upon different probe/target pairs. In this case, the binding affinity of the protein probe/target pairs appear largely unaffected by the presence of PAC. However, those of the DNA probe/target pairs are significantly diminished.

In terms of performance, the OPD coating provided the highest affinities for the DNA1, DNA2, and anti-IgG probe compounds. The DNA probe/target pair affinities, in particular, were significantly higher than those obtained on the AS and PEM coatings. This result illustrates pros and cons with use of the OPD coating. On one hand, the PAC-washed OPD coating immobilizes significantly less DNA probe in comparison to the PAC-washed AS and PEM coatings. On the other hand, the DNA probe which does immobilize onto the OPD coating shows an affinity value over two times greater than that obtained on the PAC-washed AS and PEM coating, as shown in Figure 4.8. In regard to microarray technology development, these performance compromises further illustrate why there is no ideal microarray surface chemistry or assay methodology, but rather, the ideal platform design and assay conditions will vary depending upon desired application and end goal.

4.4.2.4   Target Background

As discussed in Section 3.6.2.5, it is typically desirable to minimize target NSB onto the platform surface, as lower NSB provides a lower the theoretical detection limit. Using the previous assay design in Chapter 3, differential levels of NSB were observed on the PBST-washed platforms depending on the platform coating and target compound, as shown in Figure 3.11. Here, the target background intensities generated on the PAC-washed platforms are examined to determine the effect of the PAC was on target NSB. The target background intensities are plotted in Figure 4.9, where the □ datapoints represent the fluorescence generated on the PBST-washed platforms and the ■ datapoints represent the fluorescence generated on the PAC-washed platforms. Each graph in Figure 4.9

was generated in the same manner used to generate the graphs in Figure 3.11, Section 3.6.2.5.

In Figure 4.9, significant reductions in the target background fluorescence are observed when utilizing the PAC wash, indicating relatively low target NSB. In most cases, the background intensities are reduced to values approaching zero on every platform and with each target sample, aside from a few exceptions. For example, when using the DNA2 target (Figure 4.9B), the PEM coating generated background intensities of around 600 when using the PBST wash, as shown by the □ datapoints. When utilizing the PAC wash, the background intensities drop, but only to 300, as shown by the ■ datapoints. As shown in Figure 4.9E, the mixed target sample also generated unwanted background fluorescence on the PAC-washed AS and PEM coating, however, the extent of fluorescence is significantly lower in comparison to that generated on the PBST-washed platforms.

The reductions in target background intensity observed on the PAC-washed platforms indicate that this new variable introduced into the experimental design effectively minimizes both probe comet tails and NSB of DNA and protein target compounds. In terms of microarray development, the inclusion of PAC in the wash step may prove highly beneficial for microarray applications which require minimal target NSB. Also, this variable can most likely be further improved upon by modifying the wash solution in terms of pH, salinity, or the additive itself in order to minimize its negative impact upon the probe immobilization densities and probe/target affinities, which were observed previously in Figures 4.4 and 4.8.

It should be noted that the advantages and disadvantages of newly introduced variables, such as the PAC wash, will be different depending on the surface properties of the platform, as shown throughout this chapter. Therefore, the effects of new variables will not be interchangeable on platforms with differing surface properties. When utilizing SI surface coatings, however, the effect of new variables, both positive and negative, should be identically interchangeable between platforms. The ability to interchange variables between platforms is a primary reason why broad utilization of SI surface coatings would enable more rapid development, advancement, and validation of microarray technology.
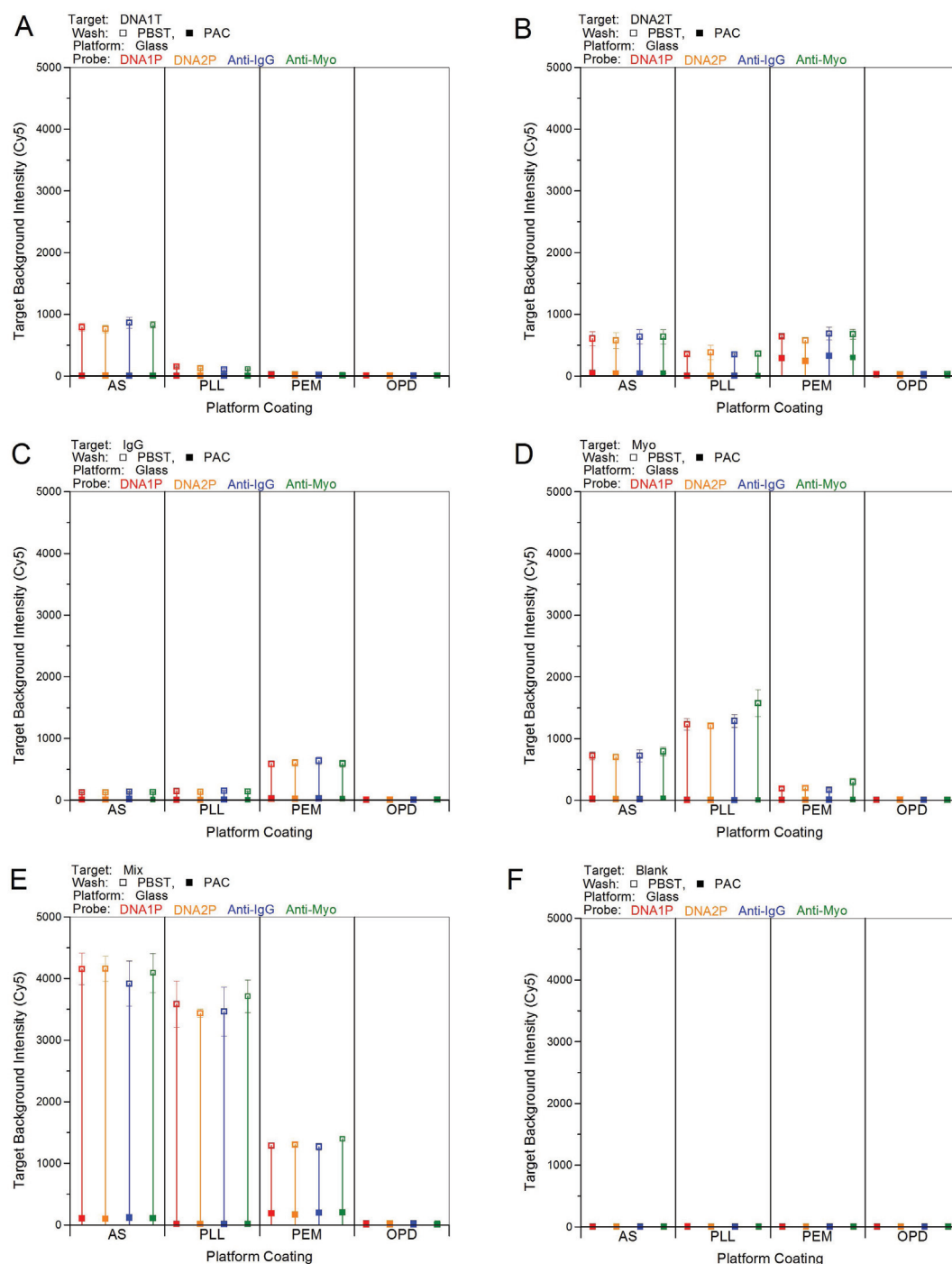
FIGURE 4.9: Effect of the PAC wash and OPD coating on the target background intensities generated by each target sample solution as a result on NSB. The □ datapoints represent values obtained on the PBST-washed platforms, while the ■ datapoints represent those obtained on the PAC-washed platforms. Graphs A-D represent the target background intensity generated by the 100nM Cy5-labeled single target samples DNA1T, DNA2T, IgG, and Myo, respectively; graph E represents the target background intensity generated by the mixed sample containing 100nM of each Cy5-labeled target; and graph F represents the target background intensity generated by a blank sample containing no target compounds.

4.4.2.5 S/N

Previously in Section 3.6.2.7, the S/N ratios on the PBST-washed platforms were calculated using Equation 3.1. Here, the effect of the PAC wash and OPD coating on the target S/N ratios is investigated. Going back to Figure 4.3D it was found that the PAC-washed platforms typically generated lower target signal responses than their PBST-washed counterparts. Because the target signal intensities form part of the numerator of Equation 3.1, a reduction in their value will serve to reduce the S/N ratio. However, the PAC-washed platforms also generated significantly lower target background intensity SDs, as shown in Figure 4.3F. Because background intensity SD is the sole component of the denominator in Equation 3.1, a reduction in their value will significantly increase the S/N ratio.

The impact of the PAC wash on the target S/N ratios can be seen in Figure 4.10, where the □ datapoints represent the target signal intensities calculated on the PBST-washed platforms and the ■ datapoints represent those calculated on the PAC-washed platforms. In Figure 4.10, positive and negative changes in the target S/N ratios are observed when utilizing the PAC wash. For example, the DNA1 target S/N ratio on the AS coating is significantly increased on the PAC-washed platform in comparison to the PBST-washed platform, as shown in Figure 4.10A. This increase in the DNA1 target S/N ratio on the AS coating when utilizing the PAC wash can be attributed primarily to the reduction in the background SD. As shown previously in Figure 4.3F, the DNA1 target generated a background intensity SD of around 100 on the PBST-washed AS-coated platform. On the PAC-washed AS-coated platform, however, the background intensity SD was close to zero, resulting in a significantly increased S/N ratio for the DNA1 target.

Although an increase in the DNA1 target S/N ratio was observed on the PAC-washed AS-coated platform, the reverse effect was observed on the PEM-coated platform. As shown in Figure 4.10A, the PAC-washed PEM-coated platform generated a significantly lower DNA1 target S/N ratio in comparison to that observed on the PBST-washed platform. In this case, the decreased DNA1 target S/N ratio can be attributed to a combination of reductions in the DNA1 probe immobilization density, target response, and probe/target affinity, as shown in Figures 4.4, 4.7, and 4.8, respectively.
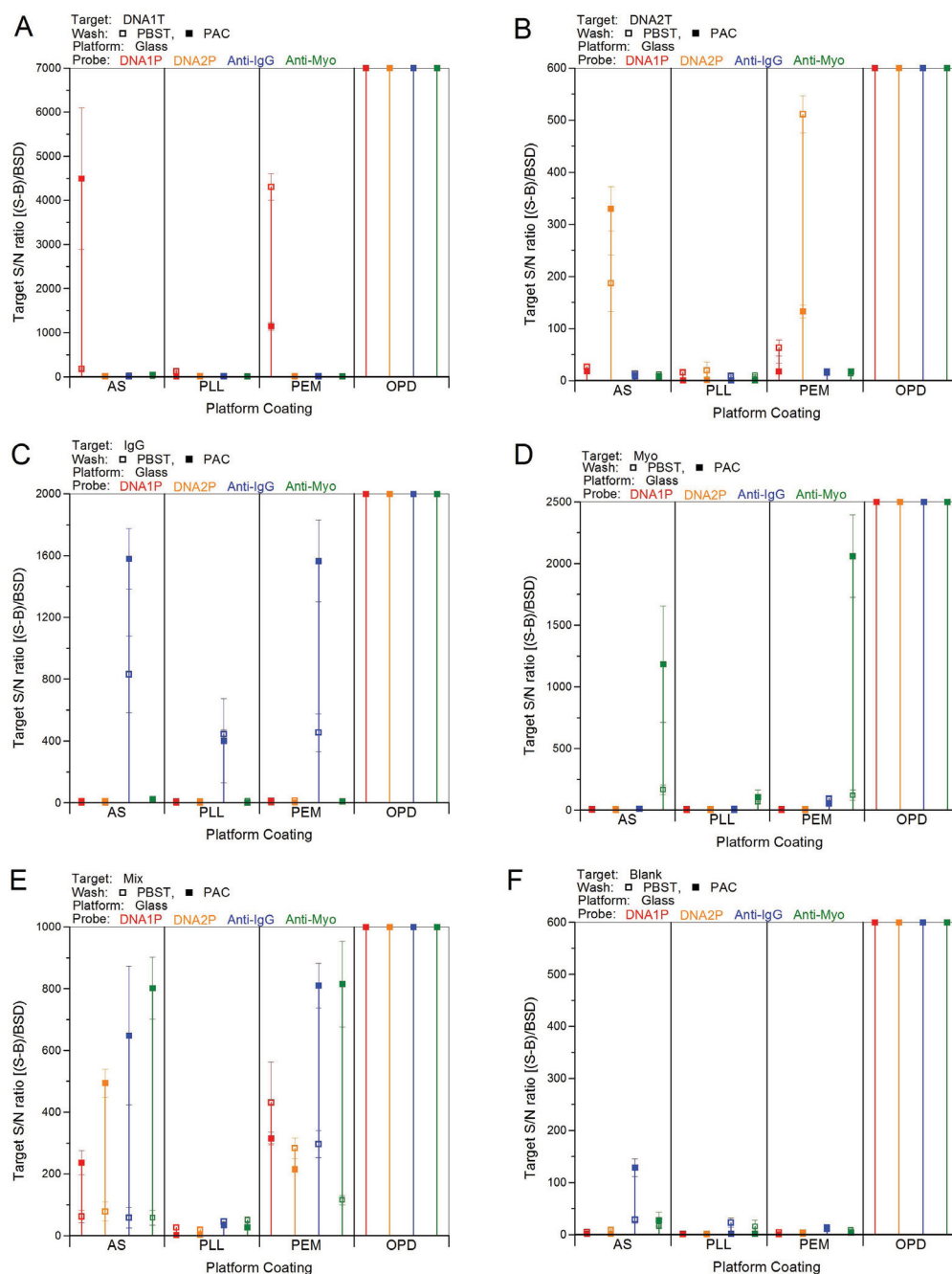
FIGURE 4.10: Effect of the PAC wash and OPD coating on the target S/N ratios calculated using Equation 3.1. The □ datapoints represent values obtained on the PBST-washed platforms, while the ■ datapoints represent those obtained on the PAC-washed platforms. Graphs A-D represent the S/N ratios generated by the 100nM Cy5-labeled single target samples DNA1T, DNA2T, IgG, and Myo, respectively; graph E represents the S/N ratios generated by the mixed sample containing 100nM of each Cy5-labeled target; and graph F represents the S/N ratios generated by a blank sample containing no target compounds.

When comparing Figures 4.10A and B, a similar trend between the AS and PEM platforms is observed regarding the DNA2 target S/N ratios. Specifically, an increased S/N ratio is observed on the AS coating, while a reduction is seen on the PEM coating. The results in Figures 4.10A and B illustrate a scenario where a newly introduced variable reverses performance between two different platforms. In this case, the best performance in terms of target DNA S/N ratios was provided by the PEM coating when using the PBST wash. When utilizing the PAC wash, though, the AS-coated platform provided the best performance. This situation represents a further obstacle preventing more rapid co-development between microarray platforms and assay design. Specifically, this finding demonstrates how a performance enhancement developed on one platform may serve to reduce performance on other platforms, bringing forth a scenario where it may be more beneficial to adopt a common, industry-wide platform to enable more rapid assay development. This solution, however, would stagnate future development in terms of platform design. To overcome this limitation, however, the use of a SI surface coating could be employed, which should enable co-development between microarray platforms and assay design.

Moving down to Figures 4.10C and D, the effect of the PAC wash on the protein target S/N ratios can be seen. In this case, significant increases in the S/N ratios are observed on both the AS and PEM-coated platforms when utilizing the PAC wash. Unlike the DNA targets, which showed increases in the S/N ratios on one platform but reductions on the other, the protein targets S/N ratios are increased on both platforms when utilizing the PAC wash, indicating that the PAC wash may be more compatible with protein microarray applications than DNA microarray applications.

Figures 4.10 A-D show the target S/N ratios generated by single target samples, designed to investigate assay performance in a single analyte microarray format. In Figure 4.10E, the S/N ratios generated in a multianalyte format can be seen when using the mixed target sample. In a multianalyte format, significant improvements in the S/N ratios are observed on the AS coating with all four target compounds when utilizing the PAC wash. In regard to the PEM coating, however, the S/N ratios were not improved with every target compound. Specifically, the protein target S/N ratios were considerably improved, whereas the DNA target S/N ratios were slightly reduced. Taking all four targets into account, though, the PAC wash provided an overall improvement in the S/N ratios on the AS and PEM coating in a multianalyte format.

Another significant observation seen in Figure 4.10 is the very large S/N ratios generated on the OPD coating. These large S/N ratios represent a limitation with both the experimental design and the S/N ratio formula defined by Equation 3.1. Because the background intensity SD represents the only component of the denominator, background SD values which approach zero will generate S/N ratios approaching infinity. In this experimental design, all platforms were scanned at a fixed PMT of 55 in order to avoid saturated signals and enable direct comparison between the fluorescence images in Figures 3.2 and 4.2. At this PMT setting, however, the PAC-washed OPD coating generated background SDs approaching zero, resulting in extremely large S/N ratios for all probe spots. Due to this limitation with the use of Equation 3.1, the S/N ratios on the OPD coating can not be utilized as an accurate performance parameter to characterize assay performance. It should be noted that this limitation can typically be overcome by increasing the PMT setting to boost the scanning sensitivity. This measure was not taken, however, as it would have prevented the ability to make a direct comparison between datasets obtained with the OPD coating and the other coatings.

4.5 Summary of New Variables Effect on Multianalyte Microarray

Analysis of the datasets in Figure 4.3 provided significant information regarding the impact of newly introduced experimental variables on different platforms and probe/target pairs. In this case, PAC was introduced into the wash solution with the hope of reducing probe comet tails and target NSB. Although these goals were achieved, the PAC wash typically reduced probe immobilization densities and probe/target affinities, especially on the PLL-coated platform. Despite these reductions in probe density and affinity, however, the PAC-washed AS and PEM-coated platforms provided the best performance in terms of S/N ratio in a multianalyte assay format, as shown in Figure 4.10E.

In regard to meeting the objectives established in Chapter 1, these results demonstrate the ability to improve microarray performance parameters on SI coatings through modification of the experimental design. For instance, utilization of the PAC wash significantly improved the S/N ratios of the protein targets on the PEM coating. It should

be noted, though, that the ability to improve assay performance is not characteristic to just SI surface coatings. For example, it was found that the PAC wash also increased the S/N ratios on the AS coating, with both DNA and protein targets. In regard to the AS coating, however, this performance enhancement will not be transferable to other platforms with the same results, as the AS is a substrate-specific (SS) surface coating. The use of SI surface coatings, on the other hand, provide a unique advantage in that performance enhancements developed on them should be identically interchangeable onto a range of platforms.

The results in Chapter 4 also provide significant information regarding the ability to tailor the functionality of SI surface coatings to perform specific applications. In Chapter 3 it was reported that the PD coating was incapable of performing DNA microarray applications and rather poor with protein microarray applications due to low probe immobilization densities. In this chapter, modification the PD surface with a PAH(PSS/PAH) multilayer system enabled the ability to immobilize larger densities of both DNA and protein probes. Furthermore, these immobilized probes went on to generate significant target signal responses, demonstrating the ability to tailor the surface properties of the PD coating to perform complex multianalyte microarray applications. Also, because the PD is a SI surface coating, modifications made to its surface properties in order to tailor and optimize the microarray assay application should be transferable to other platforms with similar results. This ability was investigated and the results are reported in the next chapter.

Chapter 5

Cross-Platform Microarray Dataset Concordance

5.1   Introduction

In Chapters 3 and 4, multianalyte microarrays were fabricated on glass platforms modified with conventionally used SS surface coatings (AS and PLL) and with multifunctional SI surface coatings (PEM and PD) in order to compare assay performance between coating types. The results in Chapter 3 showed that assay performance was significantly better on the AS and PEM coatings than on the PLL and PD coatings. In regard to the PD coating, however, it was found that assay performance could be improved upon through chemical modification of its surface, as demonstrated in Chapter 4. Furthermore, because the PD and PEM coatings are SI, it was predicted that the assay performances obtained on these surfaces would be interchangeable with other platforms. To test this hypothesis, different platform materials were introduced into the experimental design in order to compare the extent of cross-platform concordance achievable when utilizing SI surface coatings versus SS surface coatings.

5.2 Sources of Cross-Platform Dataset Discordance

The use of different microarray platforms introduces many complexities which negate the ability accurately compare inter-laboratory and cross-platform datasets[75]. Cross-platform dataset discordances can arise from virtually any aspect of the experimental design. In addition to intrinsic differences in the platforms themselves[37–39], sources of discordance commonly attributed to limiting the extent of cross-platform dataset agreement are the use of different probes, references, assay protocols, and analysis techniques[43–45]. In the experimental design reported here, common probes, references, assay protocols, and analysis methods were used with all the microarray platforms investigated. Since these aspects of the experimental design were kept consistent, they can be considered standardized, and therefore were not considered as variables contributing to cross-platform dataset discordance.

One source of possible cross-platform discordance in this experimental design lies with the method of detection. Specifically, the detection method is based on the use of a PMT to capture the fluorescence emission of excited dye-labeled compounds bound to a platform's surface. Use of this detection method can elucidate differences in autofluorescence and fluorescence interference on different platforms.

5.2.1 Intrinsic Platform Fluorescence

Typically, dissimilar platforms exhibit different intrinsic autofluorescence when exposed to light. To investigate these differences in autofluorescence, glass, polymer, and silicon platforms were scanned at multiple PMT settings to examine the autofluorescence generated by each material. Furthermore, two different scanning wavelengths were used to examine the extent of autofluorescence generated at different wavelengths. Specifically, wavelengths of 543nm and 633nm were used, as these are the same wavelengths used to excite the fluorescent dye-labeled compounds utilized throughout this thesis. The autofluorescence data generated by these scans are plotted in Figure 5.1, where the green axis correspond to the green curves and the red axis corresponds to the red curves. In Figure 5.1, the green curves represent the autofluorescence generated on each platform using a LP of 100%, a PMT range between 50% and 100%, and a wavelength of 543nm; while the red curves represent those obtained using the same settings but at

a wavelength of 633nm. It should be noted that the lower and upper X-axis scales are reversed in order to ease visual discrimination between scans obtained at 543nm and 633nm, respectively.
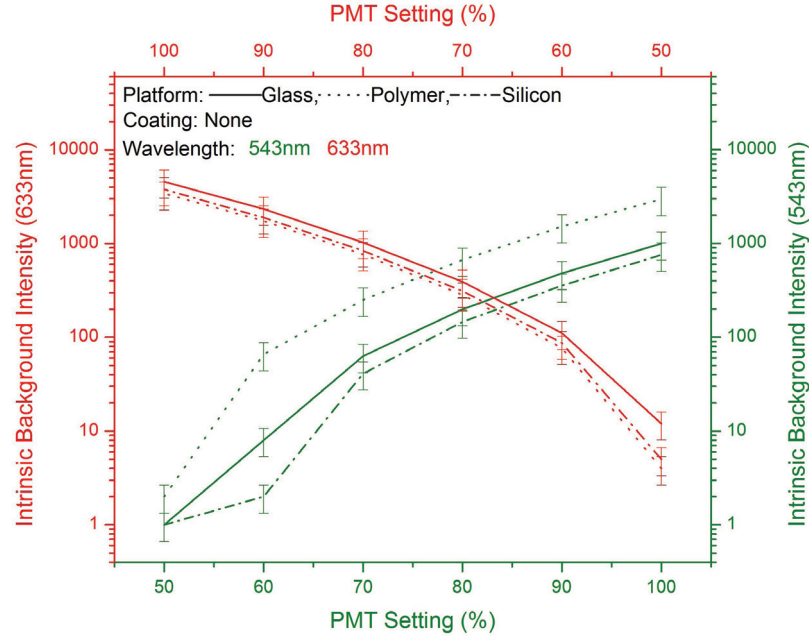
FIGURE 5.1: Intrinsic autofluorescence generated by glass, polymer, and silicon platforms using a LP of 100%, two different scanning wavelengths, and a range of PMT settings. The green axis and curves correspond to scans performed at a wavelength of 543nm, while the red axis and curves correspond those performed at 633nm. The upper and lower X-axis scales are reversed to ease visual discrimination between the fluorescence curves generated at each wavelength.

When comparing between the green and red curves in Figure 5.1, the intrinsic background intensities generated at a wavelength of 543nm are significantly lower than those obtained at 633nm. For example, at a PMT setting of 100%, the 543nm wavelength generates fluorescence intensities around 1000 on each material, whereas the 633nm wavelength generates fluorescence intensities closer to 5000. Moreover, when looking specifically at the green curves, the fluorescence intensity generated by the polymer (dotted line) is significantly larger than the fluorescence intensity generated by the glass (solid line) and silicon (dash-dot line), indicating that the polymer produces more autofluorescence at 543nm than the other two materials. This observation suggests that the extent of autofluorescence generated at a specific wavelength will vary depending on the platform material. Differences in autofluorescence between platforms were also observed when using the 633nm wavelength. In this case, however, glass generates the

highest autofluorescence and the extent of autofluorescence differences between platforms are smaller in comparison to the differences observed at 543nm. These results indicate that the extent of intrinsic autofluorescence, as expected, is both platform and wavelength-dependent.

In terms of multianalyte microarray development, these differences in autofluorescence can significantly limit cross-platform dataset agreement and complicate the ability to validate new technologies which utilize different platform materials or fluorophores. Additionally, it should be noted that these differences in cross-platform autofluorescence represent a particular source of cross-platform discordance which cannot be overcome with the use of SI surface coatings such as PEM and OPD.

5.2.2 Fluorescence Interference

In Chapters 3 and 4, all microarray assays were performed on glass platforms. Because a common platform material was used, differences in autofluorescence and fluorescence interference between each platform were minimal, and therefore, datasets obtained at a fixed scanning LP and PMT could be used to accurately compare the relative amount of Cy3 and Cy5 dye-labeled compounds across microarray platforms.

When using fluorescence detection on platforms constructed from different materials, however, the observed fluorescence of dye molecules will vary due to either constructive or destructive interference[76]. The extent of fluorescence interference will vary depending on the distance of the dye molecule from the surface and the reflectivity of the platform. These cross-platform differences in fluorescence interference can be seen in Figure 5.2.

The images in Figure 5.2 depict unwashed arrays of Cy3-labeled DNA1 probe printed onto OPD-coated glass, polymer, and silicon platforms according to the layout shown in Figure 5.3. Spots in the top row of each image were obtained by printing a 10μM solution of Cy3-labeled DNA1 probe. Each subsequent row of spots are a 2x dilution of the previous rows spotting solution. The OPD coating was utilized in order to eliminate differences in the surface properties between materials, thereby minimizing differences in the spot sizes and densities of the DNA1 probe.

The printed DNA1 probe arrays were scanned using a fixed wavelength of 543nm, LP of 100%, and PMT setting of 65%. Because microarrays were left unwashed, it was
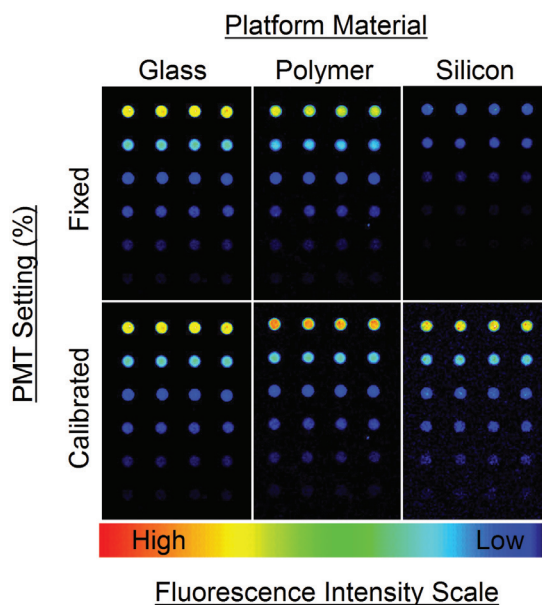
FIGURE 5.2: Identical unwashed DNA1P arrays printed onto OPD-coated glass, polymer, and silicon platforms. Images in the upper row show fluorescence scans performed at a fixed wavelength of 543nm, LP of 100%, and PMT setting of 65%; while images in the bottom row show those obtained using calibrated PMT settings. The upper row of spots in each array were obtained by spotting a $10\mu M$ solution of Cy3-labeled DNA1P, while each subsequent row was a 2x dilution of the previous rows spotting solution.
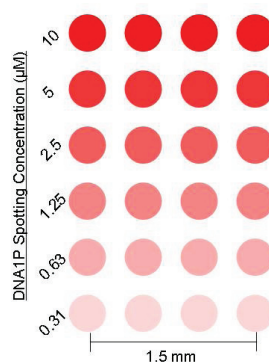
FIGURE 5.3: Layout of Cy3-labeled DNA1 probe microarrays printed onto OPD-coated platforms used to investigate cross-platform fluorescence interference

assumed that the absolute number of Cy3-labeled DNA1 probes was identical between corresponding spots on each platform. Based on this assumption, it was expected to see similar fluorescence intensities generated on each platform when scanning with a fixed PMT setting. This was not the observed result, however, as shown by the images in the top row of Figure 5.2. In particular, the silicon platform generated significantly lower fluorescence intensities than the glass and polymer platforms when scanned at a fixed PMT setting. Additionally, the polymer platform generated slightly lower fluorescence intensities than the glass platform, suggesting that each platform exhibits a different fluorescence interference.

These differences in the fluorescence interference observed on different platforms exemplifies yet another source of cross-platform discordance that cannot be overcome with the use of SI surface coatings in conjunction with fluorescence detection. It should be noted, though, that these specific sources of cross-platform discordance, associated with the use of optically-based detection methods such as fluorescence emission, can be avoided with the use of alternative detection methods. Utilization of alternative detection methods, however, may bring forth other detection-dependent sources of cross-platform discordance.

5.2.2.1 Fluorescence Scan Calibration

Although fluorescence interference can vary depending on the platform material used, this particular source of dataset discordance can be minimized with the use of a common cross-platform reference, or control, to calibrate the scanning LP or PMT. Specifically, the scanning LP or PMT can be increased or decreased relative to a defined cross-platform reference in order to compensate for dissimilar fluorescence interference on different materials. For many applications, it is desirable to use a reference which generates a signal larger than any other, in order to avoid saturation of other signals which may be of importance for analysis. For instance, a common cross-platform reference for the array layout shown in Figure 5.3 could be defined as the row of DNA1 probe spots deposited at a concentration of 10μM, as this row generated the largest fluorescence intensities. Using this spot row, the microarray scanner was calibrated by adjusting the PMT setting until the fluorescence intensity generated by these spots was 20% below saturation. Once this PMT setting was found, the microarray platforms were rescanned

using their respective calibrated PMT settings to obtain the images in the bottom row of Figure 5.2. In this case, the calibrated PMT settings for the glass, polymer, and silicon platforms were found to be 65%, 67%, and 83%, respectively.

The microarray images in Figure 5.2 were used to compare the fluorescence intensities generated on each platform when using a fixed PMT setting versus a calibrated PMT setting. For this, the images were analyzed according to the procedure described in Section 3.5. The datasets obtained from this analysis are plotted in Figure 5.4.
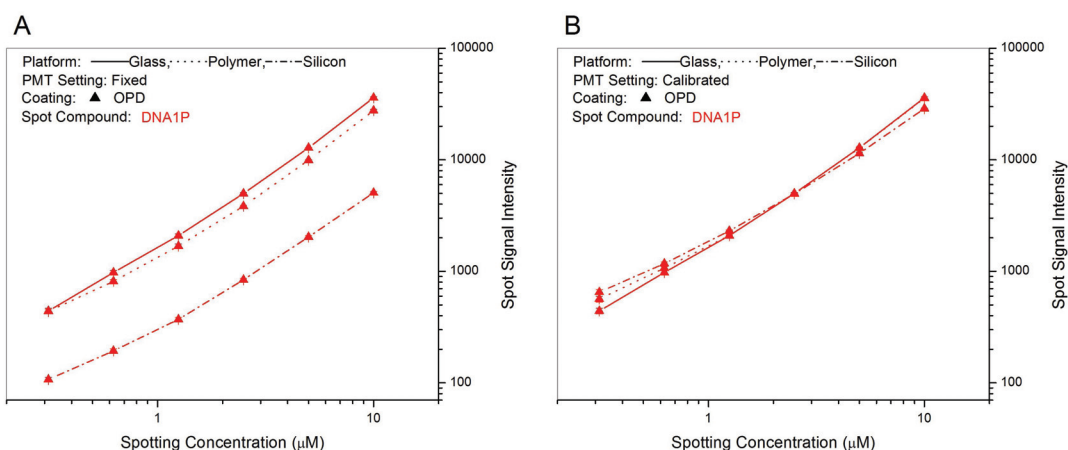
FIGURE 5.4: Fluorescence signal intensities generated by the identical unwashed Cy3-labeled DNA1P arrays printed onto the OPD-coated glass, polymer, and silicon platforms shown in Figure 5.2. Graph A shows the intensities obtained at a fixed PMT setting of 65%, while graph B shows those obtained at the calibrated PMT settings.

Each curve in Figure 5.4A represents the change in the DNA1 probe spot fluorescence intensity as a function of the spotting concentration and platform material when scanned at a fixed PMT setting of 65%. In Figure 5.4A, the lower curve represents the DNA1 probe spot intensities generated on the OPD-coated silicon (dash-dot line). When plotted on a logarithmic scale, a linear increase in the fluorescence intensity is observed on the OPD-coated silicon as the DNA1 probe spotting concentration increases. Similar linear increases in the fluorescence intensity are also observed on the OPD-coated glass (solid line) and polymer (dotted line), with curve slopes nearly identical to that obtained on the OPD-coated silicon, indicating similar rates of fluorescence increase in response to DNA1 probe spotting concentration on each platform.

While the rate of fluorescence increase appears similar on all three platforms, the absolute fluorescence intensities are not. Specifically, the fluorescence signals generated on the glass and polymer platforms are significantly higher than those obtained on the

silicon platform. Because the platform material represents the only experimental variable in Figure 5.4A, this result suggests that the silicon platform significantly reduces the observed fluorescence of the Cy3-labeled DNA1 probes. When scanning at a fixed PMT, differences in the observed fluorescence on different platform materials will ultimately result in dissimilar detection ranges. For example, increasing the DNA1 probe spotting concentration further will eventually generate saturated signals on each platform. Once saturation is reached, the fluorescence intensity plateaus and further increases in the spotting concentration cannot be detected. Fluorescence saturation will be reached at a lower spotting concentration on glass in comparison to silicon, however, as the silicon platform exhibits a lower observed fluorescence. Because saturation will be reached at a lower spotting concentration on glass, the silicon platform will have a higher concentration detection limit. Alternatively, at the other end of the concentration spectrum, decreasing the spotting concentration will eventually result in fluorescence intensities which approach zero. In this case, zero fluorescence will be reached at a higher spotting concentration on silicon, meaning that the glass platform will have a lower concentration detection limit, as the glass platform exhibits a higher observed fluorescence.

In terms of cross-platform microarray performance, intrinsic differences in fluorescence interference will result in different platforms having dissimilar theoretical target detection ranges. These cross-platform differences in observed fluorescence can be minimized, though, when utilizing a PMT setting calibrated against a common cross-platform reference. As shown in Figure 5.4B, use of the 10μM DNA1 probe spots as a common cross-platform reference generates similar absolute fluorescence intensities on all three platforms, suggesting that the cross-platform target concentration detection ranges will be more similar.

5.2.2.2   Cross-Platform Concordance

In this chapter, cross-platform dataset concordance is measured using the Pearson product-moment correlation coefficient (CC)[77]. Pearson product-moment CCs are often used to estimate the concordance between two paired datasets, or curves[38,43]. For example, if there are two datasets, X and Y, both comprising a series of n measurements written as x_i and y_i, where $i = 1, 2, \ldots, n$, then the extent of correlation between the datasets can be estimated from the equation:

$$r_{xy} = \frac{\sum(x_i - \bar{x})(y_i - \bar{y})}{(n-1)s_x s_y}, \tag{5.1}$$

where r is the CC, $\bar{x}$ and $\bar{y}$ are the sample means of X and Y, s_x and s_y are the sample SDs of X and Y, and the sum is from $i = 1$ to n. A CC of 1 calculated using Equation 5.1 indicates perfect correlation between the X and Y datasets, while a CC of 0 means there is no correlation between the datasets.

To demonstrate the use of Equation 5.1, the CCs of the curves shown in Figure 5.4 A and B were calculated. The values obtained from these calculations are shown in Table 5.1. To calculate each CC, one curve within each graph was first defined as the reference dataset (X) from which to calculate the CCs of the other datasets (Ys) in that graph. For example, the upper two values in the rightmost column of Table 5.1 represent the CCs between the fluorescence intensity curves generated on the microarray platforms when scanned at a fixed PMT setting. In this case, the fluorescence intensity curve generated on OPD-coated glass platform was defined as the reference dataset from which to calculate the CC of the datasets obtained on the polymer and silicon platforms. For consistency, the CCs of the fluorescence intensity curves obtained with the calibrated PMT settings were also calculated using the dataset obtained on the OPD-coated glass defined as the reference.

Dataset	PMT Setting	Reference Substrate	Substrate	CC
DNA1P Spot Intensities	Fixed	Glass	Polymer	1.00000
			Silicon	0.99915
	Calibrated	Glass	Polymer	1.00000
			Silicon	0.99932

TABLE 5.1: Comparison of cross-platform CCs between the DNA1P microarray fluorescence datasets obtained on platforms scanned using a fixed PMT setting versus a calibrated PMT setting. CCs were calculated from the datasets plotted in Figure 5.4 using Equation 5.1.

In Table 5.1, all CCs are above 0.999, indicating nearly perfect cross-platform correlation regardless of whether a fixed or calibrated PMT setting is used. Although the use of fluorescence detection creates differences in cross-platform autofluorescence and fluorescence interference, it was still possible to generate highly concordant cross-platform

datasets, according to the CCs calculated in Table 5.1. This result reflects both negative and positive aspects with the use of Pearson product-moment CCs as a measure of dataset concordance. On the negative side, Pearson product-moment CCs cannot be used to estimate dataset concordance in terms of absolute fluorescence intensity. For example, in Figure 5.4A the silicon platform generated significantly lower fluorescence intensities than did the glass platform when scanned at a fixed PMT setting of 65%. Despite these differences in the absolute fluorescence intensities between silicon and glass, a CC of close to 1 was still calculated, suggesting nearly perfect correlation between the two datasets. In this case, a CC close to 1 was still obtained due to similar curve shapes and slopes generated between each platform.

This limitation with the use of Equation 5.1, however, can also be considered a positive for this particular experimental design, in that it does not take into account the absolute value of the datasets, but rather, trends in the datasets. Specifically, the CCs are sensitive to changes in the fluorescence intensity in response to changes in the DNA1 probe density, but not sensitive to differences in the overall magnitude of the fluorescence intensities between the two datasets. Therefore, cross-platform dataset concordance measured with the use Pearson product-moment CCs will be largely unaffected by the fluorescence scanner settings, assuming saturated signals and zero value signals are avoided.

5.3   Cross-Platform Multianalyte Microarrays

In the previous sections of this chapter, sources of cross-platform dataset discordance were identified and methods to minimize them were discussed. Here, multianalyte assays will be performed on different platforms to determine the extent of cross-platform dataset concordance achievable when using a significantly more complex microarray design. For this, DNA and antibody probes were arrayed onto a variety of platform materials coated with either SS or SI surface coatings. These arrays were then used to perform multianalyte assays with target samples of varied concentration in order to examine the dose-response curves generated on each platform.

5.3.1 Microarray Platforms

To compare cross-platform microarray assay performance, AS, PLL, PEM, and OPD coatings were deposited onto glass, mica, silicon, and polymer substrates to provide a total of 16 microarray platforms. The use of such a diverse set of coatings and materials was deliberately chosen in order to mimic real-world and practical applications where it may be required to compare and cross-validate assay datasets obtained on dissimilar microarray platforms. The coatings were deposited onto each material using the same protocols described previously in Chapters 2 and 3.

5.3.2 Microarray Fabrication

Following deposition of the surface coatings, microarrays were fabricated onto each platform according to the procedure described in Chapter 3 and using the array layout shown in Figure 3.1. Following probe deposition, the microarray platforms were washed in PBST containing 2 mg/ml PAC according to the procedure described in Section 3.3. The PAC wash was utilized in this experimental design as it was shown to significantly reduce probe comet tails, reduce target NSB, and increase the target S/N ratios in a multianalyte assay format, as demonstrated previously in Chapter 4. Following the PAC wash, each microarray platform was blocked with BSA according to the procedure described in Section 3.3.

5.3.3 Multianalyte Dose-Response Assays

The ability to detect changes in the concentration of multiple analytes is a requirement for complex microarray applications such as gene expression profiling[3] and proteome analysis[11]. In the previous experimental designs, each sample had a fixed target concentration of 100nM in order to evaluate aspects of microarray assay performance such as target response, NSB, affinity, specificity, and S/N. Because a fixed target concentration was used, changes in assay performance due to differences in target concentration could not be investigated. In the experimental design reported here, the target concentration of each sample was varied in order to mimic real-world samples and determine whether changes in the concentration can be detected.

To perform multianalyte dose-response assays, a mixed target sample was prepared according to the procedure described in Section 3.4, except here, at a concentration of 25nM as opposed to 100nM. From this 25nM mixed target sample, a 4x dilution series was prepared to obtain a total of six samples, each of decreasing concentration. Using this set of samples, multianalyte dose-response assays were performed on each platform according to the procedure described in Section 3.4.

5.3.4   Fluorescence Scans

Following the multianalyte dose-response sample assays, each microarray platform was scanned at wavelengths of 543nm and 633nm, respectively, to measure the fluorescence intensities generated by the Cy3-labeled probes and the Cy5-labeled targets. Prior to scanning, the PMT setting was calibrated at both wavelengths for each microarray platform, in order to minimize differences in the absolute fluorescence intensity caused by the differences in cross-platform fluorescence interference identified in Section 5.2.2.

PMT calibration was performed according to the method described in Section 5.2.2.1. In this case, a common cross-platform reference was defined as the fluorescence intensity generated by a row of anti-IgG probe spots exposed to a reference sample containing 100nM of each Cy5-labeled target during the sample assays. These spots were used to calibrate both the 543nm (Cy3) and 633nm (Cy5) wavelengths. It should be noted that the reference sample was prepared at a higher concentration than the assay samples to ensure that it generated the largest fluorescence intensities, thereby avoiding saturation of other fluorescence signals.

Each wavelength was calibrated separately by adjusting the PMT setting until the fluorescence intensities of the reference anti-IgG spots were 50% below saturation with the 543nm wavelength and 20% below saturation with the 633nm wavelength. Using the calibrated PMT settings, each microarray platform was scanned to acquire the image sets shown in Appendix A. Spot analysis of these images was performed according to the procedure described in Section 3.5.

5.4 Cross-Platform Dataset Analysis

In this chapter, all aspects of the experimental design were kept consistent aside from the platform materials, surface coatings, and scanning PMTs. In regard to the scanning PMT, though, it was found that highly concordant cross-platform datasets can still be generated regardless of using fixed or calibrated PMT settings, as determined by the Pearson product-moment CCs displayed in Table 5.1. Therefore, the platform materials and surface coatings were the only variables considered to influence cross-platform dataset concordance. Here, cross-platform dataset concordance was investigated in terms of probe immobilization density (Cy3 fluorescence intensity), probe/target affinity (Cy5/Cy3 fluorescence intensity ratio), and target response (Cy5 fluorescence intensity).

Prior to dataset analysis, it should be noted that the comparability of cross-platform datasets obtained using a common reference is only as comparable as the reference itself. For example, in the bottom row of images in Figure 5.2, the common cross-platform reference on the OPD-coated platforms was defined as the fluorescence intensity generated by the Cy3-labeled DNA1 probes spotted at a concentration of 10μM. Because the arrays were unwashed, it was known that the total amount and density of the DNA1 probe within those spots was identical on each platform, and therefore, should have provided an accurate cross-platform reference. As shown in Figure 5.4B, fluorescence analysis of those images generated highly concordant datasets on each platform in terms of slope and magnitude, indicating that the use of the 10μM DNA1 probe spots was indeed an accurate cross-platform reference.

In the multianalyte microarray design, the fluorescence intensity generated by the anti-IgG probe spots exposed to a 100nM mixed-target sample was defined as the cross-platform reference. In this case, however, the spotted microarrays were washed prior to fluorescence scanning, meaning that the amount of Cy3-labeled anti-IgG probe and Cy5-labeled IgG target were different due to the dissimilar cross-platform probe immobilization densities and probe affinities which were identified in Chapters 3 and 4. Because the fluorescence intensities of the anti-IgG spots are defined as the common cross-platform reference, the comparability of datasets obtained using this reference varies depending on the extent of probe immobilization density and affinity differences between each microarray platform.

It should also be noted that this limitation on the accuracy of the anti-IgG reference spots cannot be overcome by defining some other reference, as differential cross-platform probe immobilization densities and affinities will be observed with any probe/target pair, as discussed previously in Sections 3.6.1.1 and 3.6.2.3. Based on this inability to define an accurate cross-platform reference, it is expected to obtain datasets of varying comparability between different platforms. Keeping this limitation in mind, the end goal of the multianalyte assay design is not to generate concordant cross-platform datasets, but rather, to determine the extent of dataset concordance achievable between platforms utilizing SI surface coatings versus SS surface coatings.

5.4.1 Probe Immobilization Density

Typically, different probes will immobilize onto a microarray platform at different densities. The immobilization density of a given probe will depend upon the probes chemical properties, the size of the probe, and the surface properties of the platform itself. To investigate cross-platform probe immobilization densities, the probe fluorescence (Cy3) intensities obtained from the analysis of the images in Appendix A were plotted in Figure 5.5.

Each datapoint in Figure 5.5 represents the fluorescence intensity of a particular probe compound on a specific platform. For example, in Figure 5.5B the upper leftmost ◆ datapoint attached to the dotted curve represents the mean fluorescence intensity generated by the DNA1 probe spots on the PLL-coated polymer platform. This datapoint was obtained by averaging the fluorescence intensities of each DNA1 probe spot exposed one of the six assay samples. Since a separate array was used for each sample and because there were four replicates of each probe within an array, each datapoint represents the mean fluorescence intensity of 24 spots.

The graphs in Figure 5.5 are grouped by surface coating and plotted as curves to enable visual comparison of the relative probe immobilization density differences between each probe compound on different platforms possessing the same surface coating. Specifically, Figures 5.5A and B represent the probe fluorescence intensities generated on the SS surface-coatings AS and PLL, respectively, while Figures 5.5C and D represent those obtained on the SI surface-coatings PEM and OPD.
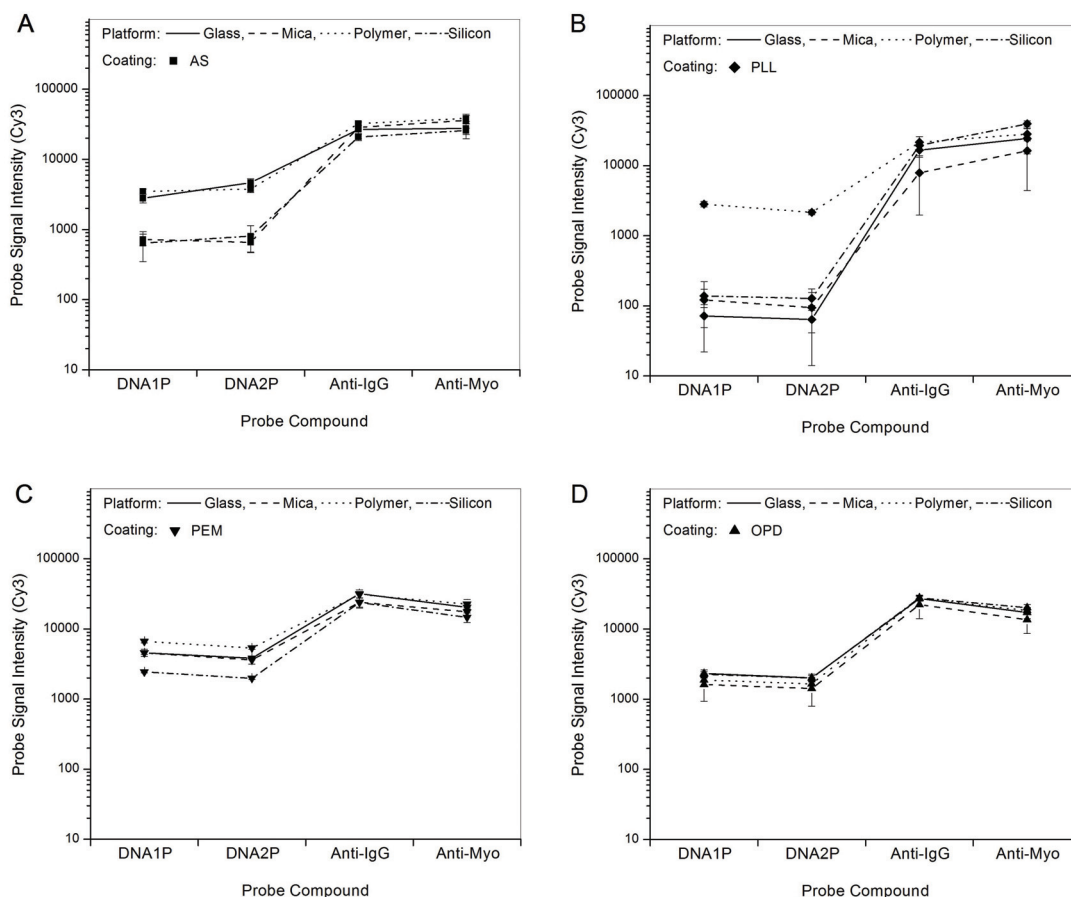
FIGURE 5.5: Probe immobilization densities (Cy3 fluorescence intensities) on glass, mica, polymer, and silicon platforms coated with SI and SS surface coatings. Graphs A and B represent the probe signal intensities generated on the AS and PLL-coated platforms, respectively; while graphs C and D represent those obtained on the PEM and OPD-coated platforms. Each datapoint was obtained from the mean of 24 replicate spots. The probe signal intensities are plotted as curves to simplify comparison of the relative changes in immobilization densities between different probes (X-axis).

In some cases, visually concordant probe fluorescence intensities are observed on platforms with SS surface coatings. For example, in Figure 5.5A the AS-coated glass and polymer platforms generated similar probe fluorescence intensity curves, indicating similar changes in the relative probe immobilization densities between the four probe compounds on these two platforms. The AS-coated mica and silicon also generated similar probe fluorescence intensity curves between each other. However, in comparison to the glass and polymer, the DNA probe fluorescence intensities are significantly lower, indicating that the changes in relative probe immobilization densities between probe compounds are dissimilar between those platform materials when using the AS coating. Moving over to Figure 5.5B, the PLL-coated platforms also show differential

probe immobilization density changes depending on the platform material and probe compound. In particular, the PLL-coated polymer generated significantly higher DNA probe immobilization densities relative to the other three platform materials. These platform-dependent and probe-dependent differences in probe immobilization density represent a primary source of discordance which limits the extent of cross-platform dataset agreement and complicates validation of microarray data generated on different platforms, especially in a multianalyte format where multiple probes are utilized.

When utilizing SI surface coatings, however, the probe immobilization densities obtained between platforms are significantly more concordant, as shown in Figures 5.5C and D. Specifically, similar changes in fluorescence intensity are observed between probe compounds and platform materials, indicating similar cross-platform immobilization density changes between different probes when utilizing SI surface coatings.

In regard to microarray technology development and validation, the ability to obtain equal changes in cross-platform probe immobilization densities represents a first step towards achieving more concordant cross-platform microarray datasets. In particular, because the relative probe immobilization density differences between probe compounds were similar on different platforms, it will be expected to generate more concordant target responses as well, assuming that the probe/target affinities are also similar on platforms coated with SI surface coatings.

It should be noted that the graphs in Figure 5.5 could have been grouped by platform material rather than surface coating. Grouping in such a manner would have enabled the comparison of relative probe immobilization density changes on the same platform material with different surface coatings. As demonstrated in Chapters 3 and 4, however, it is known that different surface coatings on the same platform material will generate significantly discordant datasets in virtually every aspect of assay performance, such as probe immobilization density, affinity, specificity, NSB, target response, and target S/N. Therefore, comparisons between the same platform material with different surface coatings will not be made in this chapter, as it is known that such a comparison will show highly discordant datasets.

5.4.1.1 Correlation of Cross-platform Probe Densities

In Figure 5.5, the cross-platform probe immobilization densities were shown to be significantly more concordant, visually, on platforms utilizing SI surface coatings in comparison to platforms using SS surface coatings. In this section, agreement of the probe immobilization densities is reported using the Pearson product-moment CCs in order to obtain a quantitative estimate of cross-platform dataset concordance. Here, the CCs were calculated using Equation 5.1. Similar to the method used in Section 5.2.2.2, datasets obtained on the glass platforms were used as the reference datasets (X) from which to calculate the CCs of the datasets obtained on the other platforms (Y). For example, the CC of the probe immobilization density datapoints on the AS-coated mica was 0.988, as shown by the uppermost CC value in Table 5.2. This value was calculated using the probe fluorescence intensity datapoints generated on the AS-coated mica platform defined as the Y dataset (dependent values), and the datapoints generated on the AS-coated glass platform defined as the reference X dataset (independent values). These datasets can be seen in Figure 5.5A, where the solid curve represents the probe fluorescence intensities generated on the AS-coated glass and the dashed curve represents those obtained on the AS-coated mica.

Dataset	Coating Type	Surface Coating	Reference Substrate	Substrate	CC
Probe Density (Cy3)	Substrate Specific (SS)	AS	Glass	Mica	0.988
				Polymer	0.993
				Silicon	0.990
		PLL	Glass	Mica	0.981
				Polymer	0.998
				Silicon	0.983
	Substrate Independent (SI)	PEM	Glass	Mica	0.996
				Polymer	0.996
				Silicon	1.000
		OPD	Glass	Mica	1.000
				Polymer	0.999
				Silicon	0.995

TABLE 5.2: Comparison of cross-platform CCs between the probe immobilization density datasets obtained on platforms with SS surface coatings vs SI surface coatings. CCs were calculated from the datasets plotted in Figure 5.5 using Equation 5.1. The upper block represents the CCs between platforms with SS surface coatings, while the lower block represents CCs between platforms with SI surface coatings.

Overall, the CCs between the cross-platform probe immobilization density datasets shown in Table 5.2 are rather high, regardless of using SS or SI surface coatings. In

this case, all CCs were above 0.980. Typically, however, the CCs calculated between platforms with SS surface coatings are considerably lower than those calculated between platforms utilizing SI surface coatings. With the exception of the PLL-coated polymer, the CCs calculated on platforms with SS surface coatings are all below 0.994, whereas the CCs calculated on platforms utilizing SI surface coatings are all above 0.994, with no exceptions.

The increased CCs observed between platforms utilizing SI surface coatings indicate that datasets obtained on these platforms are significantly more concordant in terms of probe fluorescence intensity changes between each probe compound. Based on this result, it will be expected to also generate more concordant cross-platform datasets in terms of target fluorescence intensity changes between different sample solutions. However, the ability to generate concordant cross-platform datasets in terms in target response will also be influenced by possible changes in probe affinity on each platform, as discussed previously in Section 5.4.1.

5.4.2 Probe/Target Affinity

As determined by the Pearson product-moment CCs calculated in Table 5.2, relatively high cross-platform concordance was observed on all platforms in terms of probe immobilization density. In order to generate concordant cross-platform microarray datasets in terms of target response, however, it must be possible to also obtain similar cross-platform probe/target affinities. To investigate the cross-platform probe/target affinities, the Cy5/Cy3 fluorescence intensity ratios were plotted in Figure 5.6. Similar to Figures 5.5A-D, the graphs in Figure 5.6 are grouped by surface coating to enable visual comparison between the Cy5/Cy3 fluorescence intensity ratios on different platform materials possessing the same surface coating. Specifically, Figures 5.6A and B represent the Cy5/Cy3 fluorescence intensity ratios generated on the SS surface coatings AS and PLL, respectively; while Figures 5.6C and D represent those obtained on the SI surface coatings PEM and OPD.

In Figures 5.6A-D, the maroon-colored axis corresponds to the DNA compounds, while the navy-colored axis corresponds to the protein compounds. The DNA compounds are represented by the red (DNA1) and orange (DNA2) curves, while the protein compounds are represented by the blue (IgG) and green (Myo) curves. Additionally, it
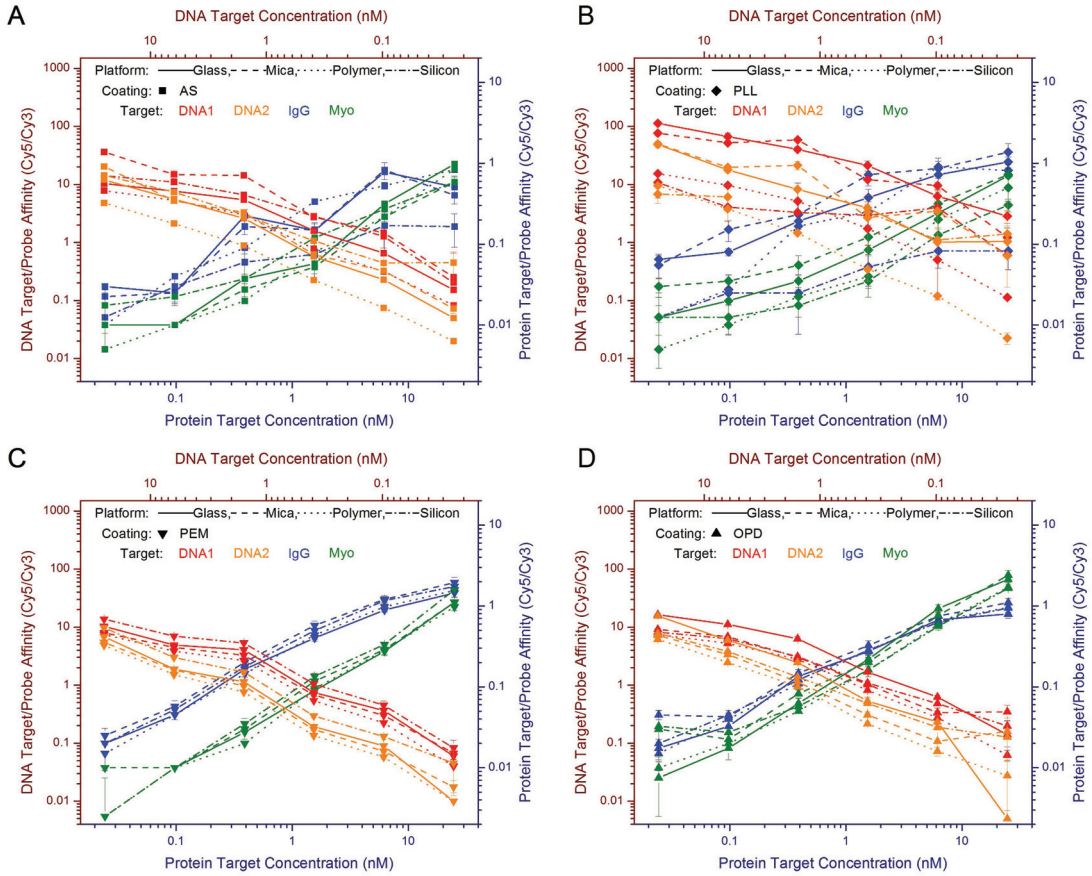
FIGURE 5.6: Probe/target affinities (Cy5/Cy3 fluorescence intensity ratios) on glass, mica, polymer, and silicon platforms coated with SI and SS surface coatings. Graphs A and B represent the affinities generated on the AS and PLL-coated platforms, respectively; while graphs C and D represent those obtained on the PEM and OPD-coated platforms. The affinity values are plotted as curves to observe the changes in the Cy5/Cy3 ratios relative to changes in target concentration (X-axis). In each graph, the maroon-colored axis corresponds to the DNA compounds, while the navy-colored axis corresponds to the protein compounds. The upper and lower X-axis scales within each graph are reversed in order to discriminate between the DNA and protein affinity curves. Additionally, each probe/target pair is color-coded to easier discern between affinity curves generated by different target compounds: DNA1, DNA2, IgG, Myo.

should be noted that the upper and lower X-axis scales within each graph are reversed in order to discern more easily between the DNA and protein affinity curves. Each datapoint in Figure 5.6 represents the mean Cy5/Cy3 fluorescence intensity ratio of a particular probe compound on a specific platform exposed to a given mixed-target sample. For example, in Figure 5.6A the upper leftmost ■ datapoint attached to the dashed curve represents the mean Cy5/Cy3 fluorescence intensity ratio generated by the DNA1 probe spots on the AS-coated mica platform which were exposed to a mixed target sample containing all four target compounds at a concentration of 25nM. Since

only one array was exposed to this sample solution, and because there are four replicates of each probe compound within an array, each datapoint represents the mean Cy5/Cy3 fluorescence intensity ratio of four spots.

In most cases, the AS and PLL-coated platforms generated differential changes in affinity values depending on the probe/target pair, the platform material, and the mixed-target sample concentration. For example, the blue curves in Figure 5.6A represent the affinity values of the anti-IgG/IgG pair calculated on the AS-coated platforms. As the concentration of the sample solution is increased, a corresponding increase in the affinity values of the anti-IgG/IgG pair is observed. This is an expected result, as more concentrated target sample solutions will generally result in an increased target response, and therefore, an increased Cy5/Cy3 fluorescence intensity ratio. As shown by the solid and dashed blue curves in Figure 5.6A, the AS-coated glass and mica platforms generated similar increases in the anti-IgG/IgG affinity values as the concentration of the sample solution was increased. As shown by the dotted and dash-dot blue curves in Figure 5.6A, however, the polymer and silicon platforms generated anti-IgG/IgG affinity values which deviate significantly from each other and from the glass and mica, indicating differential changes in the anti-IgG/IgG affinity depending upon the platform material.

Although similar changes in affinity were obtained on the AS-coated glass and mica with the anti-IgG/IgG pair, the same was not observed with the DNA1 probe/target pair, as shown by the solid and dashed red curves in Figure 5.6A. In this case, significant deviations in curve shape and magnitude can be seen between the glass and mica, indicating that the affinity values change differentially depending upon the both the platform material and probe/target pair. Due to these platform-dependent and probe-dependent affinity changes, it is difficult to visually discern the affinity curves between each probe/ target pair and platform material when utilizing conventional SS surface coatings such as AS and PLL, as shown in Figures 5.6A and B.

When utilizing the SI surface coatings, however, the ability to visually discern the affinity curves between each probe/target pair and platform material is considerably easier, as shown in Figures 5.6C and D. In this case, the affinity curves between platforms and probe/target pairs are significantly more concordant in terms of shape and magnitude, indicating that similar changes in cross-platform probe/target pair affinities are obtained when utilizing SI surface coatings. The ability to obtain similar probe/target

affinity changes has profound implications upon cross-platform dataset agreement. In particular, because both the probe immobilization densities and probe/target affinities are more concordant when utilizing SI surface coatings, it should also be possible to obtain more concordant cross-platform microarray datasets in terms of target response.

5.4.3 Target Signal Intensity

Often, the target signal response is the focal point of microarray analysis, because without it, the detection and quantification of target analytes is not possible. In this section, the target signal responses generated by the multianalyte dose-response assay on each platform are investigated. As shown in Figures 5.5 and 5.6, more concordant and discernible cross-platform probe immobilization densitiy and probe/target affinity curves were generated on platforms utilizing SI surface coatings in comparison to SS surface coatings. Based on those results, it was also expected to observe more concordant target response curves on platforms utilizing SI surface coatings.

To compare the cross-platform target responses, the target fluorescence intensities were plotted in Figure 5.7. Each graph in Figure 5.7 was plotted in the same manner used to plot those in Figure 5.6, except that here the datapoints represent the target fluorescence intensities (Cy5) as opposed to the probe/target fluorescence intensity ratios (Cy5/Cy3). For example, in Figure 5.7A, the upper leftmost ■ datapoint attached to the solid curve represents the mean Cy5 fluorescence intensity generated by the four DNA2 probe spot replicates on the AS-coated glass platform which were exposed to a mixed-target sample at a concentration of 25nM. Similar to Figure 5.6, the graphs in Figure 5.7 are grouped by surface coating to enable visual comparison of the target fluorescence intensities generated between different platform materials possessing the same surface coating. Specifically, Figures 5.7A and B represent the target fluorescence intensities generated on the SS surface coatings AS and PLL, respectively; while Figures 5.7C and D represent those obtained on the SI surface coatings PEM and OPD.

Similar to the curve concordances observed in Figures 5.5 and 5.6, the target fluorescence intensity curves in Figure 5.7 are significantly more discernible on platforms utilizing SI surface coatings as opposed to SS surface coatings. Specifically, the AS and PLL-coated platforms generate differential changes in target response depending on the probe/target pair, the sample concentration, and the platform material. For example,
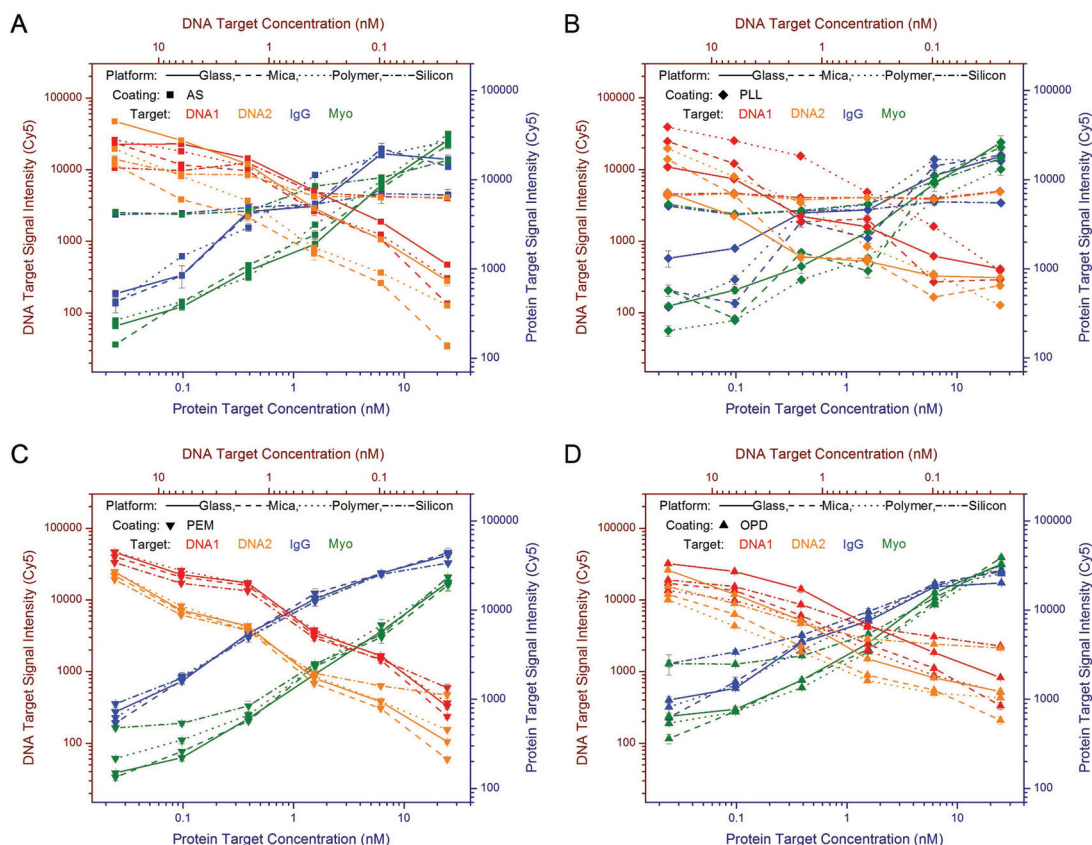
FIGURE 5.7: Target signal responses (Cy5 fluorescence intensities) on glass, mica, polymer, and silicon platforms coated with SI and SS surface coatings. Graphs A and B represent target responses generated on the AS and PLL-coated platforms, respectively; while graphs C and D represent those obtained on the PEM and OPD-coated platforms. The target responses are plotted as curves to observe changes in the Cy5 fluorescence intensity relative to changes in target concentration (X-axis). In each graph, the maroon-colored axis corresponds to the DNA compounds, while the navy-colored axis corresponds to the protein compounds. Additionally, the upper and lower X-axis scales within each graph are reversed in order to discriminate between the DNA and protein target signal response curves. The target compounds are color-coded to easier discern between the signal responses generated by different target compounds: DNA1, DNA2, IgG, Myo.

the blue curves in Figure 5.7A represent the fluorescence intensity generated by the anti-IgG spots on the AS-coated platforms. In concordance with the affinity curves plotted in Figure 5.6A, the glass and mica platforms generated similar IgG signal response curves in terms of shape and magnitude, as shown by the solid and dashed blue curves in Figure 5.7A. When looking at the dotted and dash-dot blue lines, however, the polymer and silicon generated IgG fluorescence intensity curves which deviate significantly from each other and from those obtained on the glass and mica. Since the only experimental variable between these curves was the platform material, it can be concluded that the

use of different platforms typically results in differential changes in the target response.

Although similar IgG fluorescence intensities were generated on the AS-coated glass and mica, significantly less agreement was observed between these two platforms in regard to the DNA1 target fluorescence intensities, as shown by the solid and dashed red curves in Figure 5.7A. In this case, significant deviations in curve shape and magnitude are seen between the glass and mica. Since similar curve shapes were observed with one probe compound (anti-IgG) but not another (DNA1P), it can be concluded that different microarray platforms will generate differential target responses depending upon both the probe compound and the platform itself. Due to these differential target fluorescence intensities, it is difficult to visually discern the target response curves between probe/target pairs and platform materials when utilizing conventional SS surface coatings such as AS and PLL, as illustrated by Figures 5.7A and B.

Differential cross-platform target responses represents a significant obstacle preventing more rapid development and validation of microarray technology, especially for complex multianalyte formats. For example, assuming the microarray design in this chapter was a single analyte format utilizing only the anti-IgG/IgG probe target pair, datasets obtained on the AS-coated glass and mica would appear highly concordant, as this probe-target pair generated similar target fluorescence intensities between these two platforms. Although similar target responses were generated on the AS-coated glass and mica with this specific target, the same result cannot be expected with other analytes, such as the DNA1 target for instance. Because the DNA1 target generated differential target responses relative to the IgG target responses between the AS-coated glass and mica, it can also be assumed that additional probe/target pairs integrated into the microarray design will generate differential target responses relative to the IgG target response. Therefore, as the complexity of the microarray design increases in terms of number and type of probe/target pairs, the concordance of cross-platform datasets will decrease uncertainly.

It should also be noted that because the IgG fluorescence intensities were similar on the AS-coated glass and mica, the IgG target response could potentially be defined as an accurate cross-platform reference between these two platforms. However, use of this reference would not be transferable to other platforms such as the AS-coated polymer and silicon platforms, as the IgG target responses on these platforms were significantly

different. Overall, these differential cross-platform target responses generated on platforms with SS surface coatings serve to impede more rapid development and validation of new microarray technologies by preventing the ability to accurately integrate common cross-platform references or new probe/target pairs.

Much of the differential cross-platform target responses observed on platforms with SS surface coatings, however, are minimized when utilizing SI surface coatings. As shown in Figures 5.7C and D, the ability to visually discern the target responses between probe/target pairs is considerably easier, as the fluorescence intensity curves generated on each platform are significantly more concordant in terms of shape and magnitude. It should be noted that differential target responses are still observed between different probe/target pairs on each platform. For example, the fluorescent intensity curves between the IgG and Myo targets on the PEM-coated platforms are significantly different in terms of shape and magnitude, as shown by the blue and green curves in Figure 5.7C. Specifically, the intensity curves of the IgG are of higher magnitude and somewhat concave on each platform, whereas the Myo intensity curves are of lower magnitude and somewhat convex. These differences in curve shape and magnitude are an expected result, however, as it is known that different probe/target pairs will behave differently on the same platform.

What is important to note from Figure 5.7C, however, is that the relative differential changes in target fluorescence intensity between target compounds are similar on each PEM-coated platform. These similar differential changes in target response between different probe/target pairs represents a significant advantage with the use of SI surface coatings in terms of cross-platform microarray development and dataset correlation. Specifically, because similar differential target response curves were obtained with four significantly different probe/target pairs on each platform, it can be assumed that additional probe/target pairs integrated into the microarray design will also generate similar differential target responses between each platform, meaning that advancements made on one platform, in terms of probe design and complexity, will be transferable onto other platforms with concordant results. It is also important to note that the use of SI surface coatings enables the ability to integrate and define more accurate cross-platform references. For example, in this experimental design a common cross-platform reference was defined as the fluorescence intensity generated by the anti-IgG probe spots exposed to a 100nM mixed target sample. Use of this control provided a significantly

more accurate reference on the SI surface coatings in comparison to the SS coatings, inferred from the increased dataset correlation observed in Figures 5.7C and D. Yet, because all the probe/target pairs generated more concordant relative target responses on the SI surface coatings, the fluorescence intensity generated by any of the probe spots could have be utilized as an accurate cross-platform reference. In terms of microarray development, these results demonstrate how the use of SI surface coatings simplifies co-development between platform design and assay methodology, even with complex multianalyte applications.

5.4.4 Correlation of Cross-Platform Assay Datasets

In Figures 5.6 and 5.7, both the affinity and target response curves obtained from the multianalyte dose-response assays were considerably more concordant and discernible, visually, on platforms utilizing SI surface coatings in comparison to platforms using conventional SS surface coatings, suggesting that the use of SI surface coatings generates significantly more concordant cross-platform microarray datasets. In this section, microarray dataset concordance is measured using Pearson product-moment CCs in order to obtain a quantitative estimate of cross-platform concordance. For consistency, datasets obtained on the glass platforms were used as the reference datasets (X values) from which to calculate the CCs of the other platforms (Y values). The CCs obtained from these calculations are provided in Table 5.3, where the upper block represents the CCs obtained between platforms with SS surface coatings, while the lower block represents those obtained between platforms with SI surface coatings.

In order to discriminate between low dataset concordance and high dataset concordance, the CCs were color-coded. Specifically, CC values below 0.98 were defined as low concordance and colored red, while CC values of 0.98 and higher were defined as high concordance and colored green. Using this red/green color scheme, significantly higher cross-platform microarray dataset concordance is observed on platforms utilizing SI surface coatings in comparison to SS surface coatings. Specifically, 92% of datasets obtained on platforms utilizing SI surface coatings generated high CC values above 0.98, as determined by the number of green CC values shown in the lower block of Table 5.3. When using SS surface coatings, on the other hand, only 35% of datasets generated CC values above 0.98.

Microarray Platform					Single Analyte CCs				Multianalyte CCs		
Coating Type	Dataset	Surface Coating	Reference Substrate	Substrate	DNA1	DNA2	IgG	Myo	DNAs	Proteins	All Four Targets
Substrate Specific (SS)	Probe Affinity (Cy5/Cy3)	AS	Glass	Mica	0.948	0.977	0.984	0.999	0.892	0.946	0.916
				Polymer	0.991	0.999	0.779	0.996	0.930	0.892	0.944
				Silicon	0.996	0.999	0.948	0.986	0.994	0.846	0.994
		PLL	Glass	Mica	0.915	0.961	0.978	0.997	0.928	0.977	0.946
				Polymer	0.997	0.998	0.941	0.997	0.979	0.953	0.983
				Silicon	0.887	0.786	0.950	0.997	0.817	0.590	0.863
	Target Response (Cy5)	AS	Glass	Mica	0.897	0.976	0.979	1.000	0.660	0.987	0.719
				Polymer	0.961	0.992	0.914	0.999	0.810	0.963	0.788
				Silicon	0.858	0.971	0.985	0.945	0.886	0.782	0.821
		PLL	Glass	Mica	0.984	0.993	0.982	0.988	0.972	0.977	0.885
				Polymer	0.976	0.993	0.928	0.993	0.980	0.853	0.562
				Silicon	0.305	0.188	0.743	0.994	0.287	0.801	0.777
Substrate Independent (SI)	Probe Affinity (Cy5/Cy3)	PEM	Glass	Mica	0.997	0.998	1.000	1.000	0.997	0.987	0.994
				Polymer	0.998	0.999	1.000	0.999	0.998	0.993	0.996
				Silicon	0.999	0.999	0.998	0.999	0.999	0.995	0.999
		OPD	Glass	Mica	0.995	0.996	0.989	0.992	0.989	0.988	0.986
				Polymer	1.000	1.000	0.990	0.996	0.995	0.978	0.992
				Silicon	0.997	0.995	0.987	0.994	0.996	0.975	0.995
	Target Response (Cy5)	PEM	Glass	Mica	0.999	1.000	0.998	0.999	0.999	0.997	0.993
				Polymer	0.997	0.999	1.000	0.999	0.998	1.000	0.999
				Silicon	1.000	1.000	0.994	0.998	0.999	0.987	0.984
		OPD	Glass	Mica	0.996	0.997	0.990	0.988	0.994	0.986	0.868
				Polymer	0.998	0.999	0.988	0.993	0.997	0.982	0.836
				Silicon	0.999	0.998	0.974	0.996	0.998	0.977	0.905

TABLE 5.3: Comparison of cross-platform affinity and target response CCs between platforms with SS surface coatings versus SI surface coatings. CCs were calculated from the datasets plotted in Figures 5.6 and 5.7 using Equation 5.1. The upper block represents the CCs between platforms with SS surface coatings, while the lower block represents the CCs between platforms with SI surface coatings. In order to discriminate between lower and higher correlation, CC values below 0.98 were colored red, while CC values of 0.98 and higher were colored green.

As mentioned in Section 5.4.3, the ability to generate concordant cross-platform datasets becomes significantly more difficult as the complexity of the microarray design increases in terms of number of probe/target pairs. This increased difficulty arises due to the differential cross-platform probe immobilization densities and affinities observed on different microarray platforms. In order to investigate the extent of cross-platform dataset concordance achievable in a single analyte format versus a multianalyte format, CCs were calculated between individual probe/target pairs and between multiple probe/target pairs. For example, the upper leftmost CC value of 0.948 in the Single Analyte CCs column represents the correlation of just the DNA1 probe/target affinity datasets between the AS-coated glass and mica platforms. These datasets can be seen in Figure 5.6A, where the ■ datapoints attached to the solid line represent the X dataset, while the ■ datapoints attached to the dashed line represent the Y dataset.

Considering now the Multianalyte CCs block, the CCs calculated using multiple

probe/target pairs can be seen. For example, in the column with the header DNAs, the bottommost CC value of 0.998 represents the correlation between the OPD-coated glass and silicon when taking into considering both the DNA1 and DNA2 target response datasets. To calculate this CC, the target fluorescence intensity curves of both the DNA1 and DNA2 on the OPD-coated glass were defined as the X dataset, while those obtained on the OPD-coated silicon were defined as the Y dataset. These datasets can be seen in Figure 5.7D, where the ▲ and ▲ datapoints attached to the solid lines represent the DNA1 and DNA2 target responses generated on the OPD-coated glass, respectively; while the ▲ and ▲ datapoints attached to the dash-dot lines represents those obtained on the OPD-coated silicon. Similarly, the CCs in the column with the header Proteins were obtained using the datasets of both protein probe/target pairs, while the CCs in the rightmost column were obtained using all four probe/target pairs' datasets.

As shown in Table 5.3, when going from a single analyte format to a more complex multianalyte format, considerable reductions in cross-platform dataset agreement are observed. For example, in a single analyte format, platforms with SS surface coatings showed high correlation between 50% of the assay datasets. In a multianalyte format, however, only 14% of datasets showed high correlation, indicating a significant reduction in cross-platform dataset agreement as the complexity of the microarray design is increased. Reductions in the CCs when going from a single analyte to multianalyte format were also observed on platforms utilizing SI surface coatings. Specifically, in a single analyte format, 98% of datasets showed high correlation. In a multianalyte format, however, only 83% of datasets showed high correlation.

Although cross-platform dataset correlation is decreased as the complexity of the microarray design is increased, the decreases observed between platforms utilizing SI surface coatings are significantly less profound. As mentioned above, platforms with SI coatings still showed high correlation between 83% of datasets in a multianalyte format, whereas only 14% of datasets showed high correlation when not using SI surface coatings. These significantly increased dataset CCs calculated between platforms utilizing SI surface coatings provide definitive evidense that SI surface coatings serve to minimize differences in cross-platform assay performance, even with complex multianalyte microarray designs. Specifically, the use of SI surface coatings eliminates differences in cross-platform surface properties, and therefore, differences in cross-platform probe density and affinity. As a result, significantly more concordant cross-platform sample assay

datasets are generated. More importantly, assay performance optimizations developed in conjunction with SI surface coatings will be interchangeable across other platforms, meaning that standardized and sustainable development of microarray technology is enabled with the use of SI surface coatings. This ability was demonstrated by the performance observed on the OPD coating, which was specifically designed to improve assay performance on the native PD coating with this specific microarray application.

5.4.5   Target Background Intensity

NSB of target compounds can have a profound impact upon many aspects of assay performance in a given microarray design. One performance parameter which may be impacted is the target S/N ratio. For example, platforms which exhibit high NSB with particular analytes will typically generate both higher background fluorescence intensities and background fluorescence intensity SDs. This effect was observed previously in Figures 4.5A and B. These increases in the observed background fluorescence intensities and background fluorescence intensity SDs ultimately translated into reduced S/N ratios, as shown in Figure 4.10. Platforms which exhibit lower NSB, on the other hand, will typically provide higher S/N ratios, assuming that the target signal responses are comparable in magnitude.

Another parameter of assay performance which may be influenced by target NSB are detection limits, especially for analyte compounds present at low concentrations. Specifically, a platform which exhibits high NSB for a particular analyte may adsorb the analyte to its surface before giving it an opportunity to bind with its immobilized probe partner, rendering the analyte undetectable below a certain threshold concentration. On the other hand, a platform which exhibits lower NSB with the same analyte will provide a lower theoretical detection limit, as the analyte will be given more opportunity to find and bind with its probe partner.

As a whole, these differences in target NSB on different platforms will serve to limit the extent of cross-platform dataset concordance. In this multianalyte assay design, all platforms were washed with PBST containing PAC in order to reduce NSB. Utilizing the PAC wash, low background fluorescence intensities due to NSB were observed on all platforms examined. In terms of assay performance, this was a desirable result, however, because the background fluorescence intensities were so low, it was impossible

to accurately compare the extent of NSB between the microarray platforms. Therefore, analysis of this performance parameter was omitted.

It should be noted, however, that an accurate comparison of target NSB could be enabled by manipulating the experimental design. For example, the PMT setting could be increased further to improve the scanning sensitivity towards dye-labeled target compounds. As shown in Figure 5.1, though, increasing the PMT setting will also generate differential increases in the intrinsic background, depending on the scanning wavelength and microarray platform material. Alternatively, the concentration of the targets in the sample solution could be increased, or the amount of BSA added to the sample solution could be decreased. Either of these methods would serve to shift the NSB competition away from BSA in favor of the target compounds, thereby increasing the background fluorescence intensities.

5.5 Summary of Cross-Platform Dataset Concordance

In this chapter, sources of cross-platform dataset discordance which arise with the use of fluorescence detection were identified and discussed. Specifically, differences in autofluorescence and fluorescence interference were observed on platforms constructed from different materials, as shown in Figures 5.1 and 5.4, respectively. Despite these differences in autofluorescence and fluorescence interference, however, it was found that high microarray dataset correlation could still be obtained as long as the rate of fluorescence intensity change in response to change in fluorophore surface density was the same between different platforms. This ability was demonstrated using identical arrays of Cy3-labeled DNA1P arrays printed onto OPD-coated glass, polymer, and silicon. The microarray datasets obtained between these platforms showed very high correlation, as determined by the CCs calculated in Table 5.1.

In terms of meeting the objectives established in Chapter 1, the experimental work performed in this chapter demonstrated the ability to generate significantly higher cross-platform assay dataset correlation in terms of probe immobilization density, probe/target affinity, and target response when using SI surface coatings. This ability was shown by fabricating microarrays onto a total of 16 different platforms possessing either SS or SI surface coatings. Specifically, microarrays utilizing two different DNA probes

and two different protein probes were printed onto glass, mica, polymer, and silicon platforms coated with AS, PLL, PEM, or OPD. Using these arrays, multianalyte dose-response assays were performed in order to examine the extent of cross-platform dataset correlation between platforms with SS surface coatings versus platforms with SI surface coatings.

Analysis of the probe fluorescence intensities in Figure 5.5 determined that the probe immobilization densities obtained between platforms with SI surface coatings were more concordant to those obtained between platforms with SS surface coatings. Specifically, the CCs calculated between datasets obtained on platforms with SI surface coatings were all above 0.94, whereas those calculated between platforms with SS surface coatings were all below 0.94, with the exception of the PLL-coated polymer. Additionally, it was found that assay datasets obtained on SI surface coatings were significantly more concordant in terms of probe/target affinity and target signal response, as shown in Figures 5.6 and 5.7, respectively. Specifically, 92% of datasets obtained on platforms utilizing SI surface coatings generated high CC values above 0.98, as shown in Table 5.3. When using SS surface coatings, however, only 35% of datasets generated CC values above 0.98. Furthermore, reductions in cross-platform assay dataset correlation were also observed when going from a single analyte format to a more complex multianalyte format. For example, when considering two or more probe/target pairs, platforms with SI surface coatings showed high correlation between 83% of datasets, whereas platforms with SS surface coatings showed high correlation between only 14% of datasets.

Another significant finding in this chapter was the ability to integrate accurate cross-platform references when utilizing SI surface coatings. Specifically, a common cross-platform reference was defined as the fluorescence intensity generated by anti-IgG probe spots exposed to a 100nM mixed target sample. Based on the cross-platform dataset correlation observed in Table 5.3, use of this reference proved to be highly accurate when utilized in combination with SI surface coatings. However, because all the probe/target pairs generated significantly more concordant fluorescence intensities on platforms with SI surface coatings, any of the probe spots could have been utilized as an accurate cross-platform reference. In terms of microarray development, these results demonstrate that the ability to integrate accurate cross-platform references is tremendously simplified when utilizing SI surface coatings. Overall, these results represent

a significant advancement which enables co-development between platform design and assay methodology, even with complex multianalyte applications.

Chapter 6

Conclusion

While the advent of microarray technology has enabled the ability to rapidly characterize complex biological and environmental systems, the technology has not yet advanced to the stage where it can be reliably utilized for practical applications such as healthcare and environmental monitoring. One of the primary reasons for this shortcoming has been attributed to a lack of cross-platform microarray dataset correlation, complicating the ability to validate assay results obtained between different platforms.

To address this shortcoming, researchers have begun working towards the adoption of standardized probe designs, assays methodologies, and analysis procedures in order to improve cross-platform microarray dataset correlation. The motivation behind this movement is to speed validation of newly developed platforms and foster more widespread implementation of microarray technology for real-world applications. In this movement towards standardization, however, intrinsic differences in the microarray platforms themselves which contribute to cross-platform dataset discordance have been largely ignored. In particular, differences in cross-platform surface properties represent a significant source of dataset discordance which cannot be overcome with the use of standardized probe designs, assay methodologies, and analysis procedures. These differences in cross-platform surface properties generate differential probe and target behaviors, preventing the ability to accurately compare datasets obtained between different platforms.

The primary objective of the experimental work carried out in this thesis was to develop a simple method which could be utilized to eliminate differences in surface

properties on any material, and therefore, obtain similar probe immobilization densities, probe/target affinities, and target NSB on different microarray platforms. Additionally, the method utilized should still enable sustainable development of the technology in terms of platform design, surface chemistry, probe design, assay protocol, detection method, and analysis technique. Satisfaction of these criteria required the ability to render the surface properties of any platform identical, the ability to modify the surface properties to suit specific microarray applications, and finally, the ability to replicate the surface property modifications onto any existing or newly developed platform with identical results. To meet these criteria, the use of SI surface coatings based on PEMs and PD were examined.

Experimental results determined that a PEM system composed of $PAH(PSS/PAH)_5$ was capable of assembling onto organic, inorganic, metallic, and semi-conducting materials without the need for any preliminary surface treatments. Once assembled, the PEM coating served to mask the surface properties of the underlying substrates and convert them into the properties of the PEM coating itself. Furthermore, it was found that subsequently deposited PE layers assembled at uniform thicknesses and densities onto the surface of different materials possessing the PEM coating. In regard to meeting the thesis's objectives, this result demonstrated the ability to render the surface properties of different materials virtually identical. Additionally, since it was possible to assemble one compound onto the surface of different materials with nearly identical results, it was assumed that other functionalities, including DNA and protein, would also assemble uniformly onto these surfaces.

To test this assumption, microarrays utilizing both DNA and protein compounds were fabricated onto PEM-coated glass platforms and used to perform multianalyte assays. In addition, another recently developed SI surface coating based on PD was examined for its potential suitability with multianalyte microarray applications. Assay performance on these two SI surface coatings was then compared to that on conventionally used AS- and PLL-coated glass platforms. The results of the multianalyte assays determined that the AS and PEM coatings provided the best performances, whereas the PLL and PD coatings provided the worst performances. Overall, however, it was found that no single surface coating provided the best performance with all the probe/-target pairs. Rather, certain coatings performed relatively well with some probe/target pairs, but not necessarily with other probe/target pairs. Based on this finding, it was

concluded that the ideal surface coating will vary depending upon the desired application and end goal. In terms of cross-platform concordance, the use of different surface coatings enabled the identification of platform-dependent sources of dataset discordance. Specifically, it was determined that differences in cross-platform surface properties have a profound influence upon virtually every aspect of assay performance: probe immobilization density, target response, target specificity, probe/target affinity, NSB, and S/N. Additionally, it was found that these platform-dependent performance differences prevent the ability to integrate accurate cross-platform controls, representing perhaps the greatest limitation negating the ability to compare and validate datasets obtained on different microarray platforms.

To determine whether the multianalyte assay performance could be improved upon, new experimental variables were introduced into the microarray design. Specifically, PAC was introduced into the wash solution with the goal of reducing target NSB and probe comet tails which were observed in the original experimental design. Although these goals were achieved, the PAC wash typically reduced probe immobilization densities and probe/target affinities. Despite these reductions in probe density and affinity, however, the PAC-washed AS- and PEM-coated platforms provided the best performances in terms of S/N ratio in a multianalyte assay format. In addition to the PAC wash, the surface of the PD coating was modified to determine whether the multianalyte assay performance on this SI surface coating could be improved upon. Specifically, the PD surface was modified with a PAH(PSS/PAH) multilayer system which enabled the ability to immobilize higher densities of DNA and protein probes. Furthermore, these immobilized probes went on to generate significantly higher target signal responses. In regard to meeting the thesis objectives, this result demonstrated the ability to tailor and optimize the surface properties of the PD coating to perform specific microarray applications. Moreover, because the PD is a SI surface coating, it was assumed that modifications made to its surface properties would be identically transferable to other platforms.

To test this assumption, microarrays were printed onto glass, mica, polymer, and silicon platforms coated with AS, PLL, PEM, or OPD. Following microarray fabrication, multianalyte dose-response assays were performed in order to examine the extent of cross-platform dataset correlation between platforms with SI surface coatings versus

platforms with SS surface coatings. Analysis of the probe fluorescence intensities determined that the probe immobilization densities obtained between platforms with SI surface coatings were more concordant to those obtained between platforms with SS surface coatings. Additionally, it was found that assay datasets obtained on SI surface coatings were significantly more concordant in terms of probe/target affinity and target signal response. Specifically, 92% of datasets obtained on platforms utilizing SI surface coatings generated high CC values above 0.98, whereas only 35% of datasets generated CC values above 0.98 when using SS surface coatings. Another significant finding was the ability to integrate accurate cross-platform references when utilizing SI surface coatings. Specifically, a common cross-platform reference was defined as the fluorescence intensity generated by anti-IgG probe spots exposed to a 100nM mixed target sample. Based on the high dataset correlation observed between platforms with SI surface coatings, use of this cross-platform reference proved to be highly accurate. However, because all the probe/target pairs generated significantly more concordant fluorescence intensities on platforms with SI surface coatings, any of the probe spots could have be utilized as an effective cross-platform reference. In terms of meeting the thesis's objectives, these results demonstrated the ability to generate significantly higher cross-platform assay dataset correlation in terms of probe immobilization density, probe/target affinity, and target response when utilizing SI surface coatings. Given the current state-of-the-art, these abilities represent a significant advancement which enable standardized and sustainable development of microarray technolgy, even for complex multianalyte applications.

6.1 Future Work

In addition to biomolecules, methods to pattern the surface of PEM and PD coatings with a broad range of functionalities such as poly(ethylene glycol)[78], metallic elements[32,79], and nanoparticles[80] have been developed. Also, preliminary experimental work has demonstrated the ability to fine-tune the hydrophobicity of surfaces, ranging from superhydrophilic ($0°$ water contact angle) to superhydrophobic ($>160°$ water contact angle). Currently, efforts are being directed towards the development of other useful properties and functionalities onto SI surface coatings.

Additionally, while the experimental work performed in this thesis utilized SI surface coatings to overcome many developmental issues associated with microarray technology, the methodologies described can readily be extended to related biochip technologies such as microfluidic devices. Future work in this area will be devoted towards integrating functionalities within microfluidic channels for the development of more complex biochip devices capable of sample preprocessing and target detection.

Appendix A

Crossplatform Multianalyte Dose-Response Assay Images

The image sets provided here were used to generate all data used to analyze and compare the cross-platform multianalyte dose-response assays performed in Chapter 5. Sample assays were performed on each microarray platform according to the layout shown in Figure A.1.
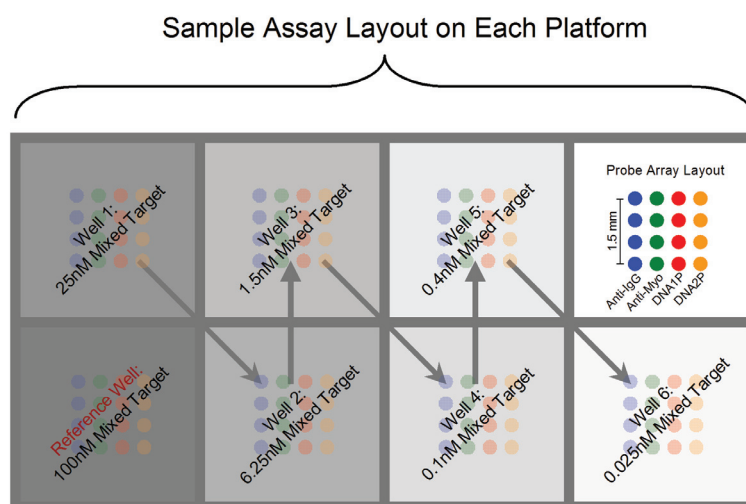

FIGURE A.1: Layout of the multianalyte sample assays performed on each microarray platform in Chapter 5. The probe layout within each well is shown in the upper right box. The lower left wells on each platform were exposed to the 100nm mixed target reference solution. The reference well was used to calibrate the fluorescence scan PMT setting according to the procedure described in Section 5.3.4. All other wells were exposed to one of the six mixed target sample dilutions according to the pathway shown by the gray arrows.
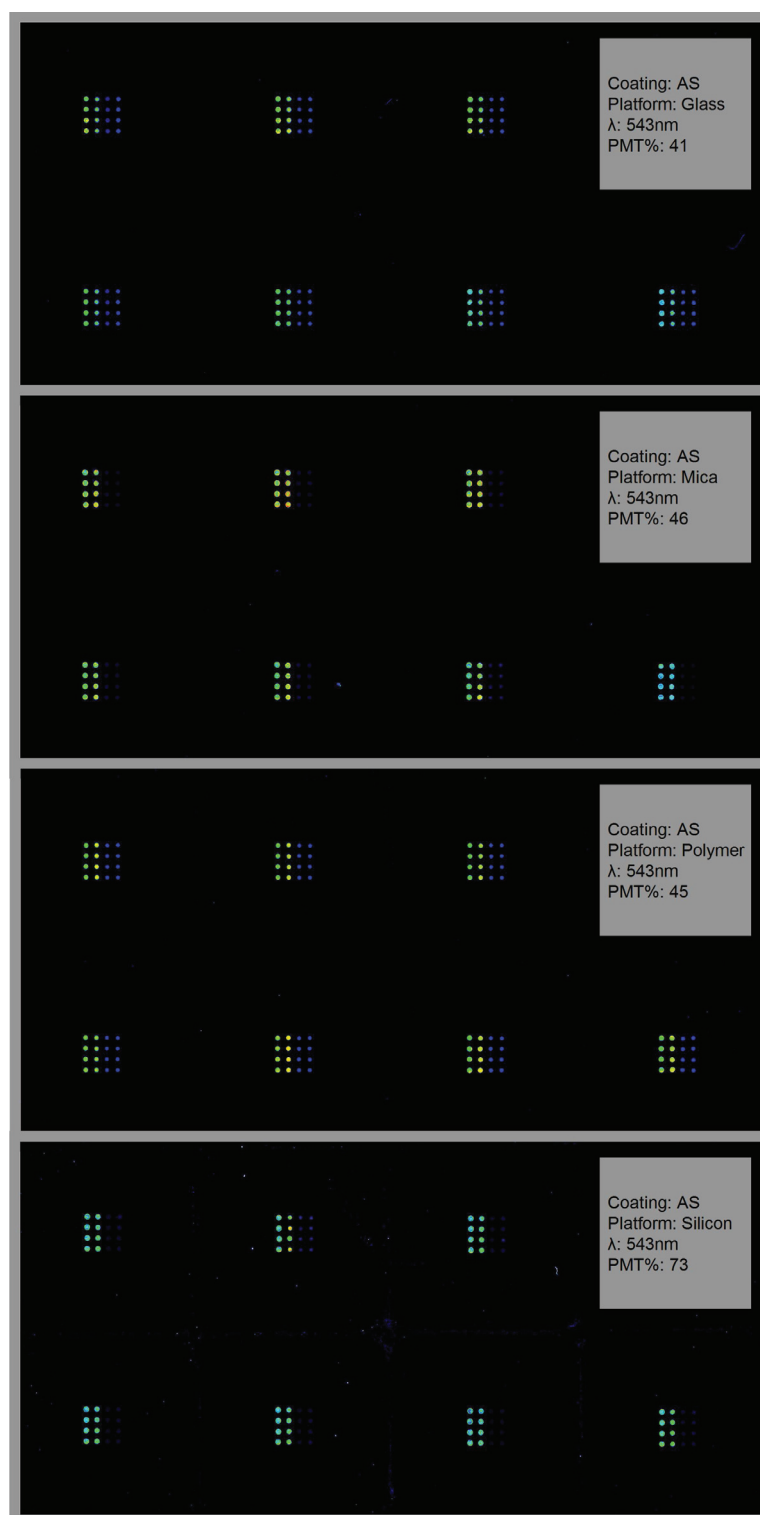
FIGURE A.2: Images of the probe fluorescence intensities generated on the AS-coated microarray platforms. The assay layout on each platform is provided in Figure A.1. Each image was acquired using a scanning wavelength of 543nm, LP of 100%, and PMT setting calibrated against the anti-IgG spots in the reference well. The platform material and calibrated PMT setting is provided in the upper left corner of each image. Datasets obtained from analysis of these images were plotted in Figure 5.5A.
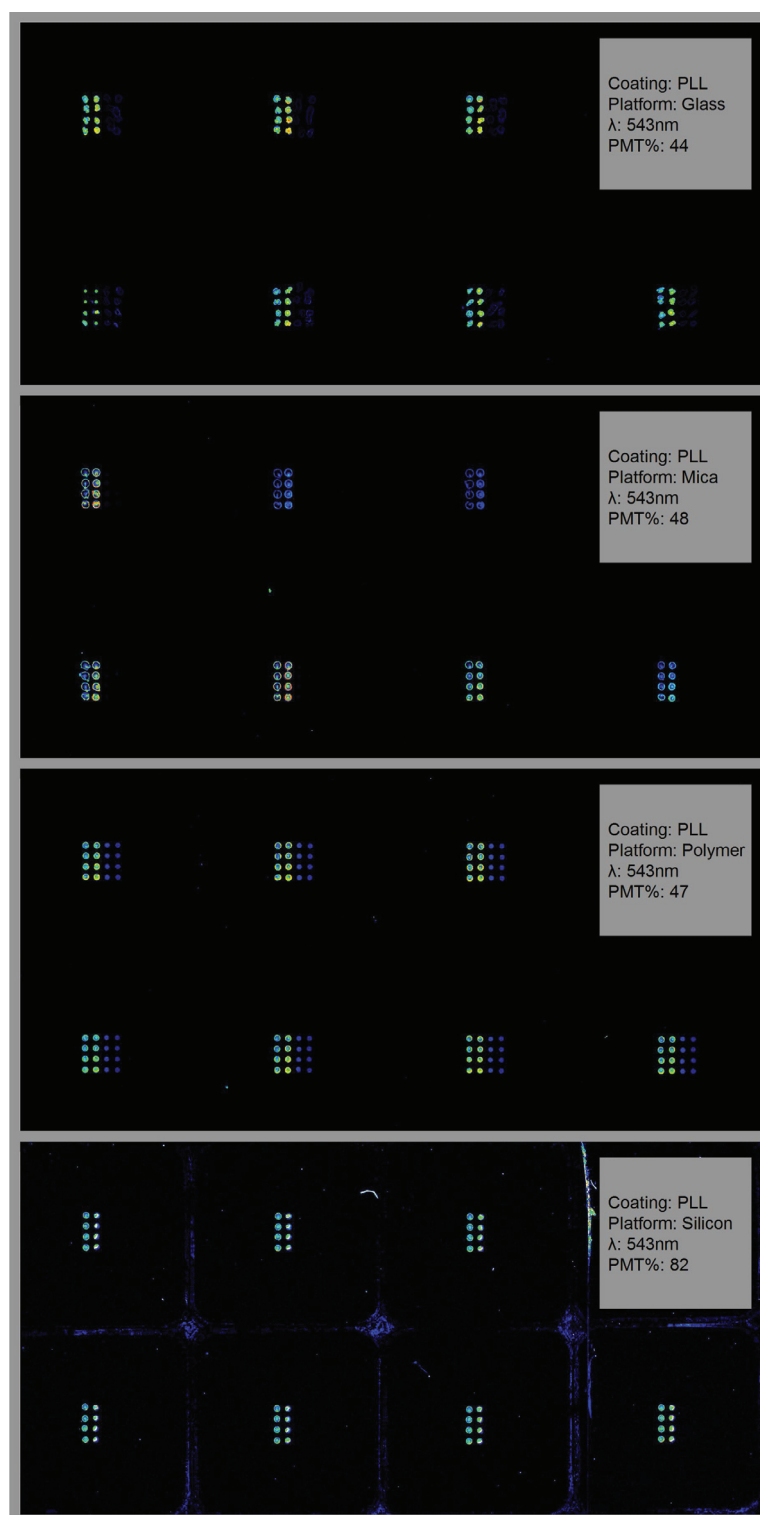
FIGURE A.3: Images of the probe fluorescence intensities generated on the PLL-coated microarray platforms. The assay layout on each platform is provided in Figure A.1. Each image was acquired using a scanning wavelength of 543nm, LP of 100%, and PMT setting calibrated against the anti-IgG spots in the reference well. The platform material and calibrated PMT setting is provided in the upper left corner of each image. Datasets obtained from analysis of these images were plotted in Figure 5.5B.
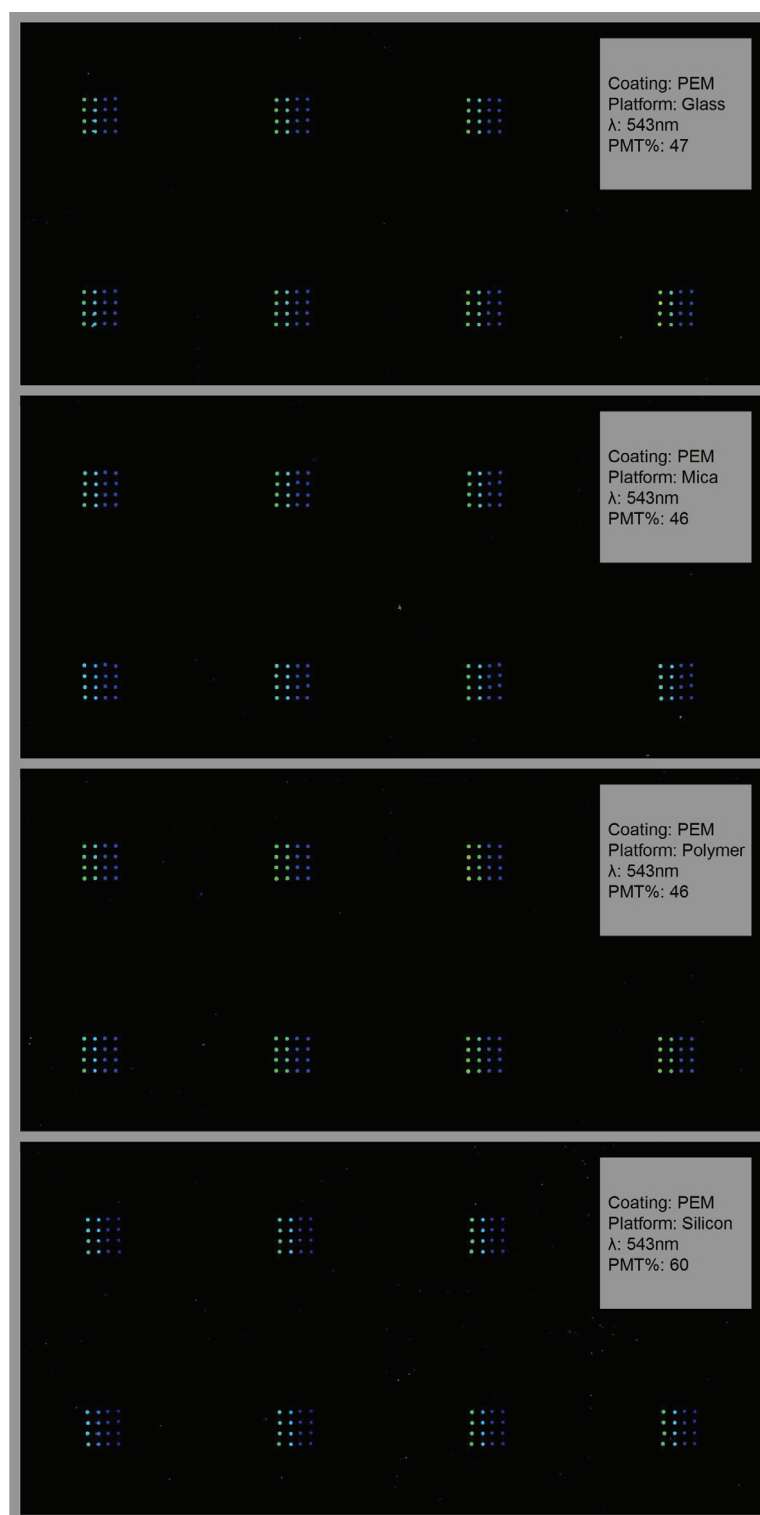
FIGURE A.4: Images of the probe fluorescence intensities generated on the PEM-coated microarray platforms. The assay layout on each platform is provided in Figure A.1. Each image was acquired using a scanning wavelength of 543nm, LP of 100%, and PMT setting calibrated against the anti-IgG spots in the reference well. The platform material and calibrated PMT setting is provided in the upper left corner of each image. Datasets obtained from analysis of these images were plotted in Figure 5.5C.
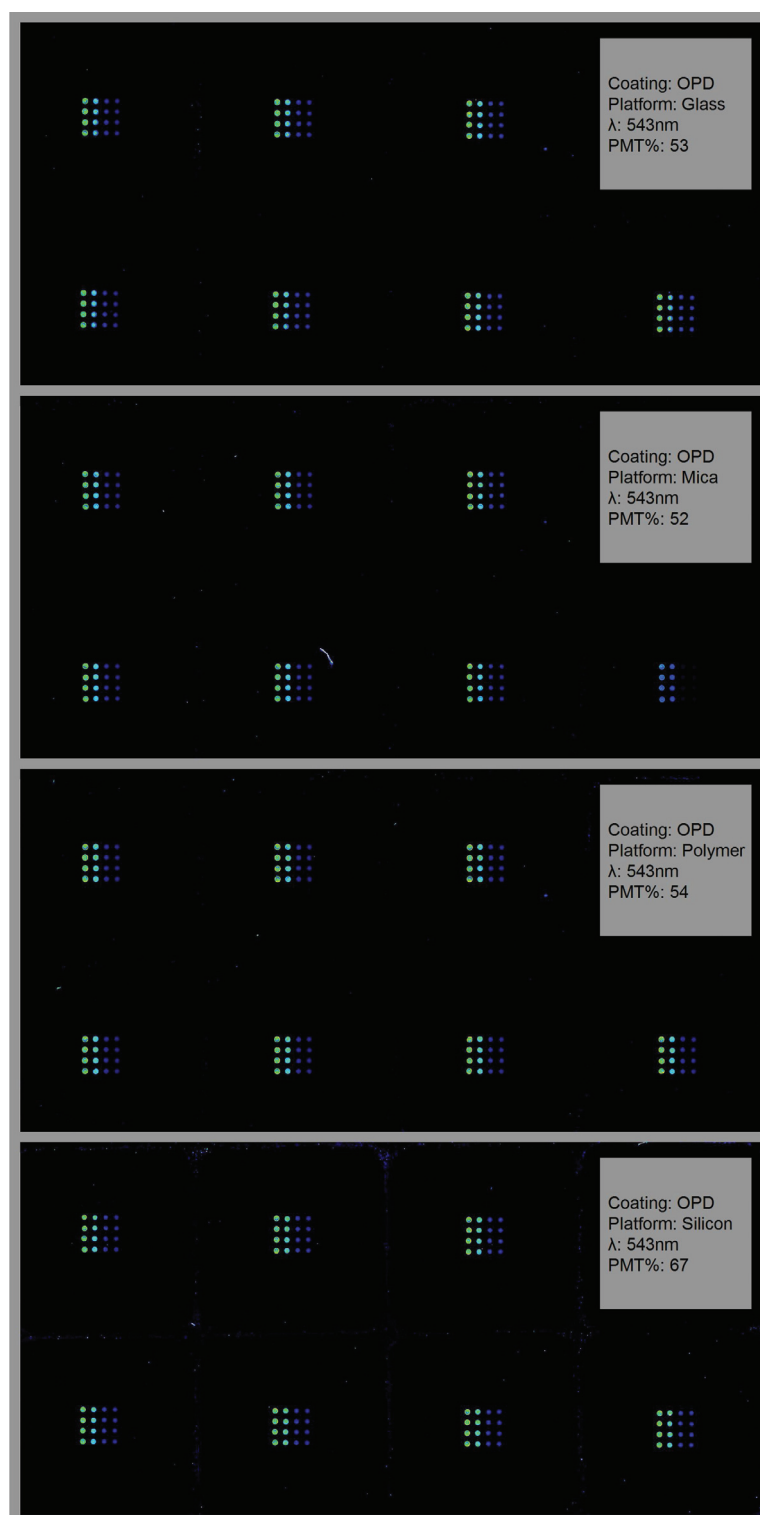
FIGURE A.5: Images of the probe fluorescence intensities generated on the OPD-coated microarray platforms. The assay layout on each platform is provided in Figure A.1. Each image was acquired using a scanning wavelength of 543nm, LP of 100%, and PMT setting calibrated against the anti-IgG spots in the reference well. The platform material and calibrated PMT setting is provided in the upper left corner of each image. Datasets obtained from analysis of these images were plotted in Figure 5.5D.
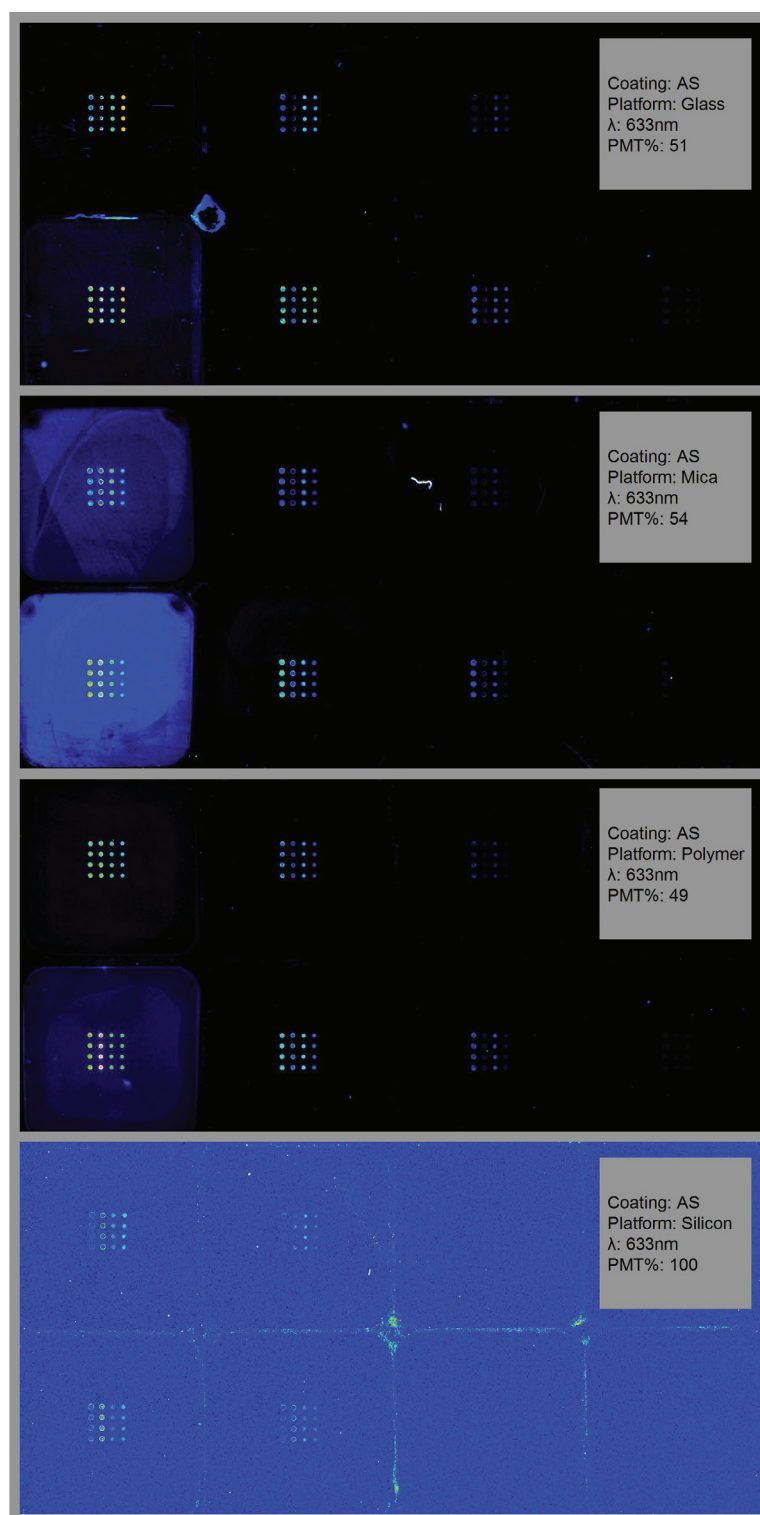
FIGURE A.6: Images of the target fluorescence intensities generated on the AS-coated microarray platforms. The assay layout on each platform is provided in Figure A.1. Each image was acquired using a scanning wavelength of 633nm, LP of 100%, and PMT setting calibrated against the anti-IgG spots in the reference well. The platform material and calibrated PMT setting is provided in the upper left corner of each image. Datasets obtained from analysis of these images were plotted in Figure 5.7A.
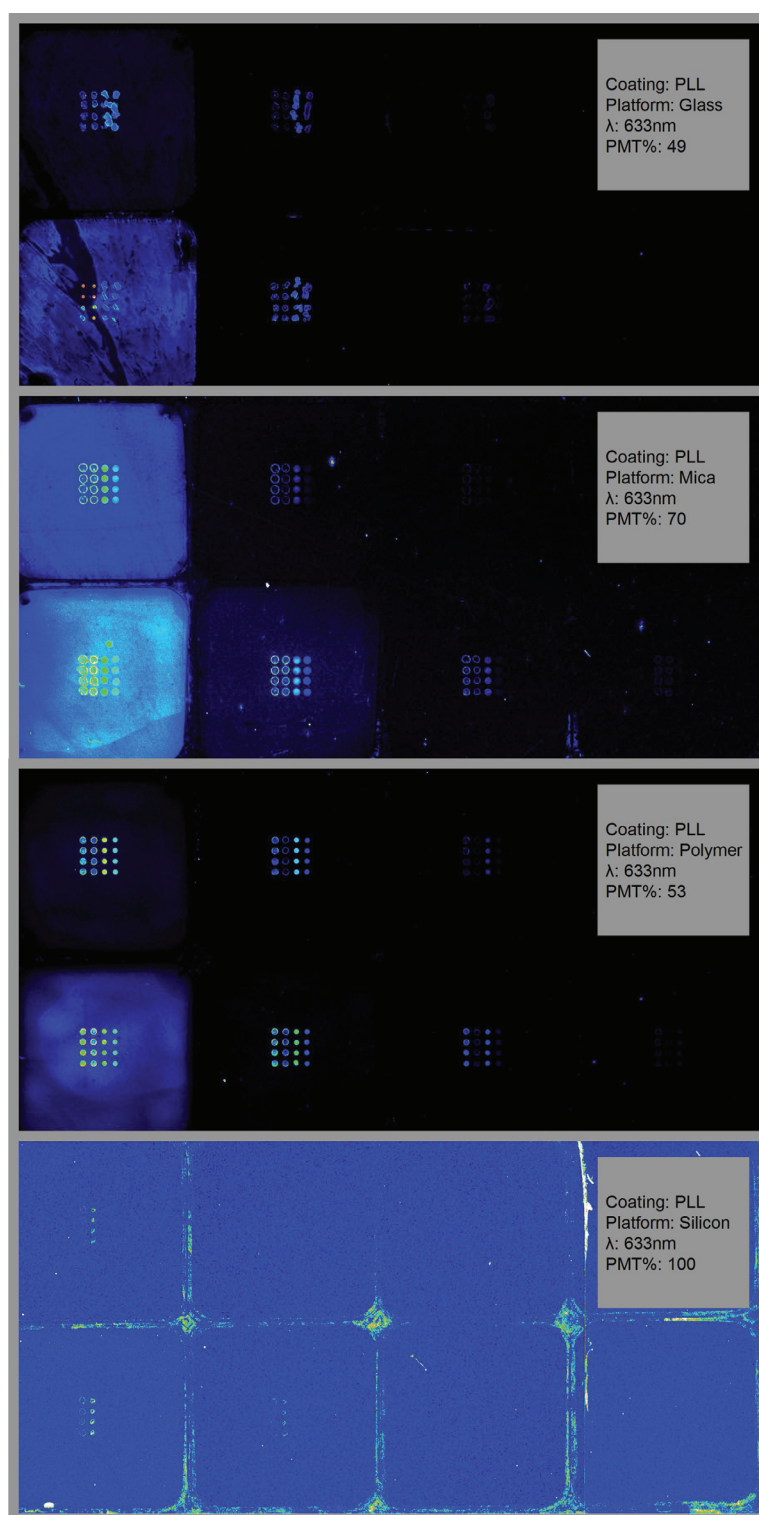
FIGURE A.7: Images of the target fluorescence intensities generated on the PLL-coated microarray platforms. The assay layout on each platform is provided in Figure A.1. Each image was acquired using a scanning wavelength of 633nm, LP of 100%, and PMT setting calibrated against the anti-IgG spots in the reference well. The platform material and calibrated PMT setting is provided in the upper left corner of each image. Datasets obtained from analysis of these images were plotted in Figure 5.7B.

FIGURE A.8: Images of the target fluorescence intensities generated on the PEM-coated microarray platforms. The assay layout on each platform is provided in Figure A.1. Each image was acquired using a scanning wavelength of 633nm, LP of 100%, and PMT setting calibrated against the anti-IgG spots in the reference well. The platform material and calibrated PMT setting is provided in the upper left corner of each image. Datasets obtained from analysis of these images were plotted in Figure 5.7C.
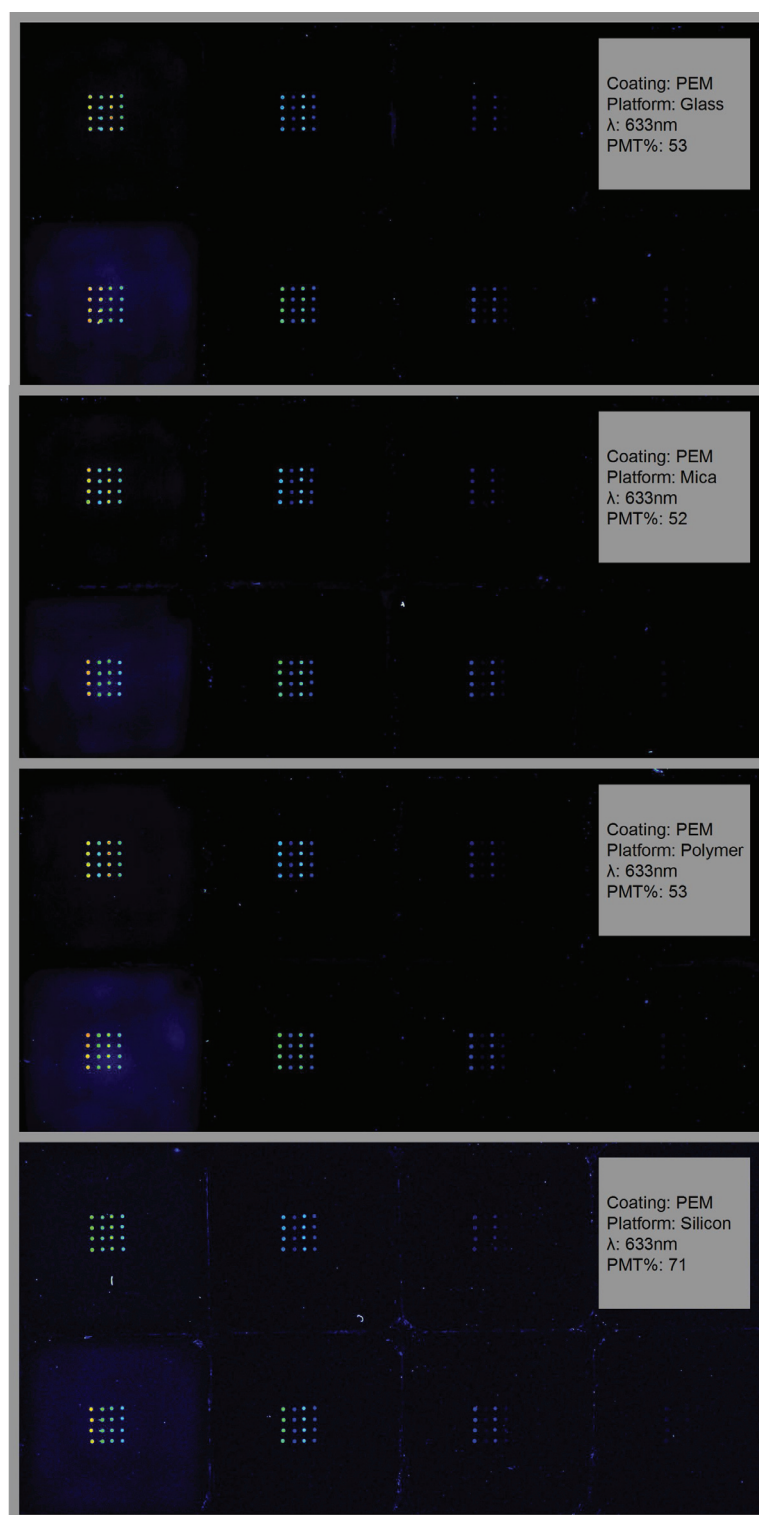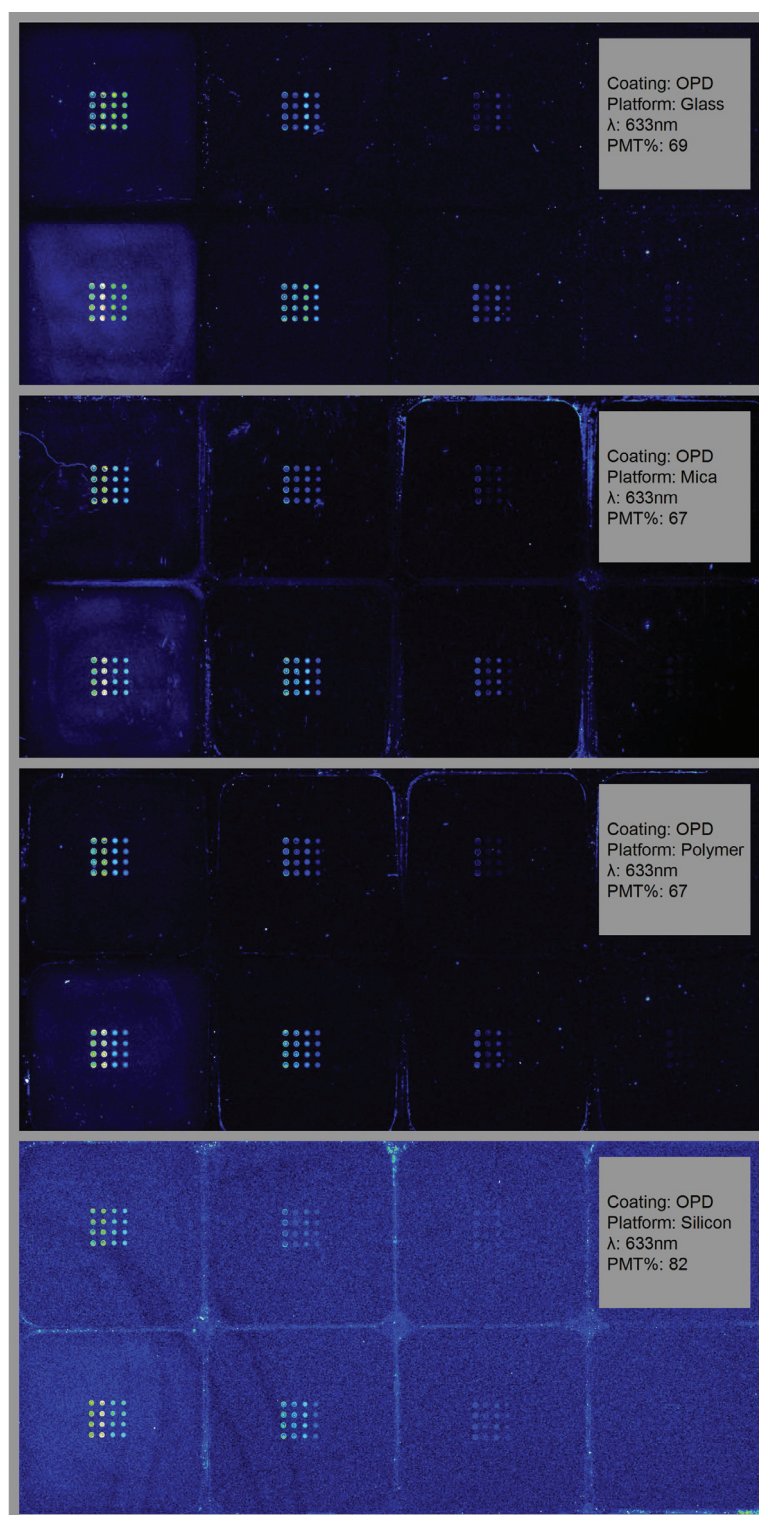
FIGURE A.9: Images of the target fluorescence intensities generated on the OPD-coated microarray platforms. The assay layout on each platform is provided in Figure A.1. Each image was acquired using a scanning wavelength of 633nm, LP of 100%, and PMT setting calibrated against the anti-IgG spots in the reference well. The platform material and calibrated PMT setting is provided in the upper left corner of each image. Datasets obtained from analysis of these images were plotted in Figure 5.7D.

Bibliography

[1] Templin, M. F., Stoll, D., Schrenk, M., Traub, P. C., Vohringer, C. F., and Joos, T. O. (2002) Protein microarray technology. *Trends in Biotechnology 20*, 160–166.

[2] Heller, M. J. (2002) DNA microarray technology: Devices, systems, and applications. *Annual Review of Biomedical Engineering 4*, 129–153.

[3] Schena, M., Shalon, D., Davis, R. W., and Brown, P. O. (1995) Quantitative Monitoring of Gene Expression Patterns with a Complementary DNA Microarray. *Science 270*, 467–470.

[4] Zhu, H., Bilgin, M., Bangham, R., Hall, D., Casamayor, A., Bertone, P., Lan, N., Jansen, R., Bidlingmaier, S., Houfek, T., Mitchell, T., Miller, P., Dean, R. A., Gerstein, M., and Snyder, M. (2001) Global analysis of protein activities using proteome chips. *Science 293*, 2101–2105.

[5] Nuwaysir, E. F., Bittner, M., Trent, J., Barrett, J. C., and Afshari, C. A. (1999) Microarrays and toxicology: The advent of toxicogenomics. *Molecular Carcinogenesis 24*, 153–159.

[6] Bains, W., and Smith, G. C. (1988) A Novel Method for Nucleic-Acid Sequence Determination. *Journal of Theoretical Biology 135*, 303–307.

[7] Hoheisel, J. D. (2006) Microarray technology: beyond transcript profiling and genotype analysis. *Nature Reviews Genetics 7*, 200–210.

[8] Dufva, M. (2005) Fabrication of high quality microarrays. *Biomolecular Engineering 22*, 173–184.

[9] Cutler, P. (2003) Protein arrays: The current state-of-the-art. *Proteomics 3*, 3–18.

[10] Angenendt, P. (2005) Progress in protein and antibody microarray technology. *Drug Discovery Today 10*, 503–511.

[11] MacBeath, G., and Schreiber, S. L. (2000) Printing proteins as microarrays for high-throughput function determination. *Science 289*, 1760–1763.

[12] Bacarese-Hamilton, T., Gray, J., and Crisanti, A. (2003) Protein Microarray Technology for Unraveling the Antibody Specificity Repertoire Against Microbial Proteomes. *CURRENT OPINION IN MOLECULAR THERAPEUTICS 5*, 278–284.

[13] Angenendt, P., Glokler, J., Sobek, J., Lehrach, H., and Cahill, D. J. (2003) Next generation of protein microarray support materials: Evaluation for protein and antibody microarray applications. *Journal of Chromatography A 1009*, 97–104.

[14] Kononen, J., Bubendorf, L., Kallioniemi, A., Barlund, M., Schraml, P., Leighton, S., Torhorst, J., Mihatsch, M. J., Sauter, G., and Kallioniemi, O. P. (1998) Tissue microarrays for high-throughput molecular profiling of tumor specimens. *Nature Medicine 4*, 844–847.

[15] Klenkar, G., and Liedberg, B. (2008) A microarray chip for label-free detection of narcotics. *Analytical and Bioanalytical Chemistry 391*, 1679–1688.

[16] Kanda, V., Kariuki, J. K., Harrison, D. J., and McDermott, M. T. (2004) Label-free reading of microarray-based immunoassays with surface plasmon resonance imaging. *Analytical Chemistry 76*, 7257–7262.

[17] Ressine, A., Ekstrom, S., Marko-Varga, G., and Laurell, T. (2003) Macro-/nanoporous silicon as a support for high-performance protein microarrays. *Analytical Chemistry 75*, 6968–6974.

[18] Situma, C., Hashimoto, M., and Soper, S. A. (2006) Merging microfluidics with microarray-based bioassays. *Biomolecular Engineering 23*, 213–231.

[19] Schwarz, A., Rossier, J. S., Roulet, E., Mermod, N., Roberts, M. A., and Girault, H. H. (1998) Micropatterning of biomolecules on polymer substrates. *Langmuir 14*, 5526–5531.

[20] Lenigk, R., Liu, R. H., Athavale, M., Chen, Z. J., Ganser, D., Yang, J. N., Rauch, C., Liu, Y. J., Chan, B., Yu, H. N., Ray, M., Marrero, R., and Grodzinski, P. (2002)

Plastic biochannel hybridization devices: a new concept for microfluidic DNA arrays. *Analytical Biochemistry 311*, 40–49.

[21] Taylor, S., Smith, S., Windle, B., and Guiseppi-Elie, A. (2003) Impact of surface chemistry and blocking strategies on DNA microarrays. *Nucleic Acids Research 31*, e87.

[22] Sobek, J., Bartscherer, K., Jacob, A., Hoheisel, J. D., and Angenendt, P. (2006) Microarray technology as a universal tool for high-throughput analysis of biological systems. *Combinatorial Chemistry & High Throughput Screening 9*, 365–380.

[23] Zhu, H., Klemic, J. F., Chang, S., Bertone, P., Casamayor, A., Klemic, K. G., Smith, D., Gerstein, M., Reed, M. A., and Snyder, M. (2000) Analysis of yeast protein kinases using protein chips. *Nature Genetics 26*, 283–289.

[24] Benters, R., Niemeyer, C. M., and Wohrle, D. (2001) Dendrimer-activated-solid supports for nucleic acid and protein microarrays. *Chembiochem 2*, 686–694.

[25] Arenkov, P., Kukhtin, A., Gemmell, A., Voloshchuk, S., Chupeeva, V., and Mirzabekov, A. (2000) Protein microchips: Use for immunoassay and enzymatic reactions. *Analytical Biochemistry 278*, 123–131.

[26] Chrisey, L. A., Lee, G. U., and Oferrall, C. E. (1996) Covalent attachment of synthetic DNA to self-assembled monolayer films. *Nucleic Acids Research 24*, 3031–3039.

[27] Kumar, A., Biebuyck, H. A., and Whitesides, G. M. (1994) Patterning Self-Assembled Monolayers - Applications in Materials Science. *Langmuir 10*, 1498–1511.

[28] Belder, D., and Ludwig, M. (2003) Surface modification in microchip electrophoresis. *Electrophoresis 24*, 3595–3606.

[29] Park, J., and Hammond, P. T. (2005) Polyelectrolyte multilayer formation on neutral hydrophobic surfaces. *Macromolecules 38*, 10542–10550.

[30] Spillman, S. D., McEvoy, H. A., and MacCraith, B. D. (2009) Fabrication of Substrate-Independent Protein Microarrays Using Polyelectrolyte Scaffolding. *Langmuir 25*, 1403–1411.

[31] Lahann, J., Balcells, M., Lu, H., Rodon, T., Jensen, K. F., and Langer, R. (2003) Reactive polymer coatings: A first step toward surface engineering of microfluidic devices. *Analytical Chemistry 75*, 2117–2122.

[32] Lee, H., Dellatore, S. M., Miller, W. M., and Messersmith, P. B. (2007) Mussel-inspired surface chemistry for multifunctional coatings. *Science 318*, 426–430.

[33] Harper, J. C., Polsky, R., Wheeler, D. R., Dirk, S. M., and Brozik, S. M. (2007) Selective immobilization of DNA and antibody probes on electrode arrays: Simultaneous electrochemical detection of DNA and protein on a single platform. *Langmuir 23*, 8285–8287.

[34] Peterson, A. W., Wolf, L. K., and Georgiadis, R. M. (2002) Hybridization of mismatched or partially matched DNA at surfaces. *Journal of the American Chemical Society 124*, 14601–14607.

[35] McKendry, R., Zhang, J. Y., Arntz, Y., Strunz, T., Hegner, M., Lang, H. P., Baller, M. K., Certa, U., Meyer, E., Guntherodt, H. J., and Gerber, C. (2002) Multiple label-free biodetection and quantitative DNA-binding assays on a nanomechanical cantilever array. *Proceedings of the National Academy of Sciences of the United States of America 99*, 9783–9788.

[36] Larkin, J. E., Frank, B. C., Gavras, H., Sultana, R., and Quackenbush, J. (2005) Independence and reproducibility across microarray platforms. *Nature Methods 2*, 337–343.

[37] Kuo, W. P., Jenssen, T. K., Butte, A. J., Ohno-Machado, L., and Kohane, I. S. (2002) Analysis of matched mRNA measurements from two different microarray technologies. *Bioinformatics 18*, 405–412.

[38] Bammler, T. et al. (2005) Standardizing global gene expression analysis between laboratories and across platforms. *Nature Methods 2*, 351–356.

[39] Tan, P. K., Downey, T. J., Spitznagel, E. L., Xu, P., Fu, D., Dimitrov, D. S., Lempicki, R. A., Raaka, B. M., and Cam, M. C. (2003) Evaluation of gene expression measurements from commercial microarray platforms. *Nucleic Acids Research 31*, 5676–5684.

[40] Shi, L. M. et al. (2005) Cross-platform comparability of microarray technology: Intra-platform consistency and appropriate data analysis procedures are essential. *Bmc Bioinformatics 6*, S12.

[41] Hultschig, C., Kreutzberger, J., Seitz, H., Konthur, Z., Bussow, K., and Lehrach, H. (2006) Recent advances of protein microarrays. *Current Opinion in Chemical Biology 10*, 4–10.

[42] Gulmann, C., Sheehan, K. M., Kay, E. W., Liotta, L. A., and Petricoin, E. F. (2006) Array-based proteomics: mapping of protein circuitries for diagnostics, prognostics, and therapy guidance in cancer. *Journal of Pathology 208*, 595–606.

[43] Shi, L. M. et al. (2006) The MicroArray Quality Control (MAQC) project shows inter- and intraplatform reproducibility of gene expression measurements. *Nature Biotechnology 24*, 1151–1161.

[44] Irizarry, R. A. et al. (2005) Multiple-laboratory comparison of microarray platforms. *Nature Methods 2*, 345–349.

[45] Mecham, B. H., Klus, G. T., Strovel, J., Augustus, M., Byrne, D., Bozso, P., Wetmore, D. Z., Mariani, T. J., Kohane, I. S., and Szallasi, Z. (2004) Sequence-matched probes produce increased cross-platform consistency and more reproducible biological results in microarray-based gene expression measurements. *Nucl. Acids Res. 32*, e74.

[46] Cretich, M., Damin, F., Pirri, G., and Chiari, M. (2006) Protein and peptide arrays: Recent trends and new directions. *Biomolecular Engineering 23*, 77–88.

[47] Kusnezow, W., and Hoheisel, J. D. (2003) Solid supports for microarray immunoassays. *Journal of Molecular Recognition 16*, 165–176.

[48] Yoshida, M., Langer, R., Lendlein, A., and Lahann, J. (2006) From advanced biomedical coatings to multi-functionalized biomaterials. *Polymer Reviews 46*, 347–375.

[49] Thevenet, S., Chen, H. Y., Lahann, J., and Stellacci, F. (2007) A generic approach towards nanostructured surfaces based on supramolecular nanostamping on reactive polymer coatings. *Advanced Materials 19*, 4333–4337.

[50] Hammond, P. T. (2004) Form and function in multilayer assembly: New applications at the nanoscale. *Advanced Materials 16*, 1271–1293.

[51] Bertrand, P., Jonas, A., Laschewsky, A., and Legras, R. (2000) Ultrathin polymer coatings by complexation of polyelectrolytes at interfaces: suitable materials, structure and properties. *Macromolecular Rapid Communications 21*, 319–348.

[52] Decher, G. (1997) Fuzzy nanoassemblies: Toward layered polymeric multicomposites. *Science 277*, 1232–1237.

[53] Choi, J., and Rubner, M. F. (2005) Influence of the degree of ionization on weak polyelectrolyte multilayer assembly. *Macromolecules 38*, 116–124.

[54] Lutkenhaus, J. L., Hrabak, K. D., McEnnis, K., and Hammond, P. T. (2005) Elastomeric flexible free-standing hydrogen-bonded nanoscale assemblies. *Journal of the American Chemical Society 127*, 17228–17234.

[55] Such, G. K., Quinn, J. F., Quinn, A., Tjipto, E., and Caruso, F. (2006) Assembly of ultrathin polymer multilayer films by click chemistry. *Journal of the American Chemical Society 128*, 9318–9319.

[56] Decher, G., and Hong, J. D. (1991) Buildup of Ultrathin Multilayer Films by a Self-Assembly Process .2. Consecutive Adsorption of Anionic and Cationic Bipolar Amphiphiles and Polyelectrolytes on Charged Surfaces. *Berichte Der Bunsen-Gesellschaft-Physical Chemistry Chemical Physics 95*, 1430–1434.

[57] Decher, G., and Hong, J. D. (1991) Buildup of Ultrathin Multilayer Films by a Self-Assembly Process .1. Consecutive Adsorption of Anionic and Cationic Bipolar Amphiphiles on Charged Surfaces. *Makromolekulare Chemie-Macromolecular Symposia 46*, 321–327.

[58] Decher, G., Hong, J. D., and Schmitt, J. (1992) Buildup of Ultrathin Multilayer Films by a Self-Assembly Process .3. Consecutively Alternating Adsorption of Anionic and Cationic Polyelectrolytes on Charged Surfaces. *Thin Solid Films 210*, 831–835.

[59] Hammond, P. T. (1999) Recent explorations in electrostatic multilayer thin film assembly. *Current Opinion in Colloid & Interface Science 4*, 430–442.

[60] Caruso, F. (2001) Nanoengineering of particle surfaces. *Advanced Materials 13*, 11–22.

[61] Sui, Z. J., Salloum, D., and Schlenoff, J. B. (2003) Effect of molecular weight on the construction of polyelectrolyte multilayers: Stripping versus sticking. *Langmuir 19*, 2491–2495.

[62] Zhou, X. C., Wu, L. Y., and Zhou, J. Z. (2004) Fabrication of DNA microarrays on nanoengineered polymeric ultrathin film prepared by self-assembly of polyelectrolyte multilayers. *Langmuir 20*, 8877–8885.

[63] Zhou, X. C., and Zhou, J. Z. (2006) Protein microarrays on hybrid polymeric thin films prepared by self-assembly of polyelectrolytes for multiple-protein immunoassays. *Proteomics 6*, 1415–1426.

[64] Dubas, S. T., and Schlenoff, J. B. (2001) Polyelectrolyte multilayers containing a weak polyacid: Construction and deconstruction. *Macromolecules 34*, 3736–3740.

[65] Duffy, D. C., McDonald, J. C., Schueller, O. J. A., and Whitesides, G. M. (1998) Rapid prototyping of microfluidic systems in poly(dimethylsiloxane). *Analytical Chemistry 70*, 4974–4984.

[66] Dai, L. M., StJohn, H. A. W., Bi, J. J., Zientek, P., Chatelier, R. C., and Griesser, H. J. (2000) Biomedical coatings by the covalent immobilization of polysaccharides onto gas-plasma-activated polymer surfaces. *Surface and Interface Analysis 29*, 46–55.

[67] Tadmor, R. (2004) Line energy and the relation between advancing, receding, and young contact angles. *Langmuir 20*, 7659–7664.

[68] Lee, H., Lee, Y., Statz, A. R., Rho, J., Park, T. G., and Messersmith, P. B. (2008) Substrate-independent layer-by-layer assembly by using mussel-adhesive-inspired polymers. *Advanced Materials 20*, 1619–1623.

[69] Lee, H., Rho, J., and Messersmith, P. B. (2009) Facile Conjugation of Biomolecules onto Surfaces via Mussel Adhesive Protein Inspired Coatings. *Advanced Materials 21*, 431–434.

[70] Bernard, A., Michel, B., and Delamarche, E. (2001) Micromosaic immunoassays. *Analytical Chemistry 73*, 8–12.

[71] Masson, J. F., Battaglia, T. M., Davidson, M. J., Kim, Y. C., Prakash, A. M. C., Beaudoin, S., and Booksh, K. S. (2005) Biocompatible polymers for antibody support on gold surfaces. *Talanta 67*, 918–925.

[72] Chen, Y. D., Kamat, V., Dougherty, E. R., Bittner, M. L., Meltzer, P. S., and M., T. J. (2002) Ratio statistics of gene expression levels and applications to microarray data analysis. *Bioinformatics 18*, 1207–1215.

[73] Laib, S., and MacCraith, B. D. (2007) Immobilization of biomolecules on cycloolefin polymer supports. *Analytical Chemistry 79*, 6264–6270.

[74] Dai, J. H., Baker, G. L., and Bruening, M. L. (2006) Use of porous membranes modified with polyelectrolyte multilayers as substrates for protein arrays with low nonspecific adsorption. *Analytical Chemistry 78*, 135–140.

[75] Brazma, A. et al. (2001) Minimum information about a microarray experiment (MIAME) - toward standards for microarray data. *Nature Genetics 29*, 365–371.

[76] Bras, M., Dugas, V., Bessueille, F., Cloarec, J. P., Martin, J. R., Cabrera, M., Chauvet, J. P., Souteyard, E., and Garrigues, M. (2004) Optimisation of a silicon/silicon dioxide substrate for a fluorescence DNA microarray. *Biosensors & Bioelectronics 20*, 797–806.

[77] Pearson, K. (1896) Mathematical contributions to the theory of evolution. III. Regression, heredity and panmixia. *Philosophical Transactions of the Royal Society A 187*, 253–318.

[78] Kidambi, S., Chan, C., and Lee, I. S. (2004) Selective depositions on polyelectrolyte multilayers: Self-assembled monolayers of m-dPEG acid as molecular template. *Journal of the American Chemical Society 126*, 4697–4703.

[79] Hendricks, T. R., and Lee, I. (2006) A versatile approach to selective and inexpensive copper patterns using polyelectrolyte multilayer coatings. *Thin Solid Films 515*, 2347–2352.

[80] Chen, K. M., Jiang, X. P., Kimerling, L. C., and Hammond, P. T. (2000) Selective self-organization of colloids on patterned polyelectrolyte templates. *Langmuir 16*, 7825–7834.